Coatings for corrosion protection of metals and alloys

By

LIJIA YANG, B.S.

A Thesis

Submitted to the School of Graduate Studies

In Partial Fulfillment of the Requirements

For the Degree

Master of Applied Science

McMaster University

MASTER OF APPLIED SCIENCE (2012)   McMaster University
(Materials Science & Engineering)   Hamilton, Ontario

TITLE: Coatings for corrosion protection of metals and alloys
AUTHOR: Lijia Yang, B.S. (Nanjing Normal University, China)
SUPERVISORS: Dr. Stephen C. Veldhuis and Dr. Igor Zhitomirsky
NUMBER OF PAGES: XI, 114

Abstract

Thin films prepared by electrochemical and physical vapor deposition (PVD) methods were investigated for corrosion protection of metals and alloys. Various electrochemical methods were developed, such as electrophoretic deposition (EPD), electrolytic deposition (ELD) and combined methods. EPD method has been developed for the deposition of polymer films, including poly(2-vinylpyridine) (PVP) and co-polymer poly(4-vinylpyridine-*co*-butyl methacrylate) (PVPBM). The method involved the electrophoresis of protonated polymer macromolecules, base generation at the cathode surface, charge neutralization and deposition of water insoluble polymer films. Nanostructured CeO_2 films were prepared by cathodic ELD and EPD. Cathodic ELD involved electrosynthesis of CeO_2 nanoparticles in the cathodic reaction and film formation. New dispersion agents were developed for CeO_2 particles for application in EPD processes. The kinetics of ELD and EPD and deposition mechanisms were investigated.

Composite polymer-CeO_2 films were deposited using various strategies, based on ELD or EPD of CeO_2 and EPD of polymers. The composite films were deposited as monolayers, multilayers or materials of graded composition. The deposition yield and film composition can be varied.

The composite films were studied by electron microscopy, X-ray diffraction, thermogravimetric and differential thermal analysis. Electrochemical testing showed that polymer and composite films provided corrosion protection of stainless steel substrates.

Corrosion protection properties of coatings deposited on commercial AMPCO and TZM alloys was investigated. CrN, CrN-D, and TiC were deposited by PVD method. Ni coatings were deposited by electroplating. The analysis of Tafel plots and impedance spectroscopy data showed that CrN and CrN-D coatings deposited by PVD showed better corrosion protection of AMPCO and TZM alloys, compared to TiC and Ni coatings. The results of this investigation pave the way for the fabrication of novel coatings with advanced corrosion protection, wear and mechanical properties, using combined PVD and electrochemical methods.

Acknowledgement

Here I would like to sincerely appreciate and thank my supervisors Dr. Stephen C. Veldhuis and Dr. Igor Zhitomirsky for guidance. I am very grateful to all the members in Dr. Igor Zhitomirsky's group and other colleagues in the MSE department. Thanks a lot to all the group members for their help in the lab and office. Besides, I do appreciate the atmosphere built in the group, which is good for study and getting along with all the members.

I also thank Professors who instructed the courses that I attended through these two years. Knowledge that I have learnt in these courses does help my study. I do sincerely appreciate all the staff in the MSE department. Ed McCaffery and Doug Culley did great job to help us, including maintenance and setting up.

I am grateful to all the agencies that have ever given financial support to our research.

Table of Contents

Table of Figures

1 Introduction

Physical vapor deposition (PVD) and electrochemical deposition (ECD) are two typical methods to form thin films at the atomic scale. These two methods are totally different, since PVD is mainly based on vacuum and plasma technologies, while ECD relies on electrode reactions and ions in electrolyte. Advantages and disadvantages of both methods have been discussed in the literature below.

As for PVD, chemical composition of deposited materials and substrate materials is almost unlimited. In addition, layered or graded structures of films can be easily achieved, due to the plasma technology. Another characteristic due to plasma is that almost no temperature limitation exists for substrates. However, PVD method requires relatively expensive and complicated vacuum and plasma equipment.

One of the major advantages of ECD is the possibility of uniform deposition on large surface area substrates of complex shape. Therefore, ECD is being used more and more in automotive industry. Further, temperature for ECD usually ranges from room temperature to 100℃. Equipment and running environment of ECD can be much simpler than that for PVD. Considering ECD has to be run in solution, the solubility of materials is definitely an obvious limit. Another problem will be waste water pollution, especially in massive industrial production.

Both of these two methods have limitations and unique advantages. Substrates for PVD have to be vacuum-resistant, while water-resistance is a similar limitation in

ECD. The choice of a specific method usually depends on the products' needs, including substrate condition, production temperature allowed, and also cost estimation.

Therefore, either of PVD or ECD performs much better than the other in some cases. For example, composite coatings, containing dispersed particles can only be achieved by ECD, especially when particles are on the nanometer range or organic materials are deposited. In contrast, PVD is definitely the irreplaceable solution when hard, wear-protective (e.g. TiN, TiC, Al_2O_3) or carbon-containing coatings are desired. In addition, PVD is also suitable for the deposition of alloys.

In many cases PVD and ECD are combined to target new and advanced applications, either is ECD-PVD or PVD-ECD.

In the ECD-PVD method, the first several electrochemically deposited layers are followed by one or more PVD coatings for final functional or decorative purposes, considering the advantage of PVD in wear-protective coating deposition. ECD interlayers of Ni and Ni-Pd, for example, increase the corrosion resistance of the substrate material (brass), while subsequent PVD-TiN coating guarantees an excellent wear resistance and nice color in addition. The sequence of ECD depends on the substrate material which finally has to be coated with films by PVD. For example, zinc die cast/ECD-Cu/ECD-Ni/PVD-TiN is a typical sequence in this ECD-PVD method.

As for the PVD-ECD method, it is totally based on the compatibility of PVD to all substrate materials, in particular by evaporation and sputter processes. The subsequent ECD process is used to achieve high-rate deposition for the fabrication of thick layers. ECD thickening of a thin gold or other precious metal layer sputtered onto the hard coating is widely used, which has been a normal method in industrial production. For example, titanium/PVD-Au/ECD/Au is frequently used to deposit gold film.

2 Literature Review

2.1 PVD

2.1.1Development of deposition methods

The method of evaporation was developed to transfer atoms from a heated source to substrates in a controllable way. Film formation and growth was expected to proceed atomistically. Evaporation differs from sputtering, which is another method for physically depositing films. In sputtering, the atoms are ejected from source surfaces, usually maintained at room temperature, through the impact of gaseous ions. The earliest sputtering experiment can be traced back to the year 1852, when metals were sputtered from the cathode using glow discharge plasma [1].

Later advances in the development of vacuum pumping equipment and fabrication of heating sources had largely promoted the progress of evaporation technology. Subsequently, sputtering was used in industrial production, such as mirror coating. Until the late 1960s evaporation became superior to sputtering, since the former method was characterized by higher deposition rates, better vacuum environments for film formation, and general applicability of all kinds of materials. Furthermore, some new technologies such as pulsed laser deposition were also related to the evaporation method [1].

Evaporation caused by absorption of thermal energy is simply one method to induce atoms to leave a liquid or solid surface. Atoms can be emitted or sputtered from solids at room temperature by bombarding the surfaces with energetic ions. These two alternatives are known as evaporation and sputtering technologies. In either way atoms, after the emission, are deposited on substrates to form a film. Since physical methods are primarily applied for film formation, both these two methods are known as physical vapor deposition (PVD).

PVD is an important alternative to chemical vapor deposition (CVD) for many thin film applications. Below some distinguishing differences between PVD and CVD are listed.

1. PVD is based on solid or molten sources, as opposed to generally gaseous precursors used in CVD
2. The physical mechanism of PVD is based on evaporation or collisional impact, which results in the transfer of source atoms into gas phase.
3. The environment for PVD is pressure reduced compared to CVD
4. Absence of chemical reactions in the gas phase and on the substrate surface [1].

Above is the brief history of PVD and related technology. However, today the choice of evaporation, sputtering, or chemically depositing for some particular applications or production depends on many factors. Some kind of competition has been formed among these alternative technologies, due to their characteristic advantages and disadvantages. Furthermore, in quite a few cases, they can be forged into some hybrid processes, which combine their advantages properly.

2.1.2 Related technology

2.1.2.1 Evaporation technology

The evaporation method is perhaps the simplest way to produce thin films composed of sequentially deposited atoms. The deposition process is controlled on the atomic scale. Thermodynamics, particularly source temperature-vapor pressure relationship, largely determines the rate of evaporation and the nature of the vapor stream. Film thickness and uniformity are basically related to the geometric placement of the evaporation source and substrate.

Pulsed laser deposition (PLD) is one of the new techniques for thin-film deposition, which is based on the interaction of laser beams with material surfaces. As the technology proceeded, almost all materials that have been deposited in the form of thin films by other PVD techniques have also been evaporated by PLD method. One significant advantage of PLD is the possibility of deposition of stoichiometric ceramic films, since stoichiometric bulk sintered ceramics are the target sources in PLD, which is totally different from the dependence of CVD on reactions between precursor gases.

Evaporation techniques for thin-film deposition have been superseded in many situations by sputtering and CVD. Despite disadvantages in maintaining stoichiometry, evaporation is still a preferred method in large operations. Another instance is the application of evaporation in the molecular beam epitaxy.

2.1.2.2 Sputtering technology

Fig.2-1 illustrates a simplified sputtering system designed to deposit metal films. Inside is a pair of parallel metal electrodes, one of which is the cathode or the material (metal here) to be deposited. This cathode is connected to the negative terminal of a DC power supply. The voltages of several kV are usually applied. Facing the cathode is the substrate or anode, which may be grounded, biased positively or negatively. After evacuation of the chamber, working gas (typically argon) is introduced and serves as the necessary medium in which the electrical discharge is initiated and sustained [1].

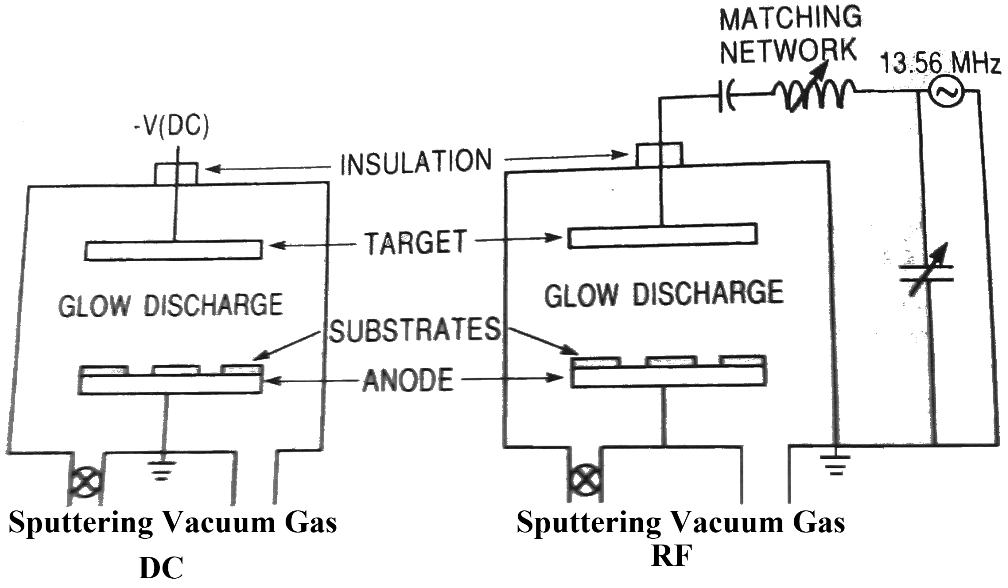

Fig. 2-1 Schematic of simplified sputtering systems (DC/RF) [1]

Microscopically, positive gas ions in the discharge strike the cathode and physically eject or sputter target atoms through momentum transfer to them. These atoms enter and move through the discharge region to eventually deposit onto the growing film. Simultaneously other particles and radiation are emitted from the target also.

2.1.2.3 Plasma technology

The term plasma was initially coined to describe the behavior of ionized gases in high-current vacuum tubes. Later it was found that plasmas actually behaved differently from simple un-ionized gases. Therefore, plasmas were termed as the fourth state of matter. 99% of matter in the universe exists in the form of plasma.

Plasma can be broadly defined as a quasi-neutral gas that exhibits collective behavior in the presence of applied electromagnetic fields. Plasmas are weakly ionized gases consisting of electrons, ions, and neutral atomic and molecular species. Fig.2-2 shows a simplified plasma deposition system.

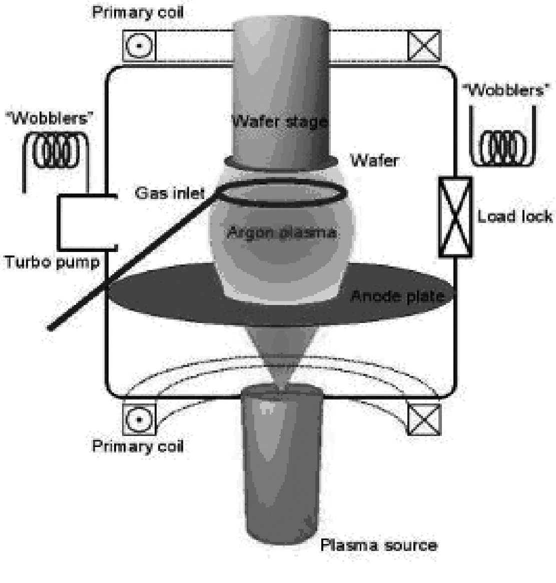

Fig. 2-2 Schematic of simplified plasma deposition system

Advances in understanding of properties and mechanisms of ionized gases have resulted in more adoption of plasma technology for deposition and surface modification. For example, integrated circuit fabrication is associated with the use of plasmas. Other areas for plasma processing include automotive, optical coatings, information recording, and aerospace industry.

2.1.2.4 Discharge

Typically a glow discharge occurs in low-pressure gas using a high-impedance DC power supply. One basic example is a discharge, in which a tiny current flows initially due to small amount of charge carriers in the system. With charge multiplication, the current increases rapidly, while the voltage, limited by output impedance of power supply, still remains constant. Eventually, the discharge becomes self-sustaining after sufficient amounts of ions are produced to regenerate the same amounts of electrons as initial ones. From this period on, the gas begins to glow and the voltage drops accompanied by a sharp rise in current. At this point normal glow takes place.

Initially, ion bombardment of the cathode concentrates near the cathode edges or other surface irregularities. With more power being applied, the bombardment extends to the entire surface and thus leading to a uniform current density. A further increase in power drives both voltage and cathode current density higher.

At still higher currents, the temperature of the cathode rises. Therefore, thermionic emission of electrons exceeds that of secondary-electron emission and low-voltage arcs propagate. Arcs are basically defined as gas or vapor discharges where cathode voltage drop is of the order of the minimum ionizing or excitation potential. The arc is a self-sustained discharge that supports high currents by providing its own mechanism for electron emission from negative or positive electrodes. Quite a few commercial PVD processes rely on arcs.

2.1.3 PVD process

Since the beginning of the 1980s ceramic PVD coatings were introduced into industry for numerous applications. Multiphase, multicomponent and composite materials have been developed for different applications, including industrial massive production. One typical example is the development of physical vapour deposition (PVD) for wear-protective multicomponent and multilayer coatings.

In PVD coating processes, film growth is usually at the atomic level and can be controlled by a series of variables, including electrical and magnetic fields, reactive atmospheres, cathode materials, and substrate temperature. The main difference among different PVD processes is the specific method used to vaporize the solid, which may entail different energy states and further result in different coating structures. Some typical PVD processes are shown below in Fig.2-3, with different methods applied.

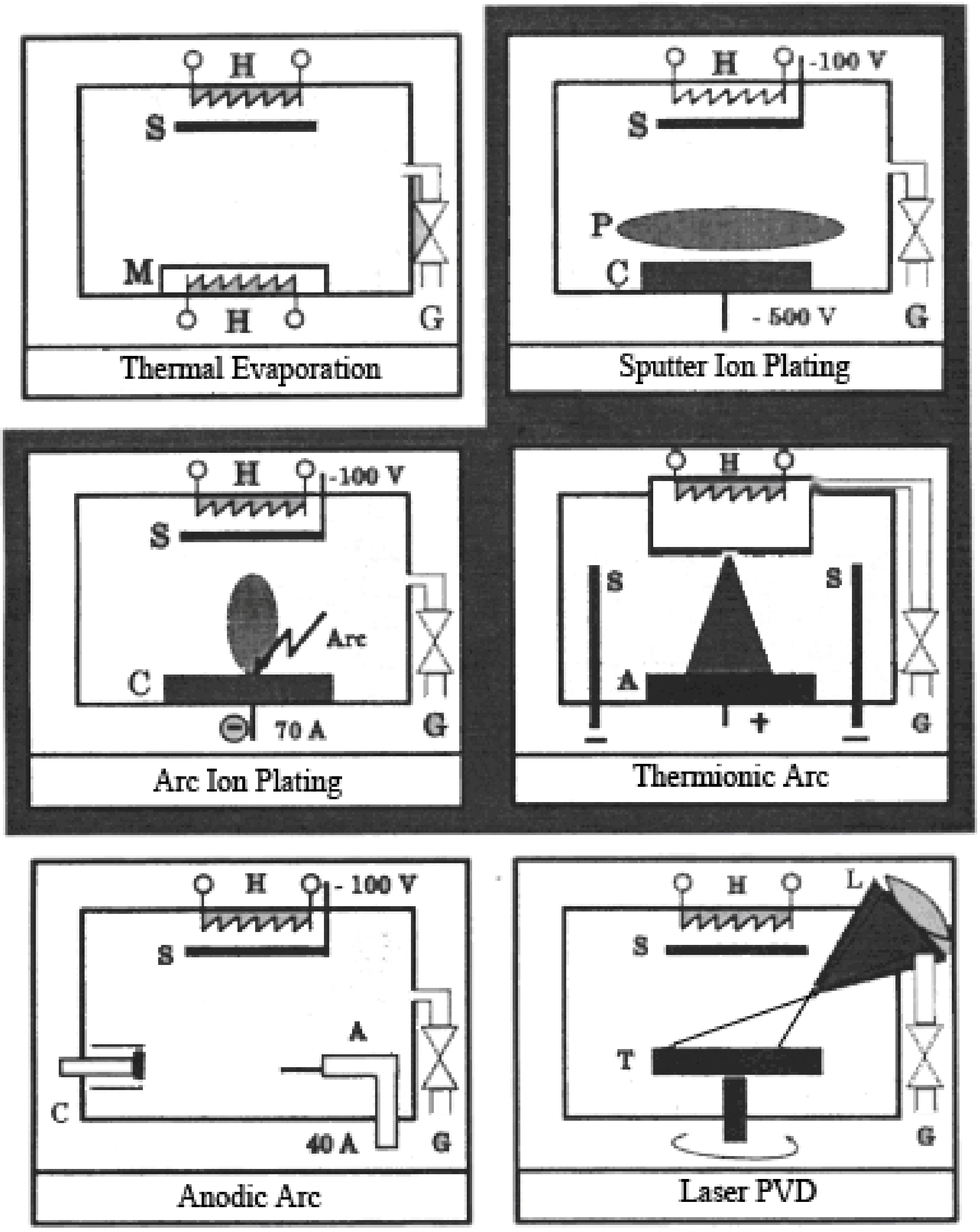

Fig. 2-3 Typical types of PVD processes [2-7]

In all PVD processes, reactive atmospheres (N_2, CH_4, O_2, C_2H_2) can be introduced into the processing chamber to form hard materials. “Ion plating” is possible with all process variants as well. In this process, an electrical bias voltage is applied to the components which are to be coated, stimulating ionic bombardment onto the substrate.

Ion plating will produce a denser film, usually associated with superior adhesion, which is a fundamental prerequisite for the real use of wear-reducing coatings on industrial tools. However, thermal stressing of the coating and substrate is simultaneously increased, which may cause damage to the surface zones of heat-sensitive tool steels or cemented carbides. Two typical types of PVD process are shown below in Fig.2-4.

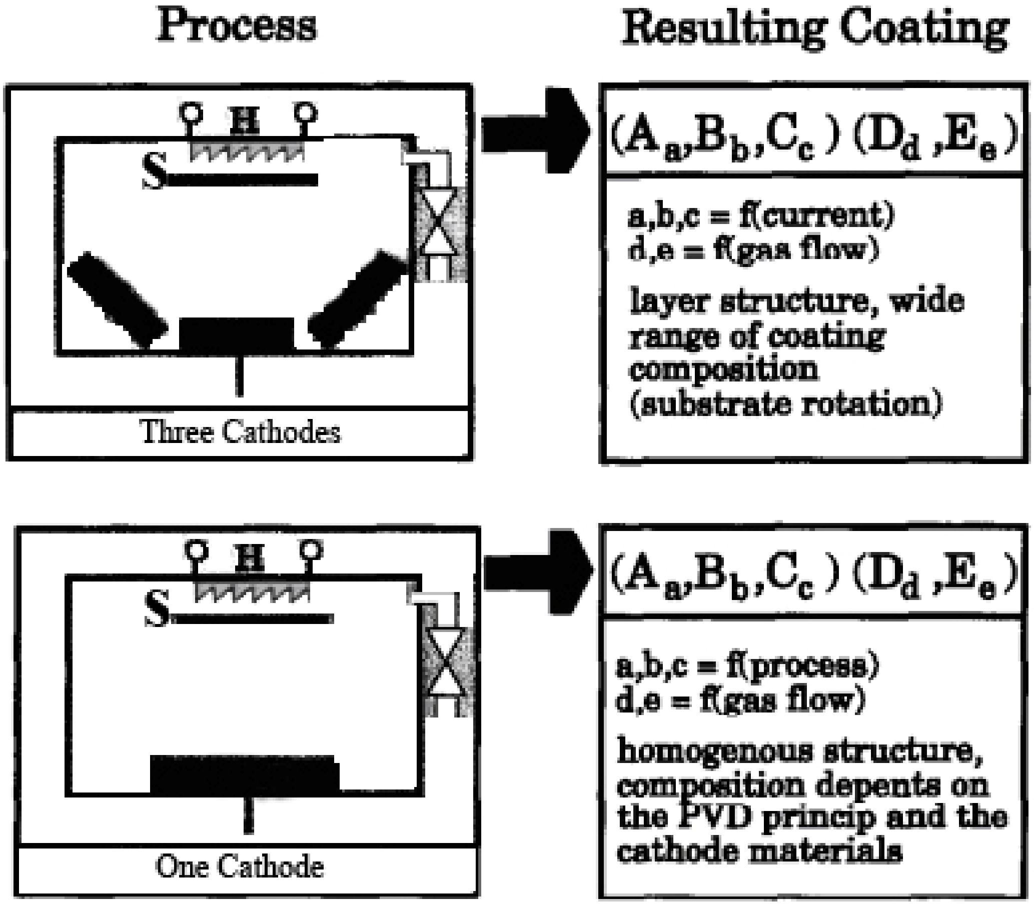

Fig. 2-4 Variants for PVD processes [2]

There are three significant variants for the PVD process. The first is number of cathodes. Films can be generated by simultaneous vaporization of several cathodes materials, since each cathode is provided with its own voltage supply. However, in real processes, it is necessary to rotate the components being coated, to guarantee a uniform layer structure of coating [3].

Another variant is use of multicomponent cathodes. For example, cathodes consisting of alloying elements can be used. The main advantage of applying multi-cathodes is homogeneous coating structure. However, due to the vaporization of cathode materials, there are probably different concentrations of alloying components within the film accordingly. For example, if a Ti/Al (50/50 (at.%)) cathode is vaporized by the arc process, a composition of roughly 90/10 (at.%) may result in the coating [8].

A third variant is reactive deposition. Usually reactive gas mixtures are used to incorporate metalloids (C, N, O) into the film. Therefore, PVD process must be controlled extremely precisely for reproduction, since reactions of the mixed gases depend on substrate temperature, gas pressure during the process, and the material effects. These factors affect the whole PVD process together and form a complex network of interrelationships, which is shown in Fig.2-5 as a schematic diagram.

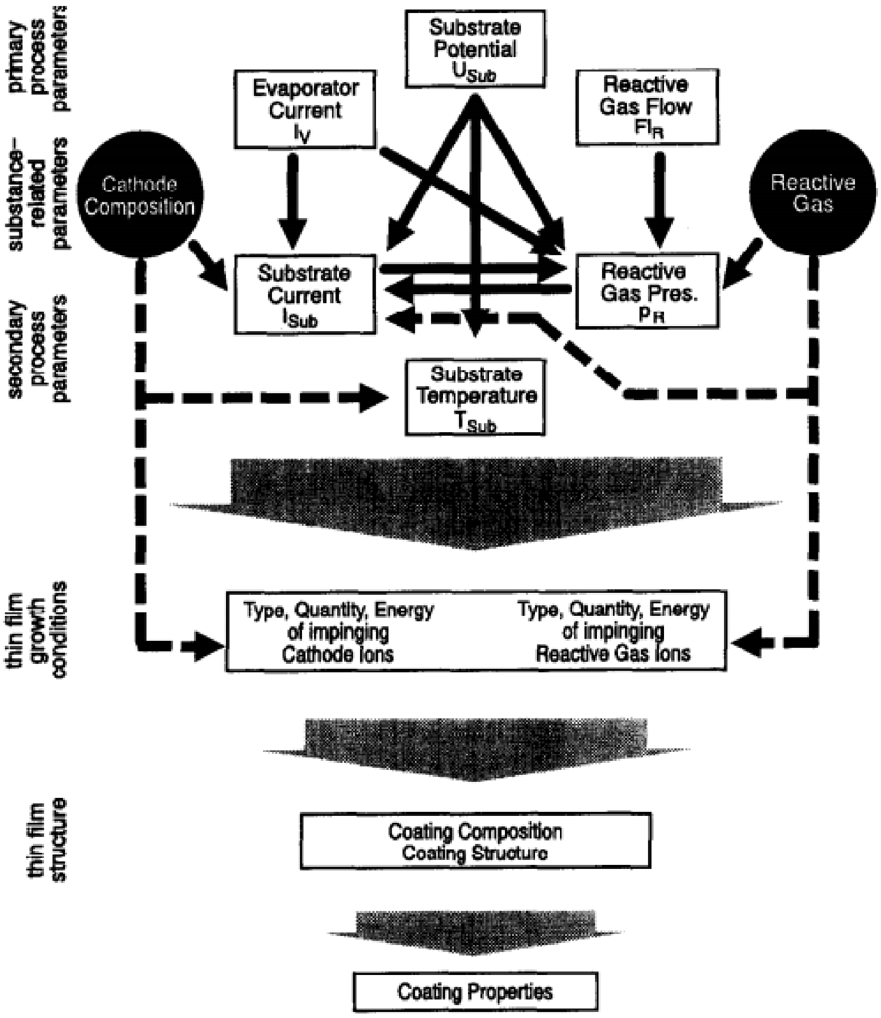

Fig. 2-5 Schematic flow chart for PVD working systems [2]

2.1.4 Multi-layer coatings

With suitable process technology used, coating composition can be varied during deposition of complex coatings by altering the gas atmosphere, to produce graded coatings or multilayer structures. Considering this method entails no interruption to the process itself, and grading of the interface zones is achieved, it can be used to produce economically extremely load-resistant films [9].

Besides from the variation of the reactive gas composition, two process variants are also significant to produce multilayer coatings. Multiple layers can be deposited by continuous movement of the tools below the cathodes during the process. This method achieves extremely good interface zones, and hence good interlayer adhesion. Since the reactive gas composition is the same for all cathodes, the metalloid constituents of the hard materials in the different layers are identical accordingly [10].

However, the method above restricts the ability to affect the composition of the individual layers. A further multilayer principle is to alter the cathode operation so that only one cathode is active at any time. Individual layers of any kind required (metal and metalloid components) can be deposited successively. The disadvantage of this method is also obvious. The interruption of the coating process, which is unavoidable every time when the cathode is changed, will probably lead to disturbances in the interface structure. Intermediate activation (e.g. ionic etching) may be a solution to achieve useful improvements.

2.1.5 Coatings of tools produced by PVD

Coatings for metal forming can be basically classified into two types, though both designed for wear and abrasion-resistance. A first type includes the traditional hard and wear resistant coatings which mainly consist of the nitrides and carbides of titanium and chromium [11]. TiN, TiCN, TiAlN and CrN can all be included into this type. These coatings are suitable to avoid galling, to prevent mechanical wear of tools [12,13].

Another type is solid lubricating coatings characterized by a low coefficient of friction. The main aim of these low friction coatings is to reduce the use of harmful lubricants in preventing wear and galling. Also, functional gradient coatings are more and more applied on metal forming tools, as shown in Fig.2-6. One possible direction in this respect is to combine a hard layer beneath another self-lubricating layer, or to deposit them simultaneously to produce composite coatings. PVD is a perfect solution for such co-deposition.

Fig. 2-6 Application of PVD to industrial tools (online source)

Tool coatings are typically applied by physical or chemical vapor deposition (PVD/CVD) [14]. In general, CVD coatings are preferred for heavy duty metal forming operations since the high deposition temperature (900–1000 °C) is beneficial for the film formation. However, in case of CVD the tools require a heat treatment after the coating deposition to harden the tool steel, which may result in dimensional changes. In comparison, coatings under PVD are deposited at lower temperatures which generally yield harder and finer deposits, thus leading to minimum of tool distortion, which is significant in the area of forming and cutting tools.

2.2 Electrodeposition

2.2.1 ELD and EPD

2.1.1.1 Definition

Electrochemical methods are frequently used to prepare thin films and coatings. Recently, microelectronic components have also been processed by these methods. Both depositions of ceramic and polymer materials have been studied intensively, due to the efficiency and low cost.

Two processes are commonly applied to prepare ceramic coatings: the electrolytic process (ELD) and the electrophoretic process (EPD), which is illustrated in Fig.2-7. The electrolytic process is based on solutions of metal salts. Ions in the solutions migrate under applied electric field. The electrophoretic process is based on the suspensions of charged ceramic particles. Suspended particles migrate under applied electric field and are then deposited on an electrode [15].

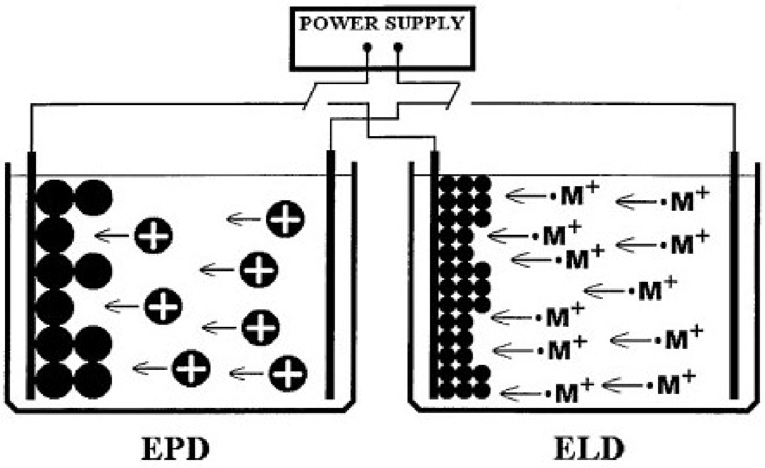

Fig. 2-7 Schematic of cathodic electrophoretic deposition EPD and electrolytic deposition ELD [15]

2.1.1.2 Different applications

Main differences between ELD and EPD include thickness of films and coatings, deposited species, and deposition rate [16, 17]. ELD enables the preparation of nanostructured thin ceramic films, while EPD is usually used to obtain thick films, as shown in the Fig.2-8 below.

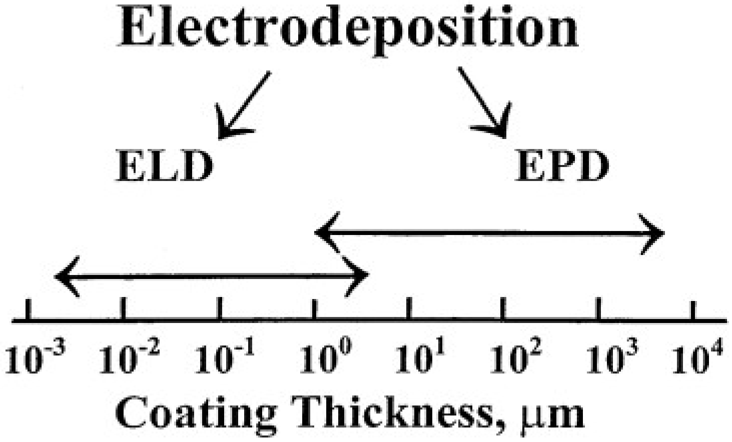

Fig. 2-8 Comparison of thickness of ELD and EPD deposits [15]

2.2.2 Basic theories

2.2.2.1 Particle interactions

Basically, hydrolysis reactions occurring in ELD processes and motion of charged particles in EPD processes result in the accumulation of ceramic particles on the electrode [18, 19]. Deposition is achieved by particle coagulation at the electrode. Recent progress in understanding ELD and EPD mechanisms was achieved using the classical Derjaguin-Landau-Verwey-Overbeek (DLVO) theory of colloidal stability [20, 21].

In DLVO theory, two main forces are considered: double-layer repulsion and Van der Waals' attraction. Besides, in most situations, various additives serve as an important parameter in the system, such as electrolytes and polymers. Interaction forces among particles in suspensions are then strongly affected by the additives.

The DLVO theory provides the basis for understanding the stability of charged colloids. In DLVO theory, the Coulombic double-layer repulsion and Van der Waals' attraction are two forces that form total pair interaction between colloidal particles together. Fig.2-9 is the sketch of double layer structure.

Therefore, the total energy V_T of interaction of two isolated and identically charged particles can be expressed **[15]**:

$$V_T = V_A + V_R \qquad \textbf{(2-1)}$$

The attractive energy V_A here can be expressed as below, if considering two identical spherical particles:

$$V_A = -\frac{A}{6}\left(\frac{2}{s^2-4}+\frac{2}{s^2}+\ln\frac{s^2-4}{s^2}\right) \text{ [15]} \tag{2-2}$$

where A is the Hamaker constant and s=2+H/a, with H the shortest distance between the two spheres and a the particle radius [20, 21]. Fig.2-10 and Fig.2-11 demonstrate the relationship between total energy and the distance H.

If H<<a, the above equation can be simplified to:

$$V_A = -A\frac{a}{12H} \tag{2-3}$$

Another part in the expression of V_T, the repulsive energy V_R is expressed as:

$$V_R = 2pee_0 a y^{2} \ln(1+e^{-kH}) \tag{2-4}$$

where ε is the dielectric constant of the solvent, ε_0 is the vacuum dielectric permittivity, ψ is the surface potential, $1/\kappa$ is the Debye length [21]:

$$k = \left(\frac{e_0^2 \sum n_i z_i^2}{ee_0 kT}\right)^{1/2} \tag{2-5}$$

The DLVO theory describes the potential energy curve for pair interaction, as shown below. Total energy of particle interaction will exhibit a maximum, if the diffuse layer repulsion is much higher than the Van der Waals' attraction. This is termed as the energy barrier to particle coagulation [15, 21].

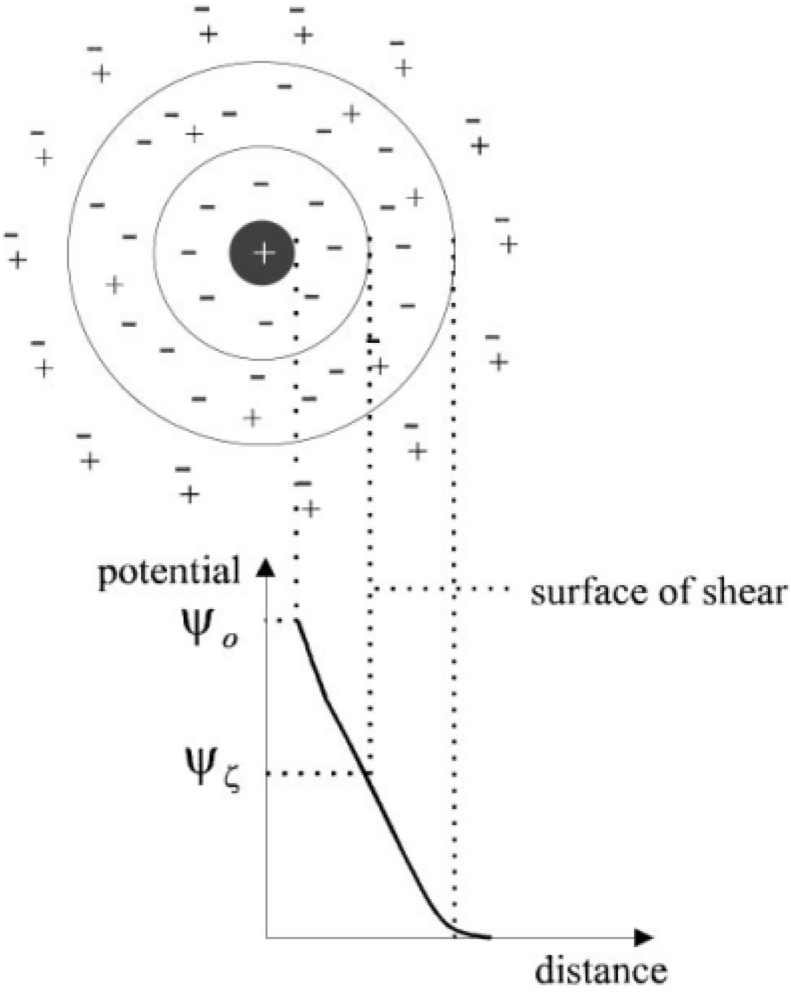

Fig. 2-9 Schematic of double-layer structure

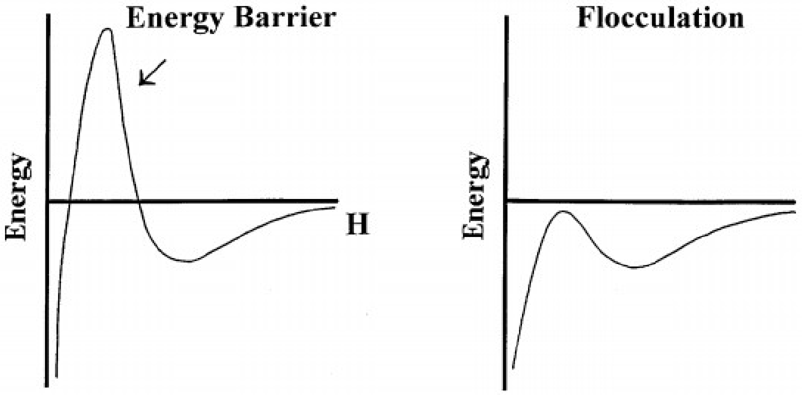

Fig. 2-10 Total interaction energy between spherical particles at low (left) and high (right) electrolyte concentration

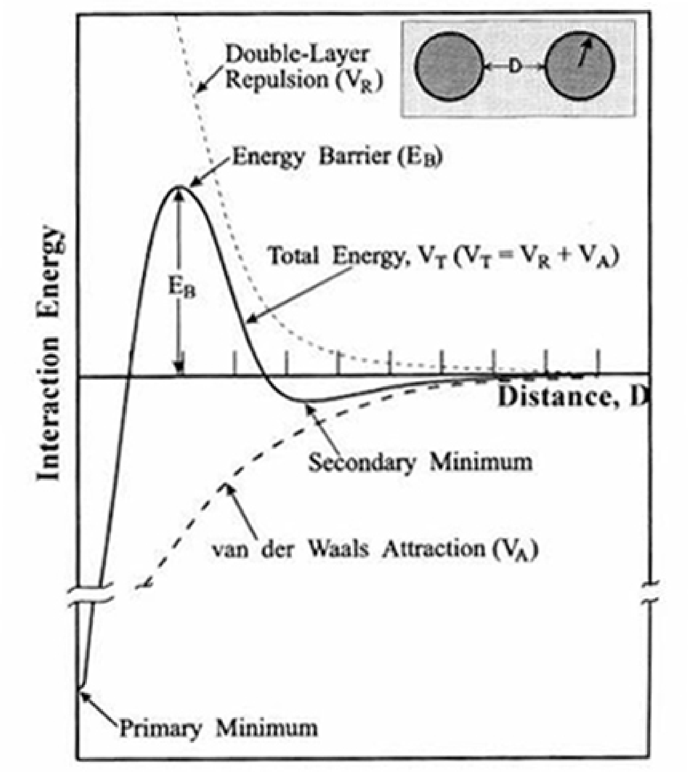

Fig. 2-11 Illustrative diagram of total interaction energy

The thickness of the double layer is characterized by the parameter of Debye length, $1/\kappa$. This thickness is extremely sensitive to the electrolyte concentration [21]. The DLVO theory terms a critical electrolyte concentration for coagulation as a flocculation value [21]. This concentration decreases with the valence of the electrolyte ions of a charge opposite to that of colloidal particles [15]. This potential energy peak decreases as the electrolyte concentration increases. After this energy barrier disappears, coagulation becomes possible. Flocculation by ions compressing the double layer also follows the Hofmeister series, which is illustrated below [21].

Within the series of ions of the same charge, the flocculation value increases in the following order:

NH_4^+, K^+, Na^+, Li^+;

Ba^{2+}, Sr^{2+}, Ca^{2+}, Mg^{2+} [15]

Therefore, negatively charged particles are flocculated by large cations at a smaller concentration rather than by small cations of the same valency. According to experimental tests, this flocculation value was found to be in the range 20- 200 for monovalent ion, 0.3-3 for divalent ions, and 0.003-0.1 for trivalent ions [21]. In conclusion, flocculation values are basically determined by solution concentration, temperature, particle size of colloids, and chemical nature of the solution.

2.2.2.2 Solvents

A solvent basically works as a vehicle that carries ions in solution (ELD) or ceramic particles in suspension (EPD). Normally there are two types of solvents used for electrodeposition: water and organic liquids [22-33].

Usually ELD requires a sufficient amount of H_2O, since typically water is consumed in cathodic reactions. Fig.2-12 demonstrates that more water is necessary for more material to be deposited. However, adsorbed water in deposits results in shrinkage and cracking during the drying process, which is a problem for coating. Therefore, non-aqueous solvents are superior for preventing the coating from hydrating [34, 35]. Repulsion among colloidal particles formed near the electrode is related to the diffuse-layer charge on the particles. The thickness of the double layer decreases in correspondence to decreasing dielectric constant of the solvent, which promotes particle coagulation.

The solvents for application in EPD should be inert with respect to powder. It is known that organic liquids are usually superior to water as a suspension medium for EPD [15, 36]. The use of water-based suspensions will cause gas formation from the electrolysis of water, which prevents the deposition of a uniform and adherent film. A variety of non-aqueous organic solvents are commonly used in the preparation of EPD suspensions, including ethanol, acetylacetone, and methyl ethyl ketone.

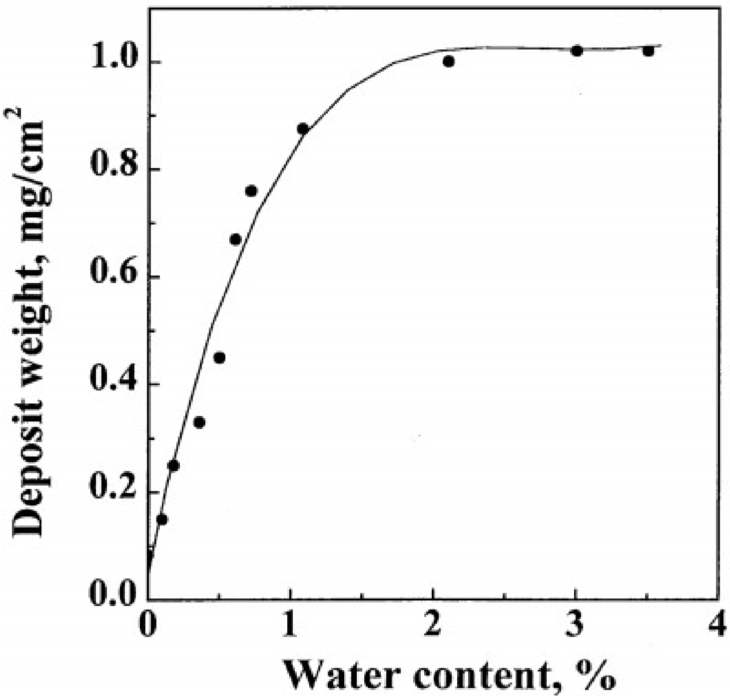

.

Fig. 2-12 Deposit weight of ELD films versus water content in 0.005 M $ZrOCl_2$ solutions in mixed ethyl alcohol-water solvent, current density 5 $mAcm^{-2}$, deposition time 5 min [15]

2.2.2.4 Electrophoretic mobility

Two theories were developed describing electrophoretic mobility of rigid particles and polyelectrolytes in EPD [15, 37-41]. These two theories of electrophoresis can be applied to either a single isolated particle or colloidal particles in concentrated suspensions [15, 37-44].

The velocity v of a particle in an electric field E is expressed by:

$$v=\mu E \quad \textbf{(2-6)}$$

where μ is the electrophoretic mobility. The electrophoretic mobility of a rigid colloidal particle can be derived from the equation below [37]:

$$m = \frac{2ee_0z}{3h} f(ka) \quad \textbf{(2-7)}$$

where z is the zeta potential and h is the viscosity of the liquid. The function $f(\kappa a)$ increases from 1 for κa<<1 to 1.5 for κa>>1. For particles whose sizes are much smaller than the Debye length, this electrophoretic mobility μ is expressed by:

$$m = \frac{2ee_0z}{3h} \quad \textbf{(2-8)}$$

For particles whose sizes are obviously large compared to $1/\kappa$, this electrophoretic mobility μ is expressed by:

$$m = \frac{ee_0z}{h} \quad \textbf{(2-9)}$$

The electrophoretic mobility of a spherical polyelectrolyte, in which fixed charges are distributed at a uniform density ρ_{fix}, can be derived from the equation below [40]:

$$m = \frac{r_{fix}}{h l^2}[1+\frac{2}{3}(\frac{l}{k})^2 \frac{1+l/2k}{1+l/k}] \quad \textbf{(2-10)}$$

However, the theory for rigid spheres differs from that for spherical polyelectrolytes. Therefore, when a rigid particle is coated by a layer of polyelectrolyte of thickness d, the general mobility is expressed by:

$$m = \frac{ee_0}{h}\frac{y_0 / k_m + y_{DON} / l}{1/k_m + 1/l} f(\frac{d}{a}) + \frac{r_{fix}}{h l^2} \quad \textbf{(2-11)}$$

where d is the thickness of polyelectrolyte layer, Ψ_0 is the potential at the boundary between the polyelectrolyte and the surrounding solution. Ψ_{DON} is the Donnan potential:

$$y_0 = y_{DON} + \frac{2n^{\infty}kT}{r_{fix}}\{1 - [(\frac{r_{fix}}{2ze_0n^{\infty}})^2 + 1]^{1/2}\} \quad \textbf{(2-12)}$$

$$y_{DON} = \frac{kT}{ze_0}\ln\{\frac{r_{fix}}{2ze_0n^{\infty}} + [(\frac{r_{fix}}{2ze_0n^{\infty}})^2 + 1]^{1/2}\} \quad \textbf{(2-13)}$$

where k is Boltzmann’s constant, T is the absolute temperature, e_0 is the elementary electrical charge, and κ_m is the Debye-Huckel parameter of the polyelectrolyte layer:

$$k_m = k[1 + (\frac{r_{fix}}{2ze_0n^{\infty}})^2]^{1/4} \quad \textbf{(2-14)}$$

$$f(\frac{d}{a}) = \frac{2}{3}[1 + \frac{1}{2(1 + d/a)^3}] \quad \textbf{(2-15)}$$

2.2.3 Cathodes

2.2.3.1 Cathodic reactions

Various cathodic reactions basically lead to a local pH increase at the cathode surface. [15, 45-53] In some cathodic reactions, H^+ ions are consumed, and H_2O is consumed in some other reactions, thus leading to a pH increase near the cathode, which is demonstrated below[47, 48].

$$2H^{+} + 2e^{-} \rightarrow H_2 \qquad \textbf{(2-16)}$$

$$NO_3^{-} + 2H^{+} + 2e^{-} \rightarrow NO_2^{-} + H_2O \qquad \textbf{(2-17)}$$

$$2H_2O + 2e^{-} \rightarrow 2OH^{-} + H_2 \qquad \textbf{(2-18)}$$

$$O_2 + 2H_2O + 4e^{-} \rightarrow 4OH^{-} \qquad \textbf{(2-19)}$$

$$ClO_4^{-} + 4H_2O + 8e^{-} \rightarrow Cl^{-} + 8OH^{-} \qquad \textbf{(2-20)}$$

The difference of pH value between the solution and the layer adjacent to the electrode increases in correspondence with increasing current density and decreases if temperature increases, respectively [54]. Data collected in tests indicated that the rate of pH change accelerated in the range 1-10 $mAcm^{-2}$ [54]. In cathodic ELD, the bulk pH is acidic, though the cathode surface pH was tested to be up to 11-12 [15, 54]. This high pH could be constant through the first 100-200 μm from the cathode surface. It was found that stirring of solutions would delay the start of alkali formation at the cathode surface.

2.3.2 Cationic species

When aqueous solutions are used, cationic species are very determining, since they are usually part of the material to be deposited. One example is the solution containing metal cations M^{z+} and anions A^{y-}. In this case, the formation of $M_a(OH)_bO_c(H_2O)_dA_x^{t+}$ species can be expected, such as mononuclear (a=1) or polynuclear (a>1) species [55,56]. The structure of polynuclear species is affected by several variants, including pH, temperature, and concentration of metal ions, anions, and additives [15].

2.2.4 Electrolytic deposition

2.2.4.1 Mechanism of ELD

The particle formation kinetics and deposit composition are determined by solvent, additives, temperature and current density [15, 57-74]. In the cathodic electrolytic deposition process, the pH in the bulk of solutions is low, though simultaneously cathodic reactions result in an increase in pH near the cathode [45-50]. The production of OH^- is due to the electrolysis of water and some other cathodic reactions. Electrosynthesis results in the accumulation of colloidal particles near the electrode. The mechanism of ELD is mainly based on the illustrated DLVO theory of colloidal stability. The formation of a deposit is caused by flocculation introduced by the electrolyte.

2.2.4.2 Features of ELD

Basically an electrochemical synthesis is achieved by passing the electric current between two electrodes separated by some electrolyte, as stated in the above chapter. Such synthesis occurs near the electrode, actually at the electrode-electrolyte interface. Typical features of electrochemical synthesis are listed as follows:

(1)Synthesis occurs very close to the electrode within the electric double layer, which is characterized by the high potential gradient.

(2)Product is deposited on the electrode (either cathode or anode) in the form of a film or coating. Besides, electrochemical synthesis can work on almost all conductive substrates of any shape.

(3)Low reaction temperature is another advantage of such synthesis, but also has some limit. Usually the technique is limited by the boiling point of the specific electrolyte.

(4)Deposition process is easy to control, by simply changing the current or voltage.

(5)Composition of coating can be conveniently changed by varying the bath materials.

(6)Cost of massive production of films is low. [56]

In typical electrosynthesis, reactant is dissolved in the electrolyte and subsequently deposited on the electrode surface as a solid product, usually in the form of film or coating. Two extremely important parameters determine the process of reactions: deposition current (density) and cell potential. Two methods of electrochemical deposition were developed accordingly: constant-current density and constant-voltage [56].

2.2.4.3 Important parameters

In a typical electrochemical synthesis, there are several significant and necessary parameters that are listed below.

(1)Electrodes

(2)Electrolyte

(3)Setting of experimental parameters, including pH value, concentration, and composition of the electrolyte solution

(4)Mode of electrosynthesis [56]

A usual problem caused by heavy precipitation over the intermetallics is cracking [15]. In contrast, ELD enables rigid control of processes of film formation and thus all kinds of variants, including thickness, uniformity, and deposition rate. The uniformity of films produced by ELD basically results from the insulating properties of deposit and the electric field dependence of the deposition rate.

Cationic surfactants and polyelectrolytes act as electrolytes when compressing the double layer of ceramic particles, which results in particle flocculation and thus increasing the deposition process efficiency [15]. The generation rate of OH^- is extremely important to the deposition process. When this generation rate is faster than the consumption rate of OH^- by hydrolysis reactions at the electrode, a fraction of the OH^- ions generated at the cathode will be transported away by the electric current and diffusion. In this case, the high pH boundary moves away from the electrode surface, thus resulting in lower adhesion of the deposits [15].

2.2.4.4 Co-deposition

Recently co-deposition of cationic species has been studied intensively as a new method, since it can be applied widely in industrial production. Some species can not be deposited alone from aqueous solutions, though they can be co-deposited with other cationic species. One example is demonstrated below.

$$10Ca^{2+}+6PO_4^{3-}+2OH^{-}\rightarrow Ca_{10}(PO_4)_6(OH)_2 \qquad \textbf{(2-21)}$$

Element P can not be deposited in aqueous solutions alone due to the solubility. Therefore co-deposition of P with Ca^{2+} ion is applied. [4]

Further, co-deposition includes several other types of materials, such as metal-polymer composites.

2.2.5 Electrophoretic deposition

2.2.5.1 Mechanism of EPD

There are numerous mechanisms of electrophoretic deposition processes [57-74]. One hypothesis is that charged particles undergo reactions at the electrode, which neutralize them. It was suggested that ceramic particles act as charge carriers and promote the circulation of electric current in the suspension. However, deposition was observed on a porous diaphragm placed between the electrodes [15,75]. According to Hamaker and Verwey, the formation of a deposit by EPD is similar to the process of sediment which is caused by gravitation. It was assumed that an applied electric field exerts sufficient force to overcome repulsion among particles [76]. The strength (*E*) required was found to follow the equation below [15,76]:

$$E=2F/3\varepsilon\xi a \qquad \textbf{(2-22)}$$

Another electrochemical mechanism of deposit formation proposed by Koelmans and Overbeek assumes that deposition is caused by flocculation, introduced by electrolyte, which is formed by the electrode reaction below [77]. The kinetics in this reaction is expressed in equation (2-24)

$$2CH_3OH + 2e^- \rightarrow 2OH^- + C_2H_6 \qquad \textbf{(2-23)}$$

$$t^* = qV^{-2}\sigma^{-2} \qquad \textbf{(2-24)}$$

where t* is the critical time in the flocculation theory, which is the time required to build up a critical electrolyte concentration. *q* is a coefficient, *V* is the voltage applied, and σ is the specific conductance of the suspension.

An electrocoagulatory mechanism of deposition is mainly based on the polarization attraction of particles to the electrode, which is proposed by Sarkar and Nicholson [78]. A mechanism based on double-layer distortion under an electric field was developed by them. In this model, the double layer becomes thinner ahead of particles, which promotes particle coagulation. However, further investigation signified errors in this mechanism. Later De and Nicholson proposed another mechanism based on a local pH increase near the cathode [79].

2.2.5.2 Influence of electrolyte in EPD

In some experiments, EPD of ceramic particles was performed in the presence of electrolytes and polyelectrolytes. These additives are usually adsorbed onto the particles to create positive charges and stabilize the suspensions [15]. These additives are important for the deposition of uniform and adherent coating. EPD of ceramic particles could be associated with electrolytic deposition of hydroxides or alkoxides, which actually forms an adhesive matrix. The adhesive materials promote particle coagulation and bind the particles to the substrate. In this case, the binder materials enhance the effect of the Van der Waals' force.

The water content and electrolyte concentration in the bath are extremely significant to the deposition process. It was supposed that reduction of water generates OH- ions, thus leading to a pH increase near the cathode substrate. It should be noted that electrode blocking by the deposited particles is also able to result in an additional pH increase in the vicinity of the cathode [15]. When the water content of suspension is low (<1%), the alkoxide is formed, which will be replaced with the hydroxide at higher water concentrations [15]. Excess water is detrimental because it results hydrogen evolution and high bath conductivity.

2.2.5.3 Different methods for deposition of composites

2.2.5.3.1 Method based on ELD of ceramic particles and EPD of polyelectrolytes

It has already been demonstrated that cathodic electrodeposition of oxides or hydroxides together with charged polymers can be achieved, which is relevant to industrial production. Typical polymers used include poly(diallyldimethylammonium chloride) (PDDA) and polyethyleneimine (PEI) [15]. Fig.2-13 is the structure sketch of these two polymers. The principle of this method is to apply EPD to polymers and

ELD to ceramic materials, respectively. Deposition is basically performed from solutions of metal salts containing polymers.

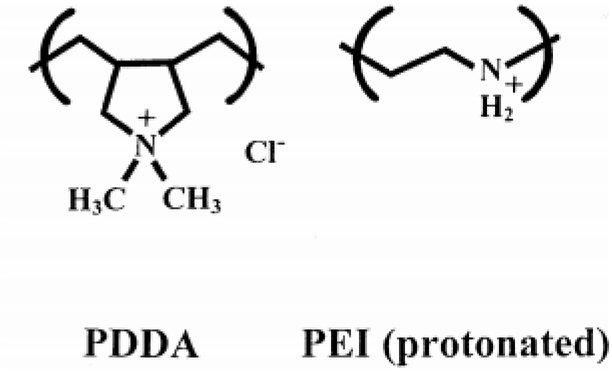

Fig. 2-13 Schematic structures of PDDA and PEI

For example, PDDA is a cationic polyelectrolyte, whose electrophoretic mobility can be calculated from the equations above. PDDA is a strong polyelectrolyte, which maintains a positive charge in a wide pH range. EPD of PDDA films can not be achieved from aqueous PDDA solutions. Electrophoresis is related to the motion of charged particles or polymer macromolecules towards the electrode. However, electrostatic repulsion of charged PDDA molecules prevents deposit formation. Depositions of Zr, Ce, Gd, Y, Fe, Ni, Cu, Co, La oxides and hydroxides from their chloride or nitrate salt solution with PDDA were all successful.

As illustrated in the chapters above, cathodic reactions cause a pH increase near the cathode, which results in the negative charge of colloidal particles. Formation of coating was thus achieved via heterocoagulation of oppositely charged PDDA and colloidal particles of oxides or hydroxides (formed near the cathode). However, the attraction of polyelectrolytes and colloidal particles can be either electrostatic or non-electrostatic. This complicated interaction is influenced by the pH value, ionic strength, and electric field.

The amount of organic phase in the coating deposited was evaluated from thermogravimetric analysis [15]. It was found that deposit composition could be controlled by varying PDDA concentration in solutions, which is very significant for film formation. Fig.2-14 illustrates that generally higher concentration of deposited material within some range leads to more deposit, although there is probably some limit. In contrast, Fig.2-15 shows that deposit amount decreases sharply after a peak, which is affected by concentration of PDDA.

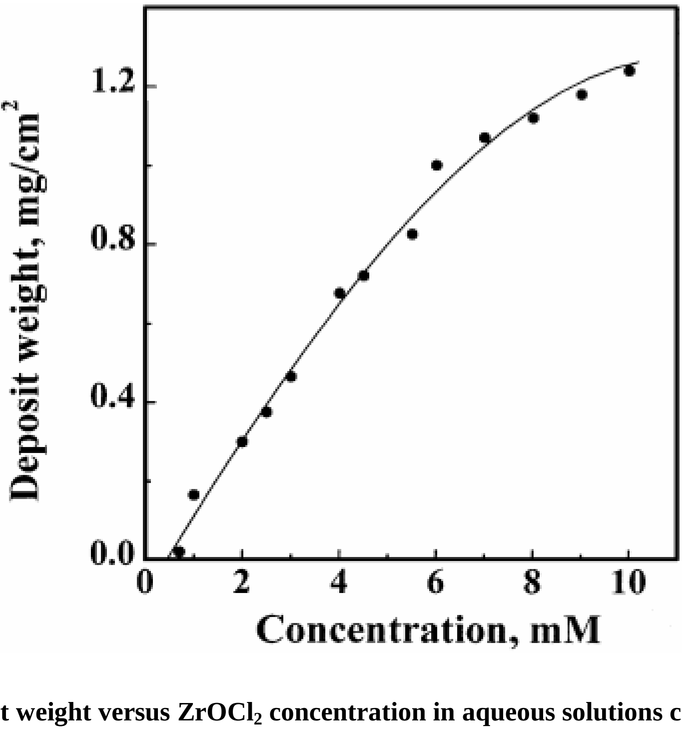

Fig. 2-14 Deposit weight versus $ZrOCl_2$ concentration in aqueous solutions containing $1gL^{-1}$ PDDA, current density 10 $mAcm^{-2}$, deposition time 6 minutes

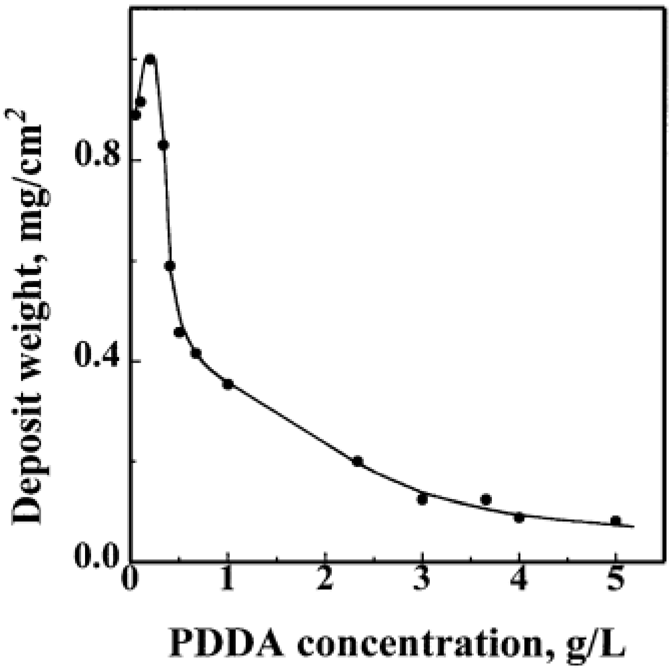

Fig. 2-15 Deposit weight versus PDDA concentration in aqueous 0.005 M $ZrOCl_2$ solutions, current density 5 mAcm^{-2}, deposition time 10 minutes

The feasibility of electrochemical intercalation of charged polymers into electrolytic deposits is of significant importance for the further development of electrolytic deposition of ceramic materials. The critical thickness of ELD deposits achievable without crack formation could be increased up to 1-2 μm using PDDA with inherent binding properties. Small additives of PDDA act as a binder, preventing cracking and increasing adhesion of the deposit [15].

2.2.5.3.2 Method based on EPD of ceramic particles and polyelectrolytes

Another method is based on the use of EPD of both ceramic particles and polyelectrolytes [15]. In this case, ceramic particles are possible to be either positively or negatively charged, depending on the pH value.

The pH of the suspension should be lower than the isoelectric point of the oxides. The particles are positively charged and driven by an electric field towards the cathode. However, a charge reversal will take place at high pH near the cathode, thus negatively charged oxide particles compensate the positive charges of PDDA. Deposit formation was achieved via heterocoagulation of PDDA and oxide particles. Fig.2-16 shows that higher concentration of ceramic materials in this EPD method generally leads to higher deposition yield. Fig.2-17 shows the influence of PDDA polymer in this method.

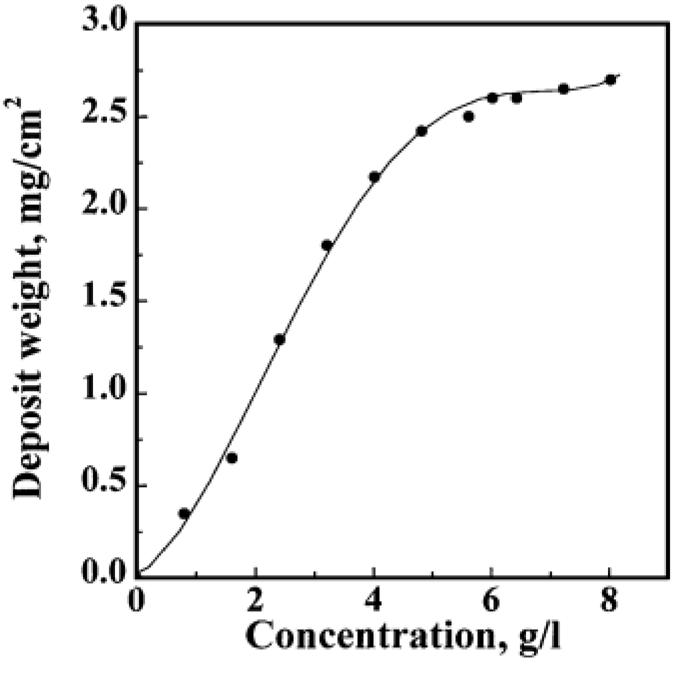

Fig. 2-16 Deposit weight of organoceramic deposits versus concentration of ceria particles in aqueous suspensions, containing 1 gL^{-1} PDDA; current density 1 mAcm^{-2}, deposition time 10 minutes

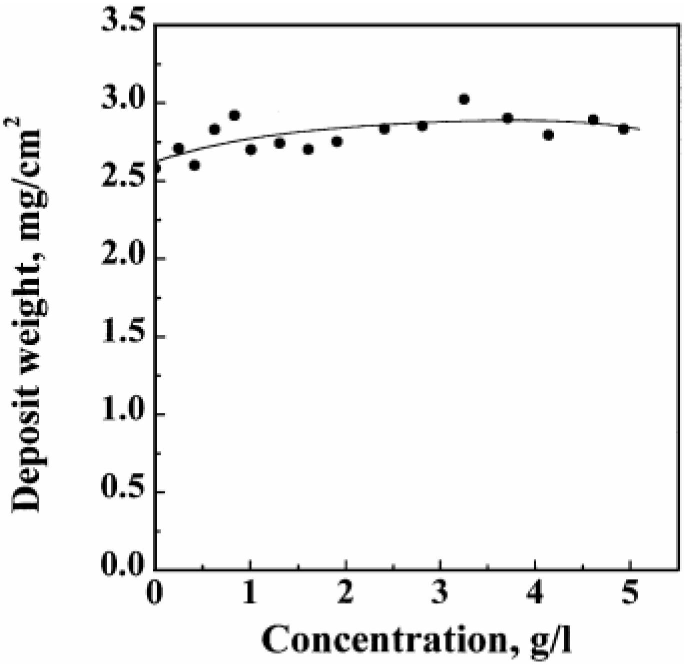

Fig. 2-17 Deposit weight versus concentration of PDDA in aqueous 8 gL^{-1} ceria suspensions; current density 1 mAcm^{-2}, deposition time 10 minutes

Influences of concentration of ceramic materials and polyelectrolyte are shown in the above two diagrams. In contrast to the other method based on ELD of ceramic materials and EPD of PDDA, no significant variation in the deposit weight versus PDDA concentration was observed in this method. The explanation is that PDDA particles accumulate near the electrode and so prevent electrosynthesis of colloidal particles [15].

3 Objectives

The objective of this work was to develop advanced coatings for corrosion protection of metals and alloys. This work involved the investigation of coatings prepared by PVD and electrochemical methods and development of electrochemical deposition methods:

-development of methods for the electrodeposition of advanced polymers

-development of advanced dispersing and charging agents for EPD of ceramic particles

-investigation of deposition mechanisms and deposition kinetics

-development of combined electrochemical methods based on ELD and EPD for the fabrication of composite polymer-ceramic coatings

-deposition of monolayer and laminated composite coatings, investigation of microstructure and composition

-investigation of corrosion protection of polymer and composite coatings deposited by electrochemical methods

-investigation of corrosion protection of composite coatings deposited by PVD method and electroplating of Ni on advanced alloy materials

-data analysis and development of practical recommendations for industrial applications.

4 Experimental Procedures

4.1 Materials and devices

CeO_2 (nano powders), $CeCl_3 \cdot 7H_2O$ and polymer materials of poly(2-vinylpyridine) and poly(4-vinylpyridine-*co*-butyl methacrylate) were used. Benzoic acid and trans-cinnamic acid were used as additives. All chemicals were produced by Aldrich Company. Power supply is the main tool to deposit films from suspensions or solutions, either in the mode of constant current density or constant voltage. Potentiostat was used for testing of electrochemical properties and corrosion protection properties of the films. N_2 was used to remove air from the electrochemical cells. Stirring device and ultrasonic tank were used to disperse powders and dissolve materials before deposition.

4.2 Preparation of suspension and solutions

4.2.1 Basic procedures before deposition

Basic substrate for deposition was stainless steel, cut in the size of 5cm×2.5cm. The volume of the deposition cell was 400 mL.

Subsequent to putting materials into solvents, it is necessary to stir the system and then perform ultrasonic treatment. These two steps were employed to disperse powders or facilitate dissolving, thus forming a stable system for deposition.

4.2.2 EPD method of CeO_2

Typical EPD processes are based on stable suspension systems. Two pieces of Pt foil were used as counterelectrodes. Stainless steel substrate is connected to another electrode. Fig.4-1 shows the typical cell for cathodic deposition. If materials are deposited on the anode, the substrate should be connected to the anode of the power supply.

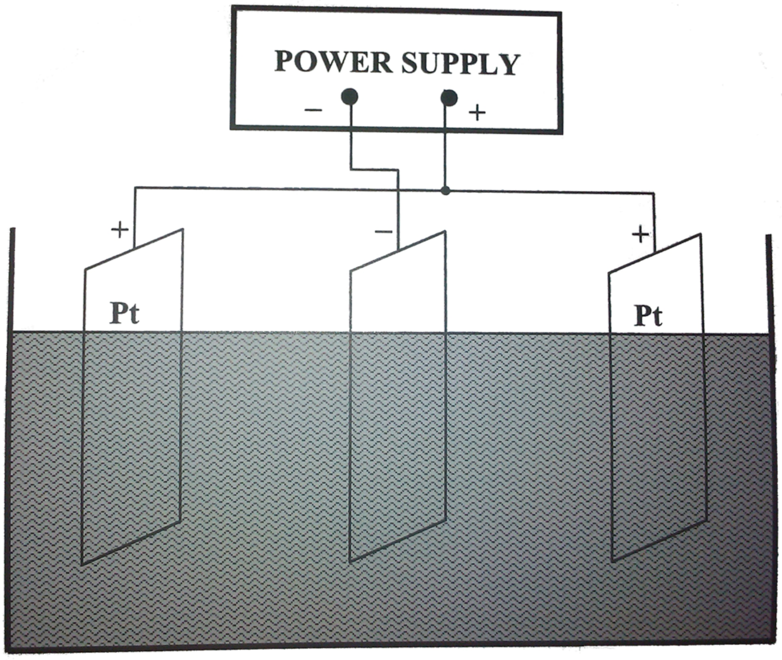

Fig. 4-1 Schematic of cathodic deposition

H_2O and ethanol are most commonly used solvents. Three types of solvents were applied in experiments, 100% H_2O, 100% ethanol, and a mixture of 80% ethanol and 20% H_2O. This ratio in the mixture was proved to be near the optimum based on a series of trials.

275 mL of mixed solution (80% ethanol and 20% H_2O) in a 400 mL beaker was used

as a solvent. The concentration of CeO_2 powders was varied in the range of 3-10 gL^{-1}. Polymers were protonated by acetic acid, dissolved and then added to the suspension. The polymers were used as binders for CeO_2 deposition in order to prevent cracks. Since polymers can not be dissolved in H_2O, acetic acid was used to protonate them. A solution of polymers was added to the suspension of CeO_2 in the concentration of $1gL^{-1}$.

After the suspension stabilized, Pt foil and stainless steel substrate were dipped into the beaker and connected to the power supply. Two modes of deposition were used: constant current density or constant voltage. Current density was controlled in the range of 1-2 $mAcm^{-2}$. Cell voltage was varied in the range from 5 V to 60 V. Duration time of deposition was varied in the range of 1 to 10 minutes

4.2.3 ELD method of CeO_2

ELD processes are based on salt solutions, instead of suspensions used in EPD. Settings of the power supply, basic placement of Pt foils, and pre-deposition treatment are similar to those in the EPD process. An obvious difference in ELD is that usually only constant current density mode can be used. Another difference is the concentration of material. Since $CeCl_3$ was dissolved in H_2O forming a solution, the concentration of $CeCl_3$ was in the range of 1-5 mM. Constant current density was controlled in the range of 1-2 $mAcm^{-2}$. Duration time for deposition was 1 to 10 minutes. PVP solution was added to $CeCl_3$ solution after protonation by acetic acid.

4.2.4 Deposition of other powders

Other materials were also tried in experiments, including titanium dioxide, clay, and CNT (carbon nanotubes). EPD was the only possible way to deposit these powders, since they could not be dissolved in solutions. Concentrations of powders varied from 0.3 g L^{-1} to 10 gL^{-1}. Usually additives such as benzoic acid or gallic acid are important to stabilize suspension systems. Deposition voltage was varied in a wide range of 10-70 V.

4.4 Methods of characterization

4.4.1 Deposition yield and rate

Investigation of deposition mass is an easy way to estimate the deposition efficiency. Masses of samples were measured both before deposition and after deposition when deposits were completely dried. The difference between these two mass values was calculated as deposit mass over a constant standard area (determined by the standard sizes of sample and beaker). The Mettler Toledo AX105 Delta Range analysis balance used has an accuracy of 0.01 mg.

In-situ measurement of deposit mass during deposition process was achieved by use of a nanobalance. In nanobalance measurement, only dilute solution can be used. Concentration of $CeCl_3$ and polymers was 0.05-0.1 gL^{-1}, which was sufficient to obtain deposit on the quartz electrode surface. As more material is deposited onto quartz surface, the vibration frequency of quartz deviated from its standard frequency. Therefore, the value of frequency deviation can be related to the mass of deposit, which is the basic principle in a quartz crystal microbalance (QCM) test.

$$-\triangle F = \frac{2F_0^2}{A\sqrt{r_q m_q}} \times \triangle m \qquad \textbf{(4-1)}$$

where ΔF is the frequency decrease of the QCM, F_0 is the parent frequency of QCM(9MHz), A is the area of the gold electrode (0.2 cm^2), ρ_q is the density of the quartz (2.65 g cm^{-3}) and μ_q is the shear modulus of the quartz (2.95×10^{11}dynecm^{-2}).

4.4.2 Electrochemical tests

The Potentiotat is a standard tool to test a coating’s electrochemical properties. EIS (electrochemical impedance spectroscopy) has been widely applied in the study of corrosion systems. It is commonly used to characterize corrosion and other electrochemical properties. EIS provides measurement of impedance of an electrochemical system as a function of the frequency of an applied electric field. The information on conductance, dielectric constant, and static properties of interfaces in the system can be reflected in EIS testing. Another significant feature of EIS is that the investigated system will not be disturbed much since EIS uses signals of very small amplitude. Typical signal amplitude is an AC potential from 5 to 10 mV applied to an electrochemical cell, with a range of frequency from 0.001 Hz to 100 kHz.

The impedance value is expressed in the form of complex numbers. The real part represents the resistance component in the system, while the imaginary part represents the capacitance component. The final result of EIS is usually presented in the form of a Nyquist plot (imaginary part versus real part) and Bode plots (absolute value of impedance and phase shift versus frequency).

Tafel testing is another important way to study corrosion systems. Tafel plots are able to reflect the potential and current density when corrosion is occurring. These values are significant when comparing materials corrosion properties. It is clearly shown on the Tafel plot which material prevents corrosion better and how the corrosion proceeds as potential is increasing. Final Tafel plot is in the form of potential versus current (logarithmic), from which corrosion rate can be calculated.

4.4.3 Characterization methods

4.4.3.1 Thermogravimetric and differential thermal analysis

TGA (thermogravimetric analysis) is useful method to determine some material thermal properties, including thermal stability and composition. The specimen experiences a mass loss in TGA, which is described by a plot showing a fraction of remaining mass. In addition to mass loss, the temperature difference between specimen and the reference is also recorded, which is DTA (differential thermal analysis). DTA is significant to monitor energy change during the heating process, either released or absorbed in chemical reactions or phase transformations.

After samples were completely dried, deposited materials were scraped carefully from the surface. These powders were tested in the thermoanalyzer (Netzsch STA-409).

Regular parameters in testing were temperature range of 25-1200℃ with a heating rate of 5℃/min.

4.4.3.2 X-ray diffraction analysis

XRD (X-ray diffractometry) is a frequently used method to probe the specimen’s phase content. Besides, XRD is significant when measuring lattice parameters, internal stress, crystal size and orientation, etc.

The phase content of deposits was investigated by a diffractometer (Nicolet I2), with parameters of monochromatized Cu K_α radiation at a scanning rate of 0.5°/min. After drying, the deposited materials were scraped from surface. XRD is important when comparing deposits via ELD and EPD respectively. Deposits obtained via two different processes had the same phase content.

4.4.3.3 Scanning electron microscopy

SEM (scanning electron microscopy) is the most commonly used tool to study morphology. A JEOL JSM-7000F scanning electron microscope was used. EDS is included on this SEM, which is used to study a specimen’s chemical composition. SEM is necessary to study the coating’s cross section. Different deposited layers and morphology characteristics such as porosity can be clearly shown via SEM.

5 Results and Discussion

5.1 Composite films based on polymer PVP

5.1.1 Electrodeposition of PVP

5.1.1.1 Mechanism and deposition method

Polymer was introduced to the deposition system to solve the problem of cracking. One obvious advantage of electrodeposition is that co-deposition and composite fabrication are enabled, which means other materials such as some polymer can be co-deposited with CeO_2. Selection of a specific polymer is significant, because both its mechanical properties and corrosion resistance should be considered. Poly(2-vinylpyridine) (PVP) was selected as the co-deposited polymer due to its advanced chemical properties. Fig.5-1 shows the structure of this polymer.

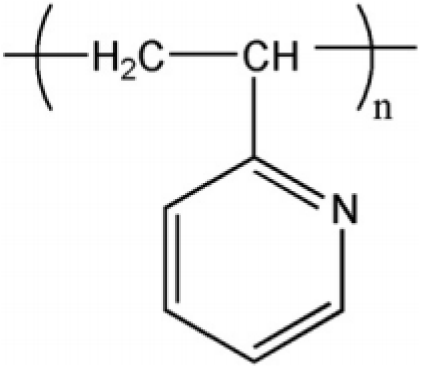

Fig. 5-1 Chemical structure of PVP

PVP is insoluble in water and electrically neutral. The nitrogen atoms possessed in its pyridine rings are able to be protonated in the presence of some acid, thus forming a soluble cationic polyelectrolyte in solution.

$$\mathrm{PVP} + n\mathrm{H}^+ \rightarrow \mathrm{PVP}\,(n\mathrm{H}^+) \qquad \textbf{(5-1)}$$

PVP ($n\mathrm{H}^+$) is converted back to precipitation of PVP at the cathode electrode during the deposition process. Electric field leads to the electrophoretic motion of the charged PVP ($n\mathrm{H}^+$) macromolecules towards the cathode. The pH value at cathode surface increases during the deposition, which promotes the reaction of PVP precipitation shown below.

$$\mathrm{PVP}\,(n\mathrm{H}^+) + n\mathrm{OH}^- \rightarrow \mathrm{PVP} + n\mathrm{H_2O} \qquad \textbf{(5-2)}$$

5.1.1.2 Deposition rate

To investigate details of PVP co-deposition, QCM method was used to record deposit mass versus deposition time. Fig.5-2 shows continuous increase in the deposit mass with increasing deposition time and indicated the possibility of the variation of film mass. The deposition rate decreased with increasing deposition time due to the formation of an insulating deposit and a decrease in electric field in the bulk of the solution.

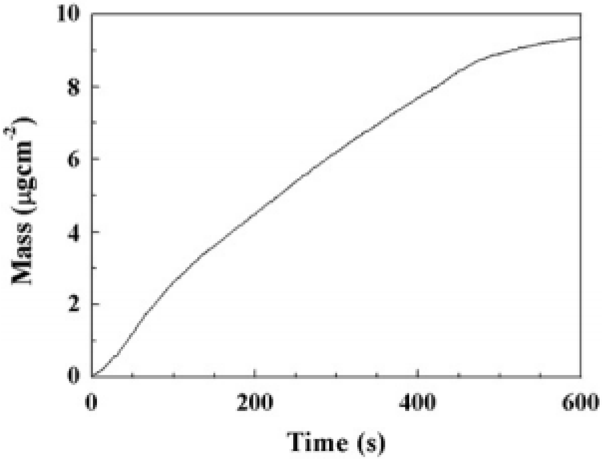

Fig. 5-2 Deposit mass versus deposition time in the deposition of PVP from 0.1 gL^{-1} PVP solution (voltage: 5V)

5.1.1.3 SEM characterization

Fig.5-3 (a) is a typical cross section image of PVP film, whose thickness can be varied from 0.1 to 3 μm depending on the concentration of PVP (0.1-1 gL^{-1}) , deposition time and voltage. A typical deposition voltage ranged from 5 V to 20 V.

Fig5-3 (b) demonstrates that such crack-free PVP films are dense and constructed of spherical PVP particles. This morphology is related to the formation mechanism of PVP film. It was assumed that precipitated hydrophobic PVP macromolecules were assembled into spherical colloidal particles, considering the precipitation process was essentially coagulation. According to the image in Fig.5-3 (b), the size of PVP molecules in the film ranges from 100 to 300 nm.

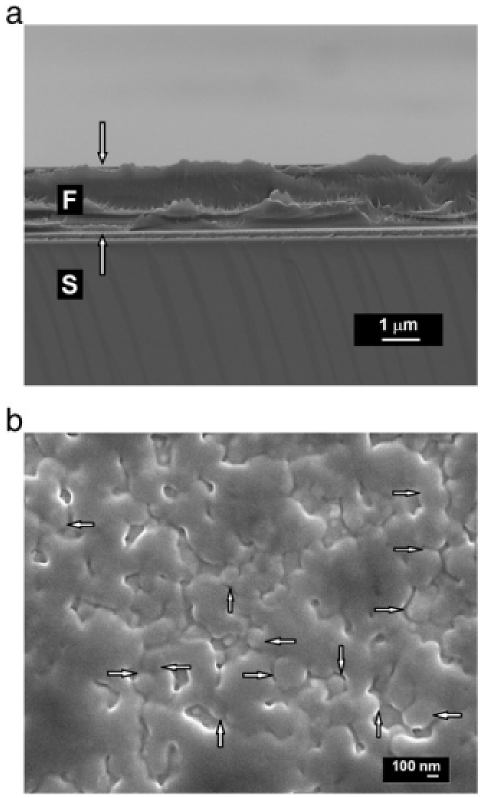

Fig. 5-3 SEM images of (a) cross section and (b) surface of the PVP film deposited from the 1 gL^{-1} PVP solution (voltage: 20 V; deposition time: 5 min)

5.1.1.4 Thermal analysis

Fig.5-4 demonstrates the thermal analysis plots, which reflects mass loss and energy change under heating. Obviously in the TGA plot there are several stages in the mass loss process of PVP film with the temperature increasing. The decrease in mass was attributed to burning out of this polymer sample. It was found that PVP was burnt out completely at some temperature close to 600 °C. Corresponding DTA plot showed a broad exotherm in the range of 300–600 °C, which exactly corresponds to the main stage of mass decrease in TGA plot.

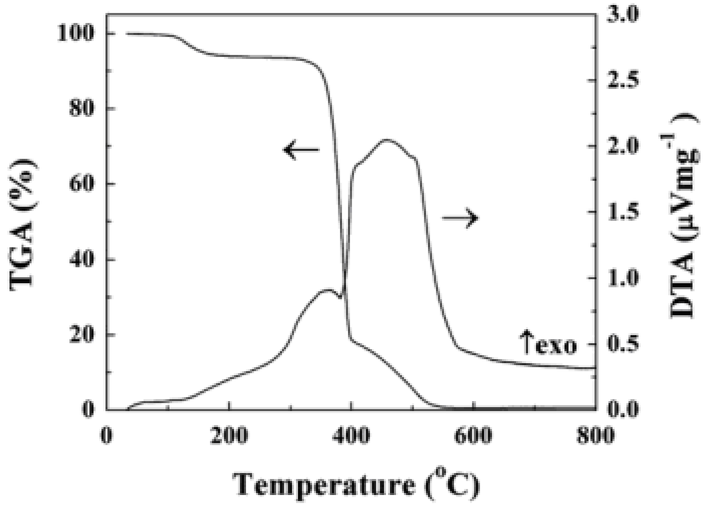

Fig. 5-4 TGA/DTA data for PVP deposit, obtained from 1 gL^{-1} PVP solution

5.1.2 ELD of CeO_2 coatings

5.1.2.1 Mechanism

Electrolytic deposition (ELD) of CeO_2 coating is essentially a galvanostatic method, which is based on the use of $CeCl_3$ solution. The most important step in this process is the electrosynthesis of colloidal CeO_2 particles and subsequent coagulation at the cathode electrode. The generation of OH^- ions in electrode reactions leads to a pH increase at the cathode:

$$2H_2O + 2e^- \rightarrow H_2 + 2OH^- \qquad \textbf{(5-3)}$$

$$O_2 + 2H_2O + 4e^- \rightarrow 4OH^- \qquad \textbf{(5-4)}$$

$Ce(OH)_2^{2+}$ was proved to exist as an intermediate ion at the cathode surface, whose formation is demonstrated below.[80]

$$4Ce^{3+} + O_2 + 4OH^{-} + 2H_2O \rightarrow 4Ce(OH)_2^{2+} \qquad \textbf{(5-5)}$$

Next step is the precipitation of CeO_2 particles, which is essentially coagulation and coating formation as shown below.

$$Ce(OH)_2^{2+} + 2OH^{-} \rightarrow CeO_2 + 2H_2O \qquad \textbf{(5-6)}$$

5.1.2.2 Deposition rate

To study deposition rate, QCM balance method was used to measure the mass of deposited material during the electrolytic deposition processing. In QCM testing, only dilute solution can be used. Fig.5-5 shows deposit mass versus deposition time in an electrolytic process. Constant current density mode was used in this measurement, which enables rigid control of deposition rate and charge passed.

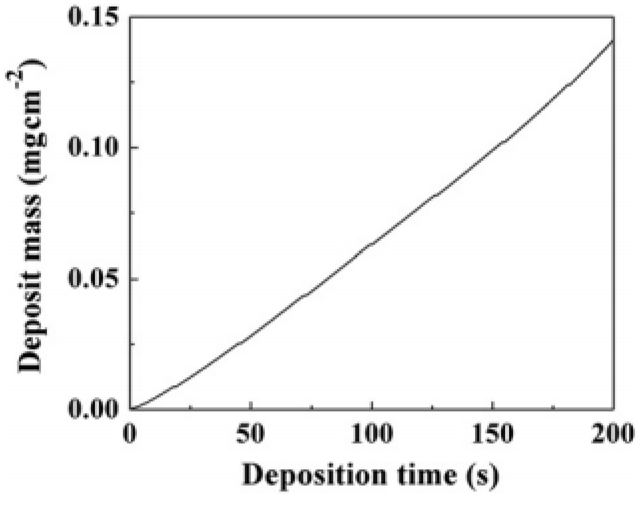

Fig. 5-5 Deposit mass of CeO_2 versus deposition time, from the 5 mM $CeCl_3$ solution at a current density of 1 mAcm^{-2}

5.1.2.3 SEM characterization

CeO_2 coatings of stainless steel substrates via ELD method was examined under SEM. A typical SEM image is shown in Fig.5-6. Obvious cracking was observed in the SEM image at low magnification. Such cracks are mainly due to the shrinkage of deposit during drying. When the magnification was higher, a more detailed porous structure was observed, which is formed by flaky particles. According to the SEM data, the size of pores ranged from 10 to 300 nm. Definitely, such film with cracks and porous structure cannot to be used for efficient corrosion prevention.

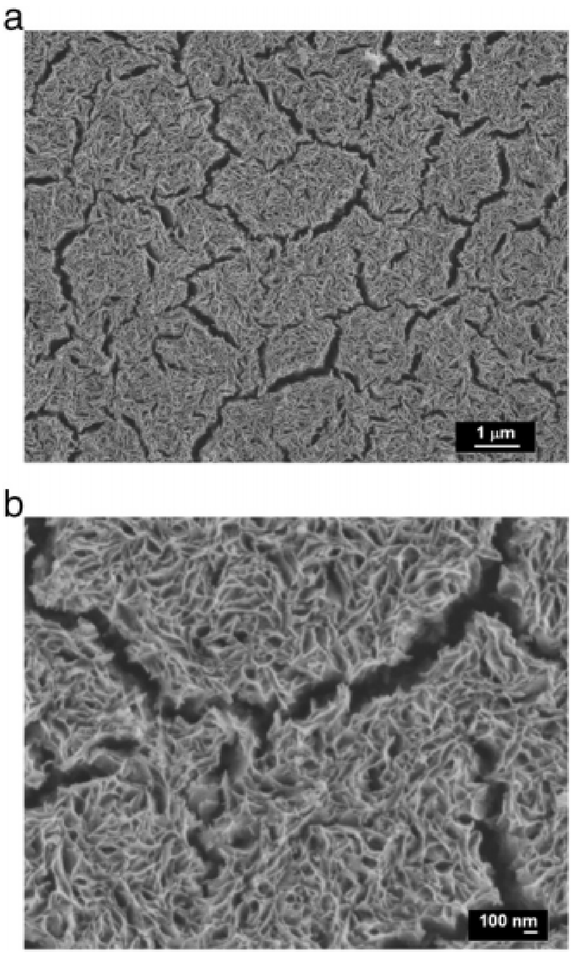

Fig. 5-6 SEM images at different magnifications of a CeO_2 film deposited via ELD from a 5 mM $CeCl_3$ solution at a current density of 1 $mAcm^{-2}$

5.1.3 Co-deposition of CeO_2 and PVP using ELD of CeO_2

5.1.3.1 Mechanism

The results presented above indicated that the ELD of CeO_2 and electrodeposition of PVP were performed cathodically in the same way. Both electrochemical strategies were based on the surface pH increase (based on OH^- generation) and charge neutralization of the cationic species at the electrode surface. Therefore, it was suggested that the electrochemical strategies can be combined for the fabrication of PVP-CeO_2 composite films, using ELD of CeO_2.

Pure CeO_2 films deposited via ELD showed unavoidable cracks. Considering that polymer can be used to bind deposits, it is promising to obtain composite films by co-deposition of PVP and CeO_2. It was expected that electrochemical properties can be retained and cracks can be avoided.

5.1.3.2 SEM characterization

To solve the cracking problem stated above, PVP was co-deposited with CeO_2 using ELD process. PVP works mainly as a binder, which prevents cracking. This co-deposition process was done in the mode of constant current density as usual ELD processes. Fig.5-7 is the SEM image of film deposited from $CeCl_3$ solution containing PVP. Basic morphology of this composite film was constructed of spherical particles in a continuous matrix. It was assumed that these spherical particles are attributed to self-assembly of PVP molecules. According to other literature data on composite materials containing PVP and CeO_2 phases, similar formation of spherical PVP particles was observed.[81, 82]

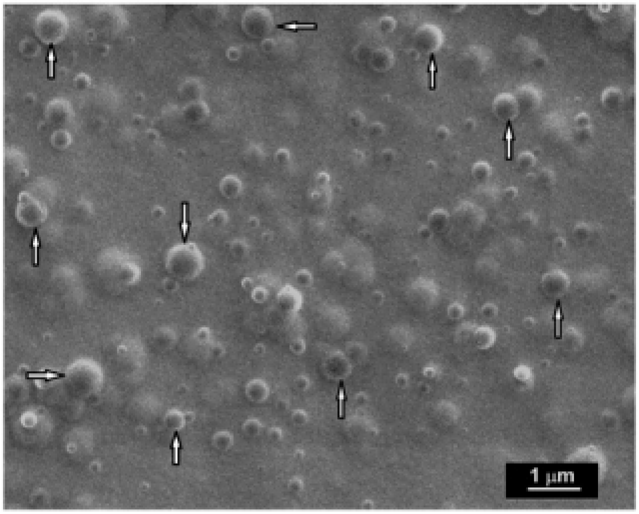

Fig. 5-7 SEM image of film deposited from a solution containing 1 gL^{-1} PVP and 5mM $CeCl_3$

5.1.3.3 Thermal analysis

Fig.5-8 shows the TGA/DTA plots of the deposited sample prepared by the combined method, based on ELD of CeO_2 and EPD of PVP. It is clear that sample mass decreased in the range of 20–600°C and then remained at some constant value even at higher temperature such as 800°C. The total mass loss at 800 °C was 18.9%, which indicated that film contained 81.1% CeO_2.

The temperature range for the exotherm in the DTA plot corresponds to the main mass decrease in TGA plot. This stage is the process of burning out of PVP polymer. It should be noted that the real kinetics of polymer’s thermal degradation in composite materials can be affected by interactions of organic and inorganic components. According to the literature, coordination of nitrogen atoms of PVP with Ce(Ⅳ) was observed when the CeO_2 phase precipitated from $CeCl_3$ solution in the presence of PVP.[83, 84]

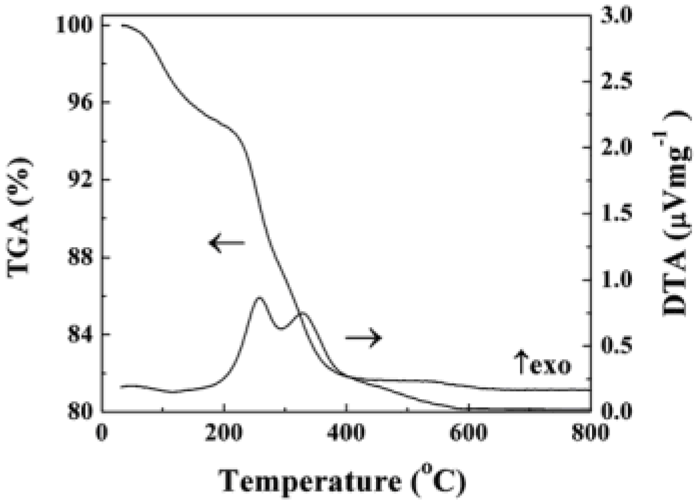

Fig. 5-8 TGA/DTA data for a deposit prepared from solution containing 1 gL^{-1} PVP and 5 mM $CeCl_3$

5.1.3.4 XRD

XRD data in Fig.5-9 is in good agreement with the results of TGA/DTA tests. The XRD pattern of the composite film prepared via codeposition shows clear peaks of CeO_2. These peaks are relatively broad, which indicates a very small size of particles formed in the polymer matrix.

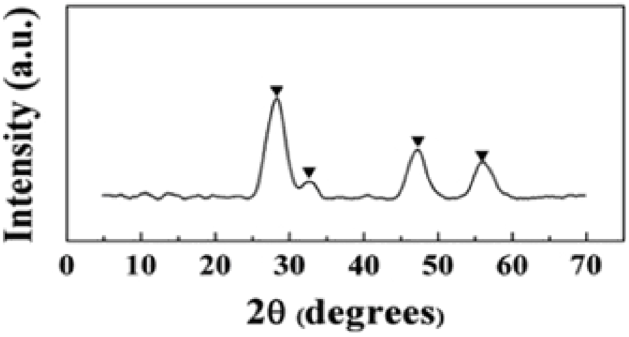

Fig. 5-9 X -ray diffraction patterns for composite deposit prepared from the solution containing 1 gL^{-1} PVP and 5 mM $CeCl_3$ (▼- peaks corresponding to JCPDS file 34–394 of CeO2)

5.1.3.5 Electrochemical tests

In Fig.5-10 Tafel plots were compared. It is obvious that uncoated stainless steel has the highest corrosion current and lowest corrosion potential. Higher corrosion current signifies a higher rate of corrosion and lower corrosion potential signifies easier occurrence of corrosion. PVP itself decreased the corrosion current obviously, which is definitely good for corrosion prevention. The PVP-CeO_2 composite film further improved the corrosion potential to a much higher value, which indicates itself as a promising type of corrosion prevention coating.

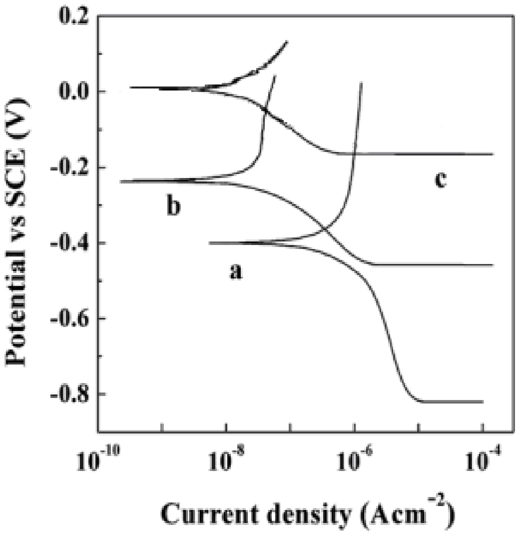

Fig. 5-10 Tafel plots for (a) uncoated and (b,c) coated stainless steel substrate: (b) coating deposited from 1 gL^{-1} PVP solution (c) coating deposited from solution containing 1 gL^{-1} PVP and 5 mM $CeCl_3$

5.1.4 EPD of CeO_2 coating

5.1.4.1 Mechanism

In contrast to ELD processes, electrosynthesis does not occur in electrophoretic deposition (EPD). In the EPD process, deposition is achieved from suspensions of oxide particles under an electric field. Particles are driven by the electric field towards the electrode and thus exert a pressure onto the deposited layer. Particles must be charged and dispersed well in the suspension. Therefore, appropriate dispersion agents should be used.

A certain value of electric field is necessary in order to overcome interparticle interactions and to allow particles to bond to the substrate. Therefore, the EPD of CeO_2 was performed at constant voltage conditions.

5.1.4.2 Dispersion and kinetics using benzoic acid

It is extremely important to disperse CeO_2 particles to form a stable suspension for deposition. Benzoic acid was used to disperse and charge CeO_2 nanoparticles. Electric field provided electrophoretic motion of charged CeO_2 nanoparticles and their deposition on the substrates.

Fig.5-11 shows the effect of benzoic acid concentration on the EPD efficiency. There is an obvious increase of deposit mass in the range of 0~0.2 gL^{-1} of benzoic acid. It is suggested that the dissociation of benzoic acid and adsorption of H^+ onto CeO_2 nanoparticle surfaces led to the electrostatic stabilization of the nanoparticles in the suspensions. The charged particles formed stable suspensions. The applied electric field provided their electrophoretic motion toward the substrate and deposition.

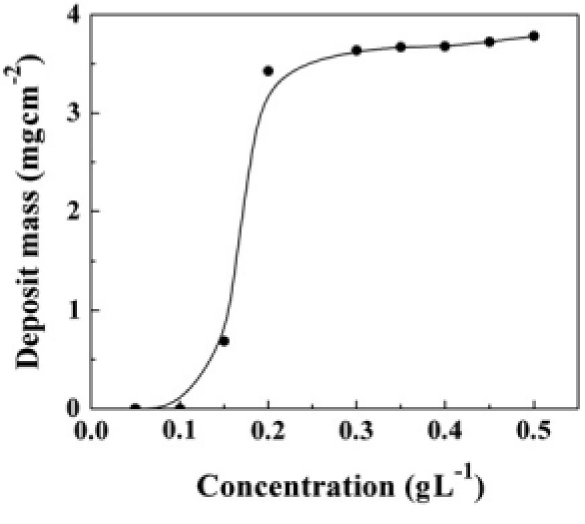

Fig. 5-11 Deposit mass versus benzoic acid concentration in the 20 gL^{-1} CeO_2 suspension

Fig.5-12 demonstrates that deposit mass increased with increasing deposition time following a nearly linear dependence. Therefore, the amount of deposited material can be varied and controlled.

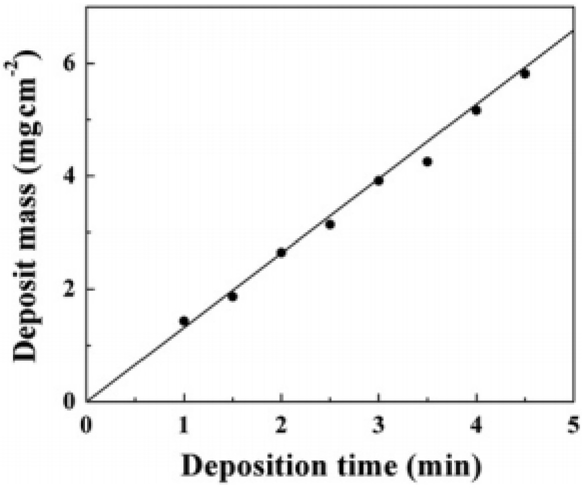

Fig. 5-12 Deposit mass versus deposition time in EPD from 20 gL^{-1} CeO_2 suspension containing 0.5 gL^{-1} benzoic acid

5.1.4.3 Dispersion and kinetics using trans-cinnamic acid

Another material used was trans-cinnamic acid, considering the possibility of EPD of CeO_2 in ethanol solvent. The suspensions of CeO_2 in ethanol or mixed ethanol–water (20% water) solvents were unstable and showed rapid sedimentation immediately after ultrasonic agitation. No EPD was observed from such suspensions. The addition of trans-cinnamic acid allowed the formation of stable suspensions. The 10 gL^{-1} CeO_2 suspensions containing 0.5-1.0 gL^{-1} trans-cinnamic acid were stable for more than 3 days (Fig.5-13).

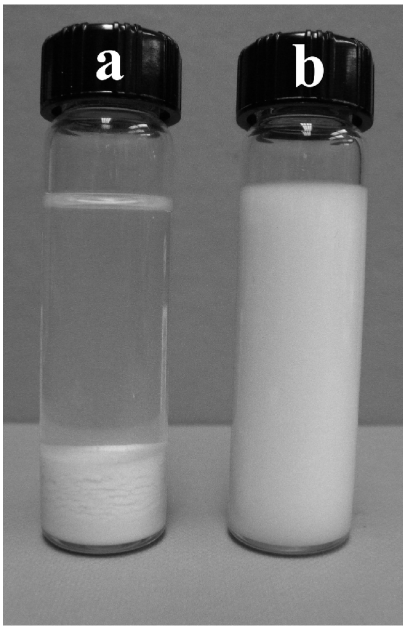

Fig. 5-13 10 gL^{-1} CeO_2 suspensions in a mixed ethanol–water (20% water) solvent: (a) without additives and (b) containing 0.5 gL^{-1} trans-cinnamic acid as a dispersant

No deposition, either cathodic or anodic, was observed from CeO_2 suspensions in ethanol when trans-cinnamic acid concentration was lower than 0.1 gL^{-1}. Higher trans-cinnamic acid concentrations allowed the formation of cathodic deposits. The deposition yield was nearly constant (Fig.5-14a) at trans-cinnamic acid concentrations in the range of 0.25-1.0 gL^{-1}. The results indicated that CeO_2 particles were positively charged in the suspensions. It is suggested that the dissociation of the trans-cinnamic acid and adsorption of protons on the CeO_2 particles resulted in electrostatic stabilization of the particles in the suspensions and allowed the formation of cathodic deposits. It is known that oxide particles, containing adsorbed protons, can be deprotonated at the cathode surface. The particle discharge was attributed to the reaction:

$$2H^{+} + 2e^{-} \rightarrow H_2 \qquad \textbf{(5-7)}$$

The consumption of H^{+} at the cathode surface results in a local pH increase, which also promotes particle discharge and deposition. However, reaction (5-7) can result in a moderate pH increase at the cathode. In contrast, significant pH changes can be expected in aqueous or mixed water-ethanol solutions due to reaction (5-3). The results presented in Fig. 5-14b for CeO_2 suspensions in a mixed water–ethanol solvent showed significant increase in the cathodic deposition yield with increasing trans-cinnamic acid concentration in the range of 0-0.1 gL^{-1}. At higher concentrations, the deposition yield from the CeO_2 suspensions in a mixed water–ethanol solvent was higher than that in ethanol. It is suggested that the charge compensation of CeO_2 particles, containing adsorbed H^{+}, by OH^{-} generated in the electrode reaction (5-3), promoted the particles deposition.

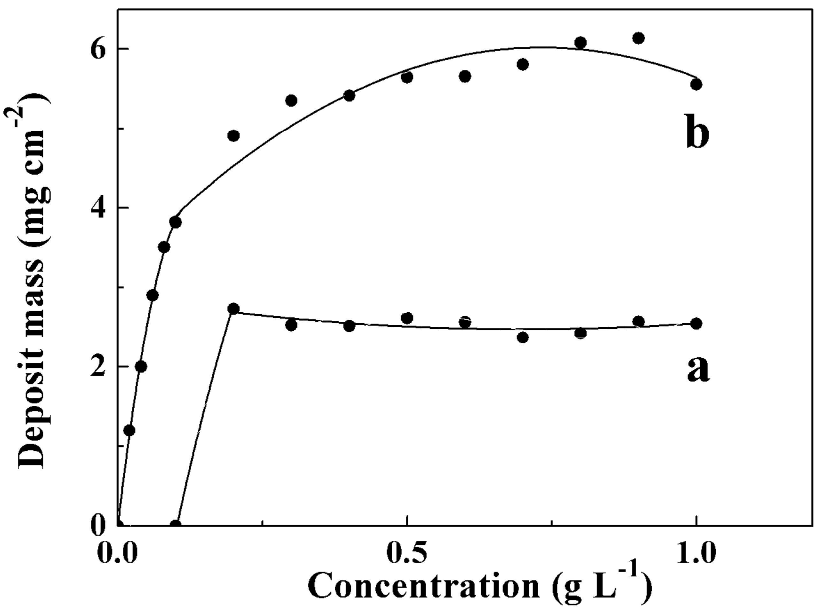

Fig. 5-14 Deposit mass for 10 gL^{-1} CeO$_2$ suspensions versus trans-cinnamic acid concentration in (a) 100% ethanol and (b) mixed ethanol–water (20% water) solvent

5.1.4.4 SEM characterization

The CeO$_2$ deposits obtained by EPD were studied by SEM. The SEM image at low magnification (Fig.5-15a) showed significant cracking. Another image at higher magnification (Fig.5-15b) indicated that the deposit consisted mainly of nanoparticles. The small pores are attributed to the packing of CeO$_2$ nanoparticles. However, such film can not be used for corrosion protection, considering porosity, cracking and even low adherence.

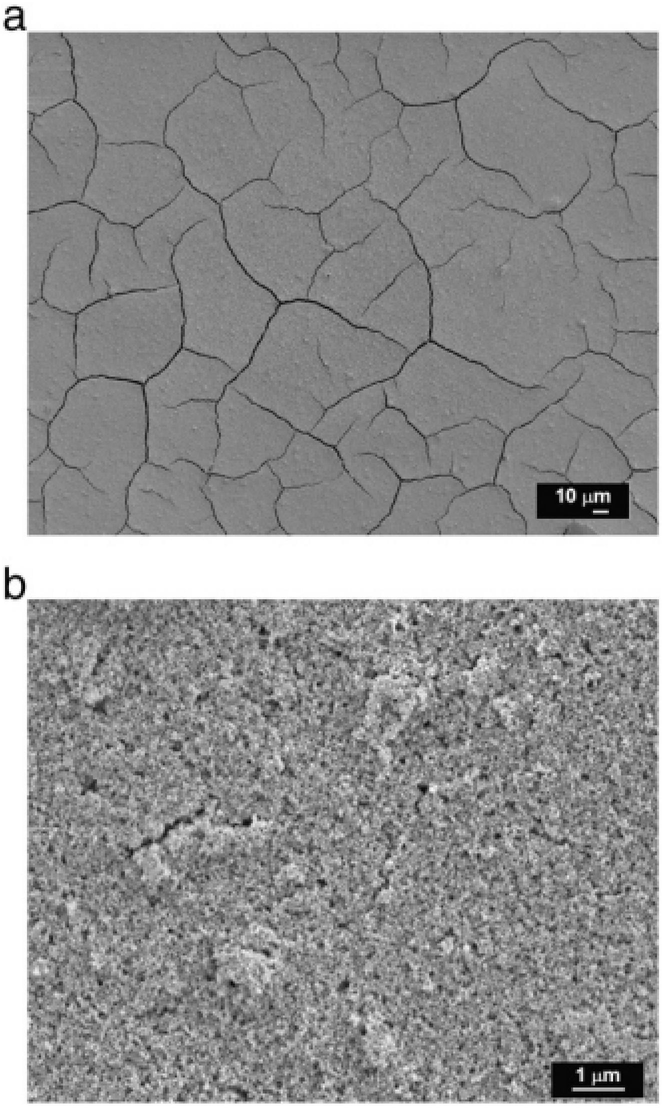

Fig. 5-15 SEM images for the CeO_2 film obtained via EPD from 10 gL^{-1} CeO_2 suspension

5.1.5 Co-deposition of CeO_2 and PVP via EPD

5.1.5.1 Mechanism

In the method based on the EPD of PVP and CeO_2, the PVP adsorption on the CeO_2 nanoparticles can be expected in the bulk of the suspensions. It was suggested that adsorbed PVP macromolecules were deposited together with CeO_2 nanoparticles under electric field. Subsequently, both of them would be bonded to the substrate.In this case, reduced assembling of PVP molecules into spherical particles can be expected. However, the PVP adsorption can promote bridging flocculation of the nanoparticles and their agglomeration in the deposited films.

5.1.5.2 SEM characterization

Fig.5-16 shows typical SEM images of film prepared from the suspension of CeO_2 containing 1 gL^{-1} PVP. The comparison of the SEM images presented in Fig.5-16a, b, c show that the increase in the concentration of CeO_2 resulted in a corresponding increase of CeO_2 amount in the film. It was seen from these SEM images that some CeO_2 particles formed agglomerates. However, spherical particles that occurred in the PVP films were not observed (Fig.5-16a, b, c). It should be noted that in an EPD process of CeO_2, the PVP adsorption onto CeO_2 nanoparticles can be expected in the bulk of suspension. It was suggested that adsorbed PVP macromolecules were deposited together with CeO_2 nanoparticles. In this case, the assembling of PVP molecules into spherical particles decreased.

PVP adsorption brought bridging flocculation of the nanoparticles and their agglomeration into deposited films, as shown in the SEM images. The SEM image under low magnification (Fig.5-16d) showed a continuous and crack-free morphology, which contrasts sharply with Fig.5-14 above. Another advantage of this approach is that problems related to sintering of ceramic materials on stainless steel substrates can be avoided.

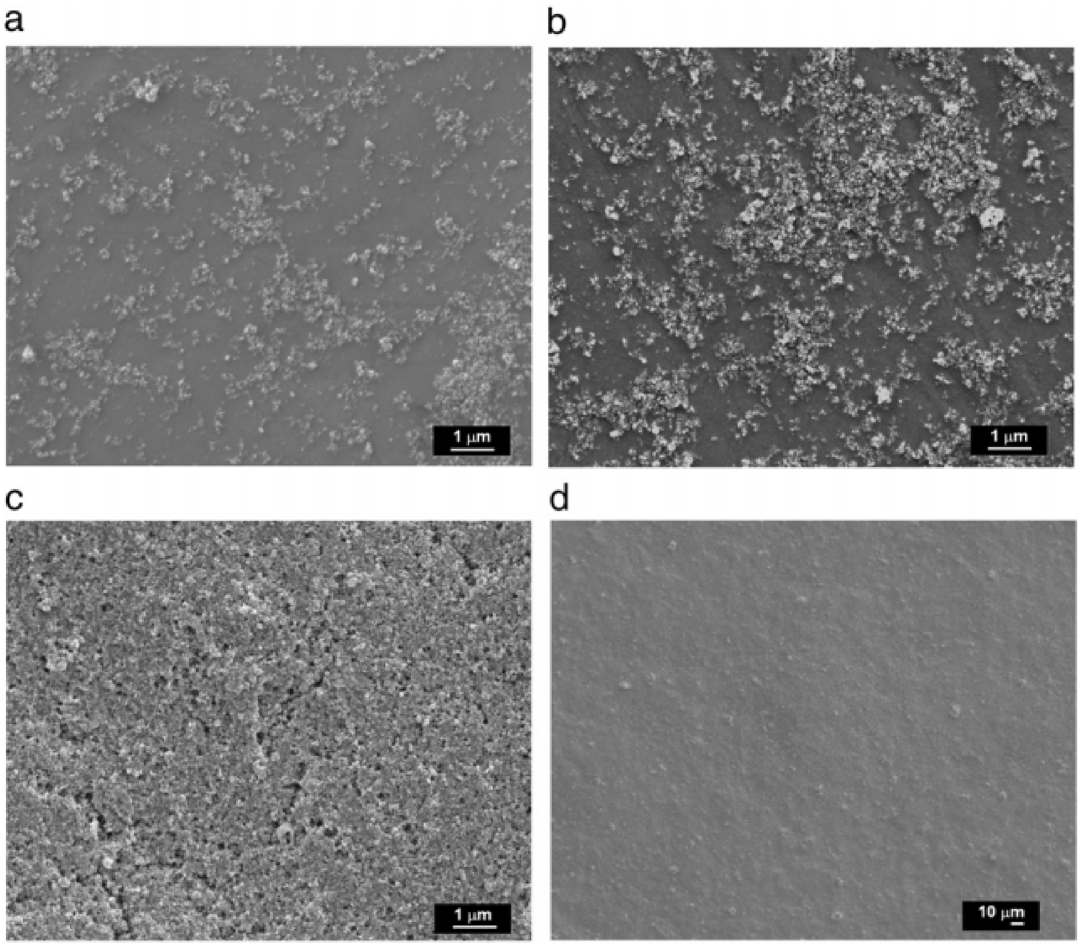

Fig. 5-16 SEM images of films prepared from 1 gL^{-1} PVP solution containing (a) 0.5, (b) 4 and (c, d) 10 gL^{-1} CeO$_2$ at different magnifications

5.1.5.3 Thermal analysis

Fig.5-17 shows the results of TGA and DTA studies of the composite film prepared from10 gL^{-1} CeO$_2$ containing 1 gL^{-1} PVP solutions. The TGA data showed significant mass loss at temperatures below 500 °C, attributed to the burning out of PVP, in agreement with corresponding DTA data. A broad exotherm was shown in DTA data in the range of 200–500 °C. It can be seen from the TGA data that sample mass was nearly constant at temperatures above 600 °C. The total mass loss at 800 °C was 28.0 mass %, which indicates that the composite material contained 72.0 mass % of CeO_2.

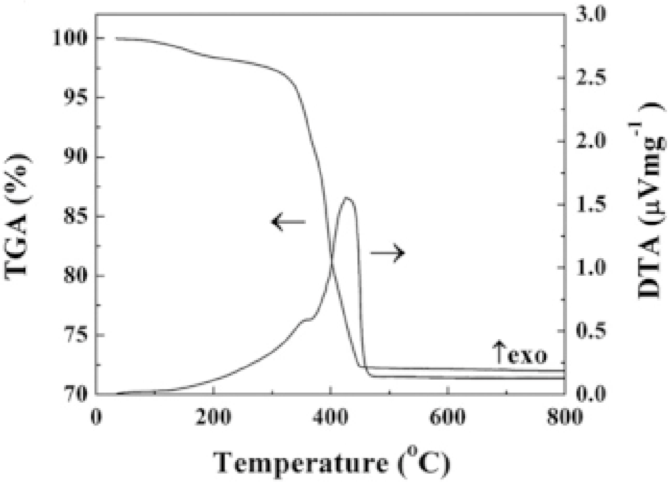

Fig. 5-17 TGA/DTA data for composite deposit prepared from the 1 gL^{-1}PVP solution, containing 10 gL^{-1} CeO_2 at a deposition voltage of 20 V

5.1.5.4 XRD

The XRD pattern of the composite film (Fig.5-18) showed well defined peaks of CeO_2 corresponding to the JCPDS file 34–394. The diffraction pattern is similar to that shown in Fig.5-9. However reduced peak broadening indicated larger size of the CeO_2 crystallites used in the EPD method.

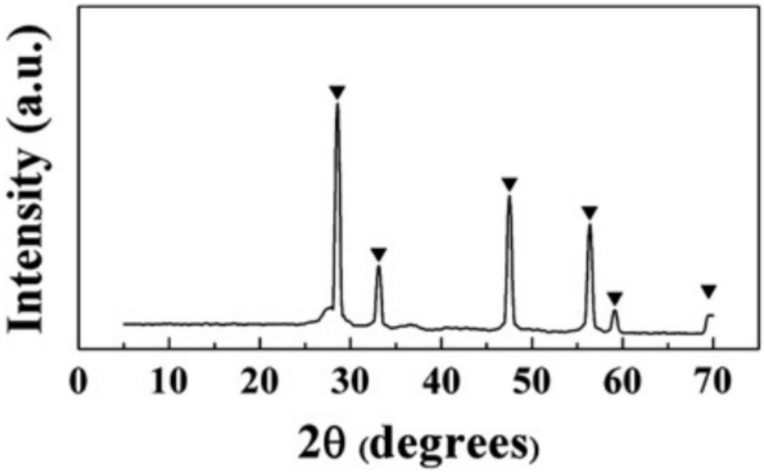

Fig. 5-18 X-ray diffraction patterns for composite deposit from the suspension containing 1 gL^{-1} PVP and 10 gL^{-1} CeO_2 (▼- peaks corresponding to JCPDS file 34–394 of CeO2)

5.1.5.5 Electrochemical tests

Fig.5-19 shows a Tafel plot of a composite PVP-CeO_2 film. The Tafel plots for uncoated stainless steel and coated with PVP films (similar to Fig.5-10) are presented for comparison. The results indicate improved corrosion protection of the composite coating and the beneficial effect of CeO_2.

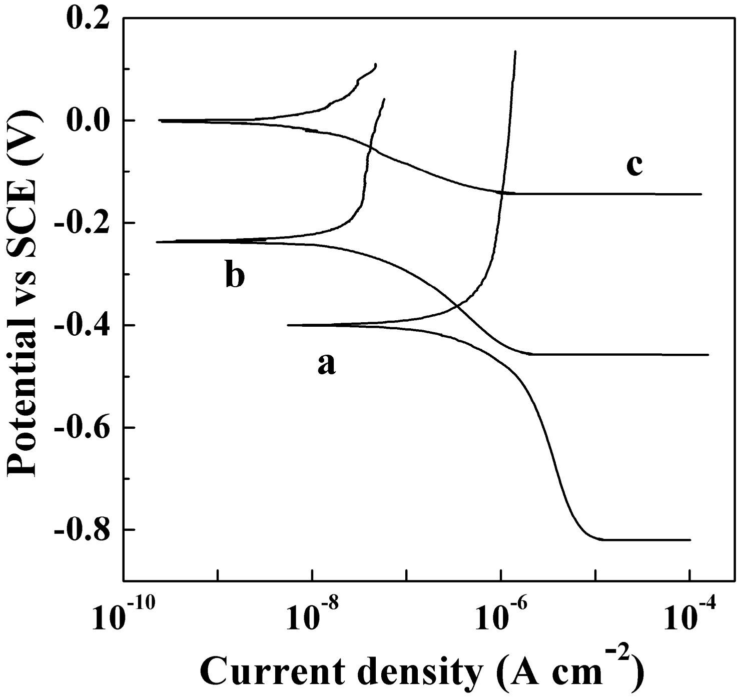

Fig. 5-19 Tafel plots for (a) uncoated and (b,c) coated stainless steel substrates: (b) coating deposited from 1 gL^{-1} PVP solution (c) coating deposited from suspension containing 1 gL^{-1} PVP and 10 gL^{-1} CeO$_2$

5.2 Composite films based on co-polymer PVPBM

5.2.1 Electrodeposition of PVPBM

5.2.1.1 Properties

Extensive studies have shown that poly(butyl-methacrylate) (PBM) and poly(4-vinyl-pyridine) (PVP) are both promising polymer materials for various applications. PBM exhibits good mechanical, electrical and thermal properties, thus being used for biomedical, thermal energy storage, optical and electromechanical devices [85-88]. PVP exhibits excellent chemical stability and can be used for efficient corrosion protection of metals and alloys.

Fig.5-20 shows the chemical structure of PVPBM used in this investigation. The properties of PBM and PVP were combined in the co-polymer of poly(4-vinylpyridine-*co*-butyl methacrylate) (PVPBM). Application of PVPBM for protective films was studied because of the combination of corrosion inhibitive properties of PVP and the excellent film forming properties of PBM[89].

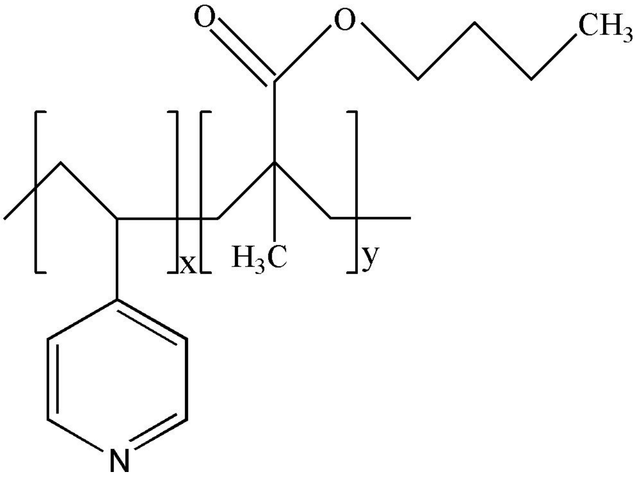

Fig. 5-20 Chemical structure of PVPBM polymer

PVPBM showed improved thermal stability and higher conductivity compared to pure PVP[90]. PVPBM offers important advantages for the fabrication of composites using colloidal methods[91,92]. It was shown that binary miscible blends and inter-polymer complexes can be obtained when sufficient specific interpolymer interactions occur between the two constituents of the mixture[93]. The introduction of PVP within the PVPBM polymer allowed the miscibility of PVPBM with other polymers and fabrication of composites with improved thermal stability [93,94].

5.2.1.2 Mechanism and deposition process

PVPBM is a water insoluble, electrically neutral polymer. It was found that the nitrogen atoms in the pyridine rings (Fig.5-20) can be protonated in the presence of acetic acid to form water soluble cationic polyelectrolyte:

$$\mathrm{PVPBM} + \mathrm{H}^+ \rightarrow \mathrm{PVPBM\text{-}H}^+ \qquad \textbf{(5-8)}$$

The protonated PVPBM was used for the fabrication of solutions for EPD. The choice of solvent is an important factor for the film formation by EPD. It is known that organic solvents, such as ethanol, offer advantages for EPD[15]. Relatively high electric fields can be applied to non-aqueous solutions and high deposition yields can be achieved. In contrast, the application of an electric field to aqueous solutions can result in significant gas evolution at electrodes, due to the electrochemical decomposition of water. Therefore, EPD in aqueous solutions or suspensions is usually performed at lower electric fields in order to reduce gas evolution. This results in lower deposition rates. However, no deposition of PVPBM was achieved from ethanol solutions. It was found that the deposition process required a certain amount of water for base generation through a cathodic reaction:

$$2\mathrm{H_2O} + 2e^- \rightarrow \mathrm{H_2} + 2\mathrm{OH}^- \qquad \textbf{(5-9)}$$

This reaction results in a local pH increase at the cathode surface. EPD of PVPBM was achieved from solutions in a mixed ethanol–water (20% water) solvent. The deposition mechanism involved the electrophoretic motion of protonated PVPBM macromolecules towards the cathode and charge neutralization at the cathode surface:

$$\mathrm{PVPBM\text{-}H^+ + OH^- \rightarrow PVPBM + H_2O} \qquad \textbf{(5-10)}$$

The charge neutralization at the electrode surface prevented electrostatic repulsions of the polymer macromolecules and promoted film formation. The method resulted in the formation of water insoluble PVPBM films.

5.2.1.3 Deposition rate

Fig.5-21 shows QCM data for the film prepared from a 0.1 gL^{-1} PVPBM solution at a deposition voltage of 4 V. The deposit mass increased with increasing deposition time, indicating a continuous film growth. The deposition rate increased with increasing polymer concentration and increasing deposition voltage. Film thickness was varied in the range of 0.5-10 μm by a variation of polymer concentration in the range of 0.5-2 gL^{-1}, and deposition voltage in the range of 5-20 V for deposition times of 0.5-20 min.

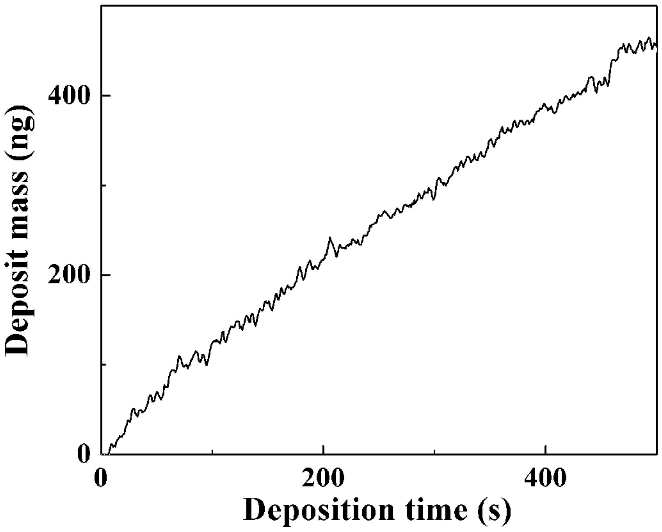

Fig. 5-21 Deposit mass versus deposition time measured using QCM for 0.1 gL^{-1} PVPBM solution in a mixed ethanol–water (20% water) solvent

5.2.1.4 SEM characterization

Fig.5-22 shows typical SEM images of the film cross sections. The images indicated that the films were relatively dense. The film thickness (Fig.5-22A, B) increased with the increasing deposition time. The films were studied by an AFM method.

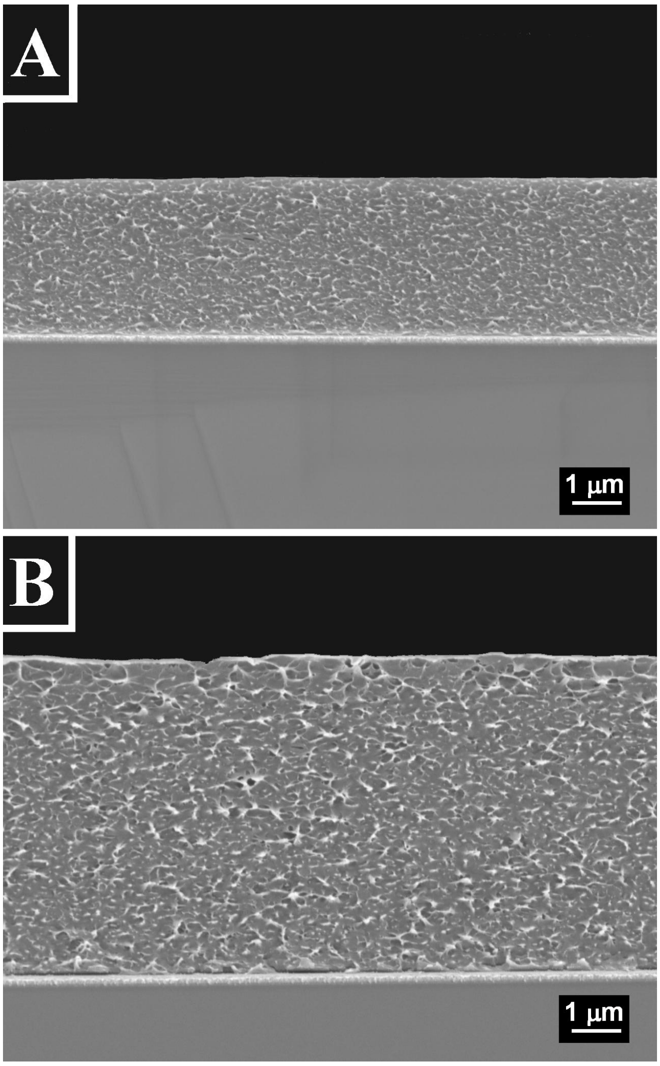

Fig. 5-22 SEM images of cross sections of the PVPBM films prepared at a deposition voltage of 20 V from 2 gL^{-1} PVPBM solutions at deposition times of (A) 5 and (B) 10 min

5.2.1.5 AFM characterization

Fig.5-23 shows an AFM image of the film prepared from 2 gL^{-1} polymer solution at a deposition voltage of 20 V. The root-mean-square (rms) surface roughness of the films was found to be 3.2 nm. The surface roughness of the films prepared by EPD could be attributed to the gas evolution at the cathode surface during deposition.

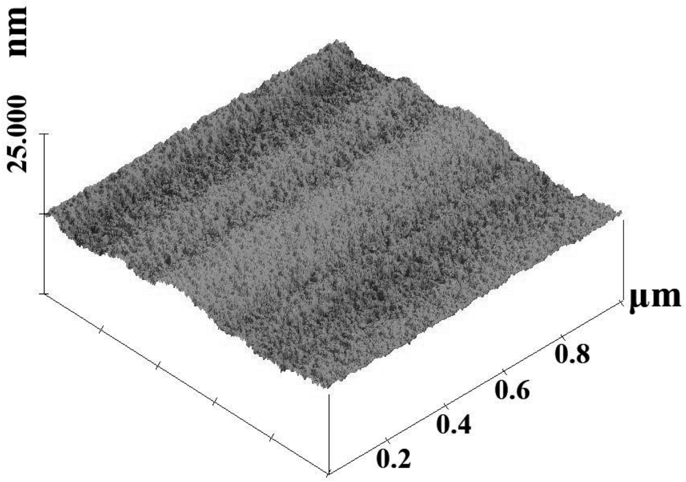

Fig. 5-23 AFM image of a PVPBM film

5.2.2 Co-deposition of CeO_2 and PVPBM using EPD

5.2.2.1 Mechanism

The possibility of EPD of PVPBM films paves the way for the fabrication of composite films. As a step in this direction, the EPD of PVPBM-CeO_2 film was investigated. The results presented above indicated that PVPBM and CeO_2 can be deposited cathodically using the polymer solutions or oxide particle suspensions in a mixed ethanol–water solvent. The OH^- generation in the reaction (5-8) allowed charge neutralization and promoted deposition of both materials. Therefore, two deposition strategies can be combined for the fabrication of composite films.

The PVPBM polymer with inherent binding properties prevented cracking and allowed the formation of adherent deposits. However, many studies indicated that the properties of individual components of composites can be utilized better in multilayer films or films of graded composition [96-99]. Previous studies of the multilayer structures obtained by EPD showed that crack propagation in such structures can be stopped or deflected at the interface of the individual layers[99].

Experiments indicated that monolayer composite films containing CeO_2 and PVPBM can be obtained by EPD. This method offered the advantages of room temperature processing of composite materials. Therefore, composite coating was not limited to monolayer any more. The formation of a layer of pure polymer with good binding and film forming properties at the interface of substrate and composite polymer–ceramic film offered benefits of improved film adhesion, whereas the properties of the ceramic component were utilized in a top polymer–ceramic layer with a high concentration of the ceramic particles in the polymer matrix[100].

5.2.2.2 SEM characterization

Fig.5-24 shows the SEM images of the films prepared from a 10 gL^{-1} CeO_2 suspension without PVPBM and containing 1 gL^{-1} PVPBM. The comparison of the SEM images shown in Fig.5-24a and Fig.5-24b indicated that the addition of PVPBM to the CeO_2 suspensions resulted in the formation of crack-free films. It was suggested that composite PVPBM-CeO_2 films were obtained by EPD from CeO_2 suspension, containing PVPBM. The binding and film forming properties of PVPBM polymer allowed the formation of crack-free films.

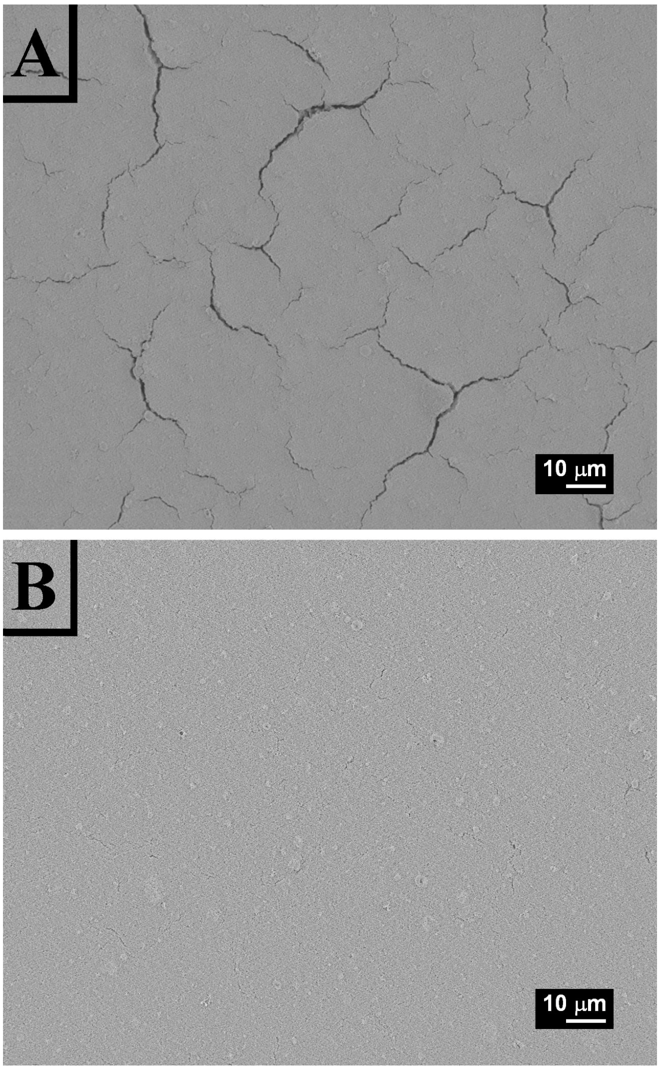

Fig. 5-24SEM images of the films prepared from 10 gL^{-1} CeO$_2$ suspensions in a mixed ethanol–water (20% water) solvent containing 1 gL^{-1} trans-cinnamic acid as a dispersant: (A) without PVPBM and (B) containing 1 gL^{-1} PVPBM

Fig.5-25 shows SEM images of film cross sections. The films were relatively uniform and adhered well to the substrates. It is known that uniformity of the films prepared by the EPD method is controlled by electric field[95]. However, the film uniformity is limited by the size of ceramic particles used for deposition[95]. The SEM images shown in Fig.5-25 indicate that the increase in the deposition time resulted in increased deposit thickness. The film thickness was varied in the range of 0.5-15 μm by the variation of deposition voltage in the range of 5-20 V and deposition time in the range of 0.5-20 min.

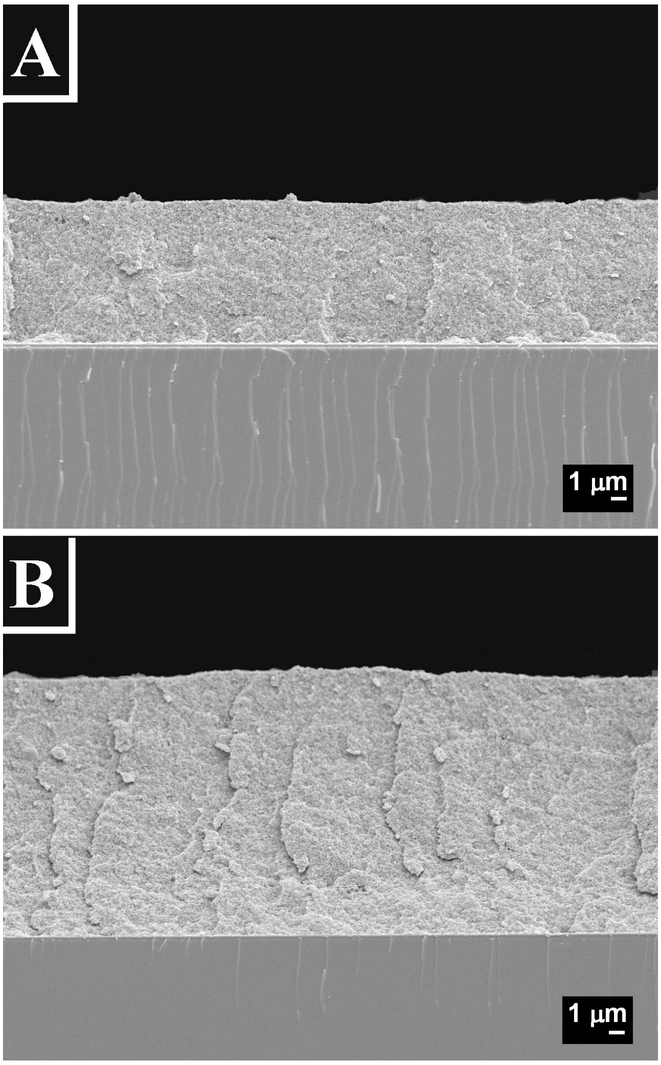

Fig. 5-25SEM images of cross sections of the films prepared from 10 gL^{-1} CeO$_2$ suspension in a mixed ethanol–water (20% water) solvent, containing 1 gL^{-1} PVPBM at a deposition voltage of 20 V and deposition times of (A) 5 min and (B) 10 min

5.2.2.3 Thermal analysis

The composite films were investigated by TGA, DTA and XRD methods. Fig.5-26 compares TGA and DTA data for pure PVPBM and composite deposit prepared from 10 gL^{-1} CeO_2 suspension, containing 1 gL^{-1} PVPBM. The TGA data for PVPBM showed reduction in sample mass in the range of 80-120 ºC, which can be attributed to the release of absorbed water. A sharp reduction of sample mass was found in the range of 320-400 ºC. The mass loss at 400 ºC was about 80% of the initial sample mass. Additional mass loss was observed in the range 400-660 ºC. The mass loss in the range of 320-660 ºC was attributed to the burning out of PVPBM. The corresponding DTA data showed an exothermic peak around 400 ºC, attributed to the burning out of PVPBM. The composite deposit exhibited mass loss in the range of 100-300 ºC and a sharp reduction of sample mass in the range of 300-400 ºC. The reduction in sample mass can be mainly attributed to the burning out of the polymer. A similar mass loss was observed for the pure polymer. The total mass loss in the range of 20-1000 ºC was found to be 16.2 %. Therefore, the composite film contained 83.8 mass% of CeO_2. The exothermic peak in the corresponding DTA data at ~390ºC was attributed to the burning out of the polymer (Fig.5-26B). It should be noted that the investigations[84] of poly(4-vinyl pyridine-co-divinyl benzene)-CeO_2 composites, prepared by a chemical precipitation method, revealed increased stability of the composites, compared to pure polymer. The increased stability was attributed to interactions of the organic and inorganic components, which involved the coordination of nitrogen atoms of pyridine with Ce(IV) of CeO_2. However, no increase in the thermal stability of PVPBM-CeO_2 films, compared to pure PVPBM, was observed in our investigation.

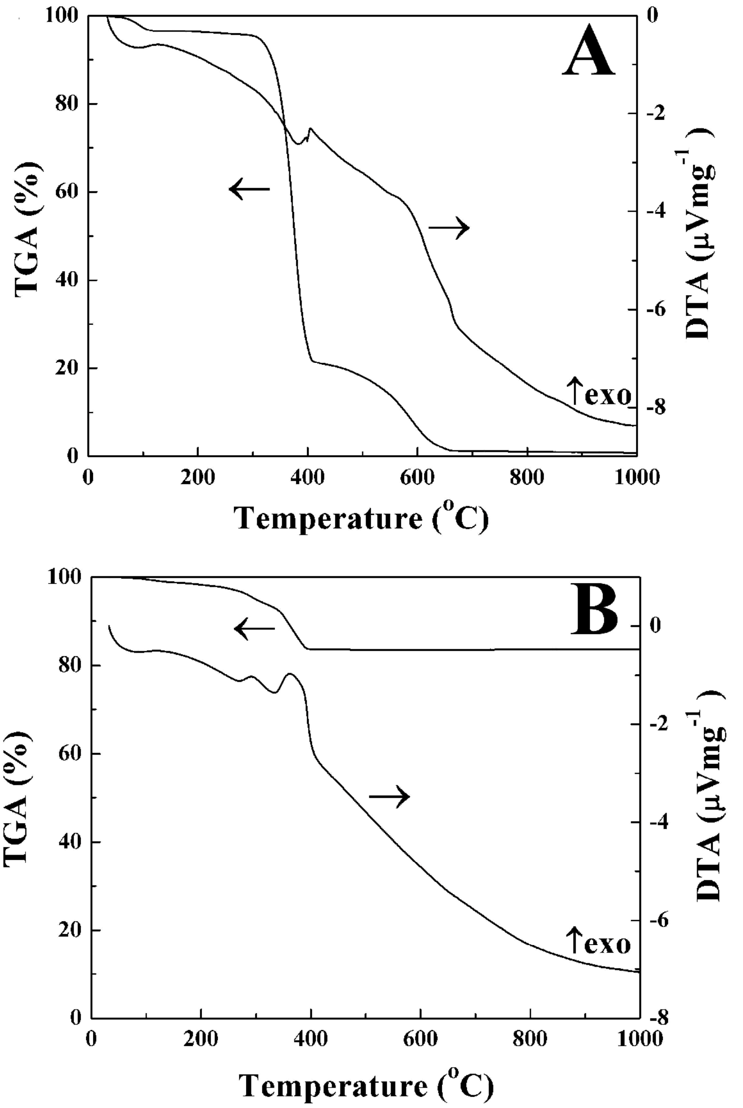

Fig. 5-26 TGA/DTA data for (A) pure PVPBM and (B) composite deposit prepared from 10 gL^{-1} CeO_2 suspension, containing 1 gL^{-1} PVPBM

5.2.2.4 XRD

The TGA and DTA data are in agreement with the results of XRD, which confirmed that the films contained CeO_2 particles. The XRD pattern of the composite deposits (Fig.5-27) showed peaks of CeO_2 in agreement with the JCPDS file 34–394 of CeO_2.

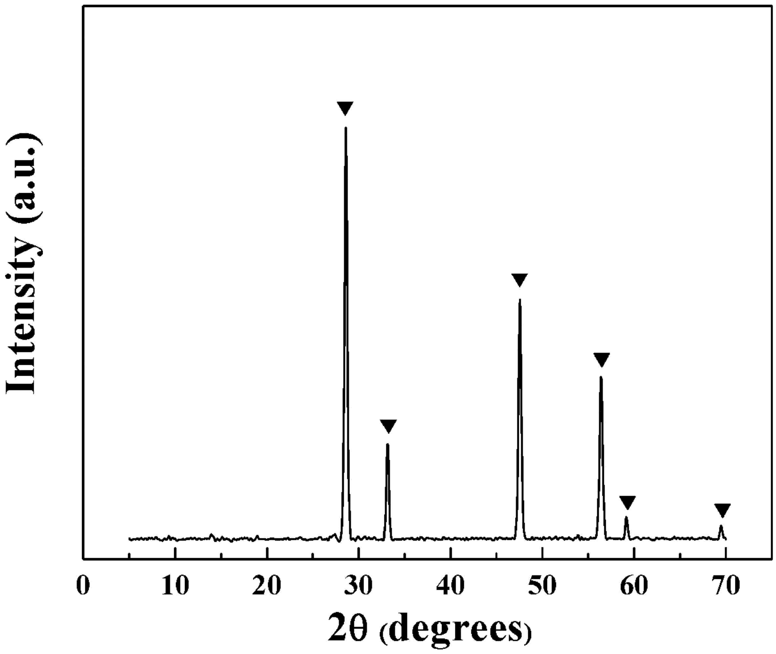

Fig. 5-27 XRD pattern for the composite deposit, prepared from 10 gL^{-1} CeO_2 suspension, containing 1 gL^{-1} PVPBM (▼- peaks corresponding to JCPDS file 34–394 of CeO_2)

5.2.2.5 SEM studies of laminated film

Problems related to the high temperature sintering of CeO_2 coatings on metallic substrates can be avoided in the composite coatings. The sintering problems involve the sintering shrinkage and cracking of the ceramic layer, oxidation of the metallic substrates, diffusion and chemical reactions at the film-substrate interface at elevated temperatures. The possibility of deposition of PVPBM, CeO_2 and PVPBM-CeO_2 films paved the way for the fabrication of laminated films with advanced properties.

Fig.5-28 shows SEM images of the surface and cross section of a bilayer PVPBM(bottom layer)/PVPBM-CeO_2(top layer) film prepared by EPD. The PVPBM solution was used for the fabrication of pure PVPBM films, whereas the composite PVPBM-CeO_2 layer was obtained from PVPBM solution, containing dispersed CeO_2. The SEM image of the surface showed CeO_2 nanoparticles in the PVPBM matrix. The small porosity with pore size of 10-30 nm can be attributed to the packing of CeO_2 particles. The SEM investigations of the cross sections of the bi-layer films showed that the films were uniform with a good bonding between the individual layers. The investigations of film cross sections of individual layers with thickness of 2-10 μm did not reveal any voids or delamination of the individual layers at their interface.

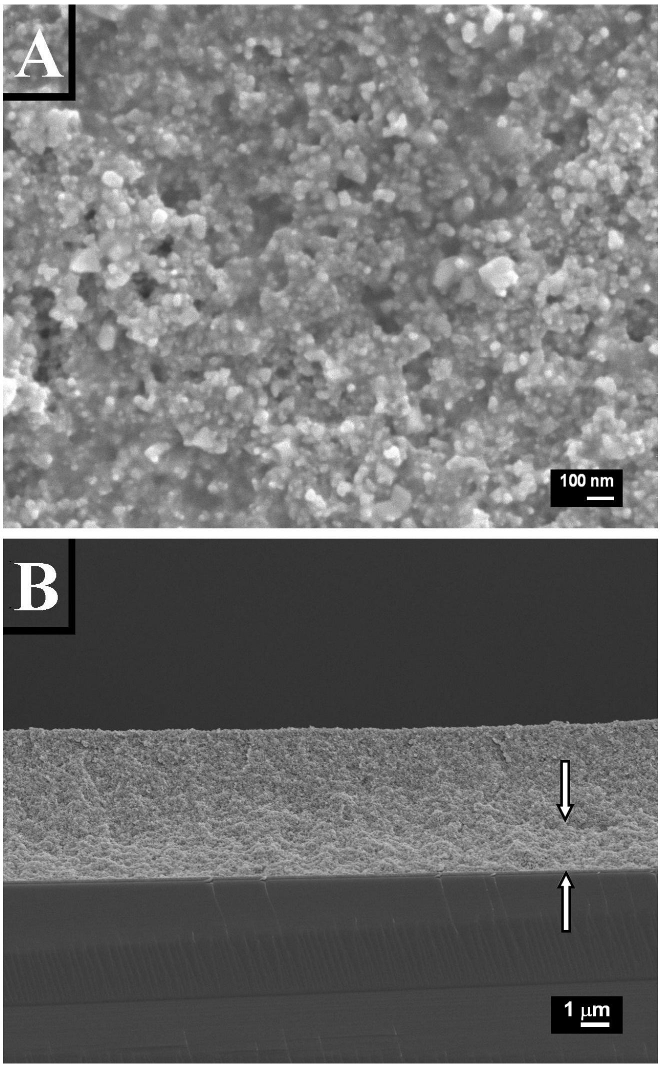

Fig. 5-28 (A) surface and (B) cross section of a composite film, containing a PVPBM bottom layer deposited from 1 gL^{-1} PVPBM solution and a PVPBM-CeO$_2$ top layer deposited from 10 gL^{-1} CeO$_2$ suspension containing 1 gL^{-1} PVPBM in a mixed ethanol–water (20% water) solvent at a deposition voltage of 20 V. (Arrows show the PVPBM layer)

5.2.2.6 Electrochemical tests

The composite films deposited by EPD on stainless steel substrates were investigated for corrosion protection of the substrates. Fig.5-29 compares the Tafel plots of uncoated stainless steel, and stainless steel with monolayer or bi-layer composite coatings. The coated samples showed increased corrosion potential and reduced anodic current compared to uncoated samples. Therefore, the composite coatings can be used for corrosion protection of stainless steel. The composite coatings can be used for other applications, utilizing functional properties of the organic and inorganic components. Moreover, film forming properties of PVPBM can be used for the deposition of new composites, containing inorganic nanoparticles of various functional materials.

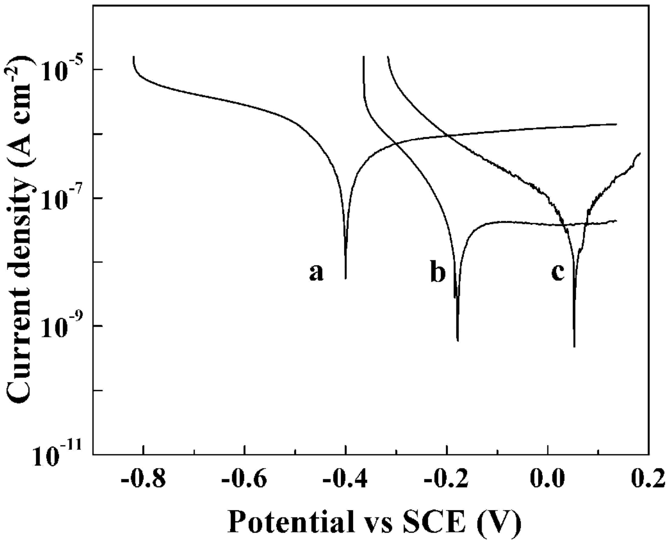

Fig. 5-29 Tafel plots for stainless steel: (a) uncoated, (b) coated with PVPBM-CeO_2 film prepared from 10 gL^{-1} CeO_2 suspension containing 1 gL^{-1} PVPBM at 20 V, and (c) coated with a bilayer film, containing a PVPBM bottom layer deposited from 1 gL^{-1} PVPBM solution and a PVPBM-CeO_2 top layer deposited from 10 gL^{-1} CeO_2 suspension containing 1 gL^{-1} PVPBM

5.2.3 Other composite films by EPD

5.2.3.1 Deposition mechanism

The method, developed for the deposition of CeO_2- PVPBM films, paved the way for the deposition of other composites. As a step in this direction, the fabrication of composites, containing inorganic clay in a PVPBM matrix, was achieved by EPD. Various organic molecules were investigated for the dispersion of clay. It was found that efficient dispersion, charging and EPD of clay particles can be achieved using crystal violet. Fig.5-30 shows the molecular structure of crystal violet. The dissociation of crystal violet in water solutions resulted in the formation of cationic species.

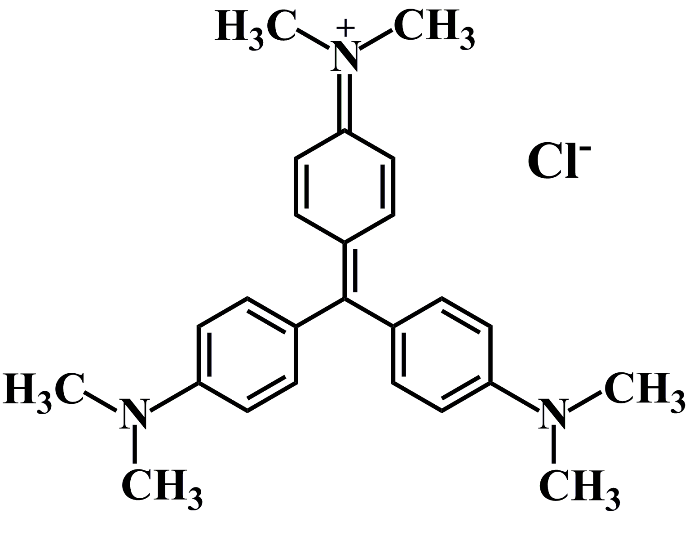

Fig. 5-30 Structure of crystal violet

However, the pH increase resulted in the charge neutralization:

$$C_{25}H_{30}N_3^+ + OH^- \rightarrow C_{25}H_{31}N_3O \qquad \textbf{(5-11)}$$

The reaction (5-11) is also illustrated in Fig.5-31.

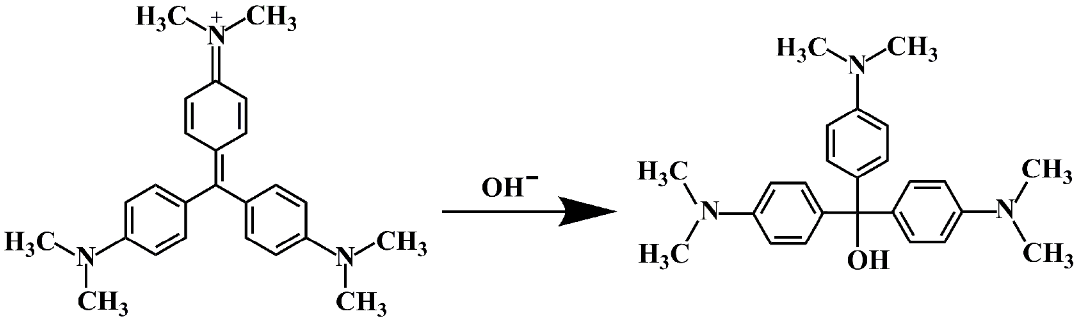

Fig. 5-31 Charge neutralization of crystal violet in basic solution

5.2.3.2 Dispersion mechanism and deposition kinetics

Subsequent to dissolving of crystal violet, $C_{25}H_{30}N_3^+$ ions were adsorbed on clay particles and charged them positively. The adsorption of $C_{25}H_{30}N_3^+$ ions resulted in electrostatic stabilization of clay particles. Under the influence of an electric field, these charged particles were driven towards the cathode, where the concentration of OH^- ions increased. The charge neutralization in the high pH region at the cathode surface promoted deposit formation. Fig.5-32 shows the relationship between deposit mass and concentration of crystal violet in the clay suspension. Fig.5-32(a) gives the data measured at a deposition voltage of 20 V and (b) presents the data at 60 V. The deposit mass increased with increasing crystal violet concentration in the suspensions. The increase in the deposition voltage resulted in higher deposition yield.

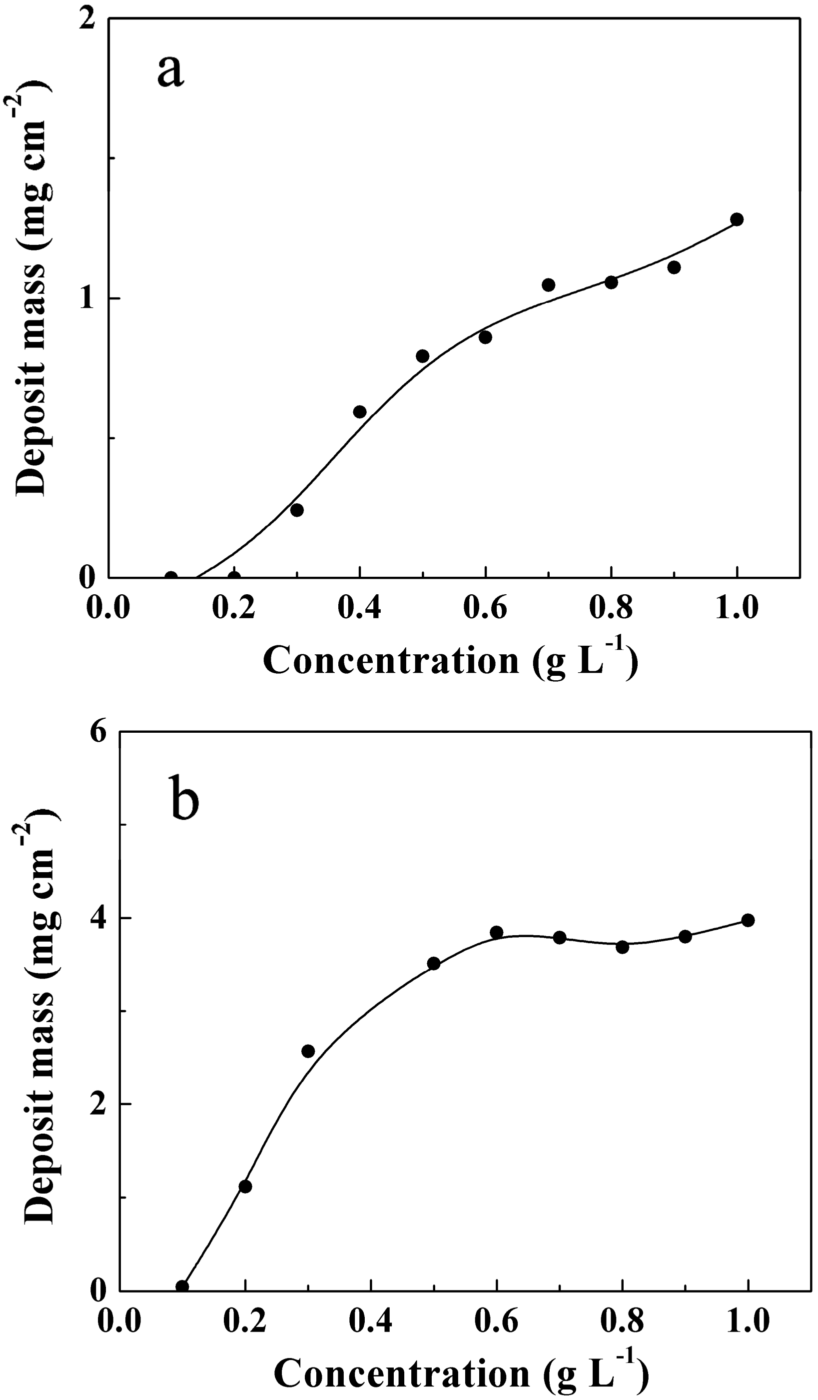

Fig. 5-32 Deposit mass versus concentration of crystal violet in 10 gL-1 clay suspension at deposition voltages of (a) 20V, (b) 60V and deposition time of 5 min.

5.2.3.3 SEM characterization

Fig.5-33 shows SEM images of the surface of a film prepared by EPD from the10 gL^{-1} clay suspension containing 1 gL^{-1} PVPBM and 0.5 gL^{-1} crystal violet. The solvent was composed of 80% ethanol and 20% water. Fig.5-33(a) showed that the films were crack free and contained clay particles in the polymer matrix. It is suggested that binding and film forming properties of PVPBM polymer allowed the formation of adherent and crack free films.

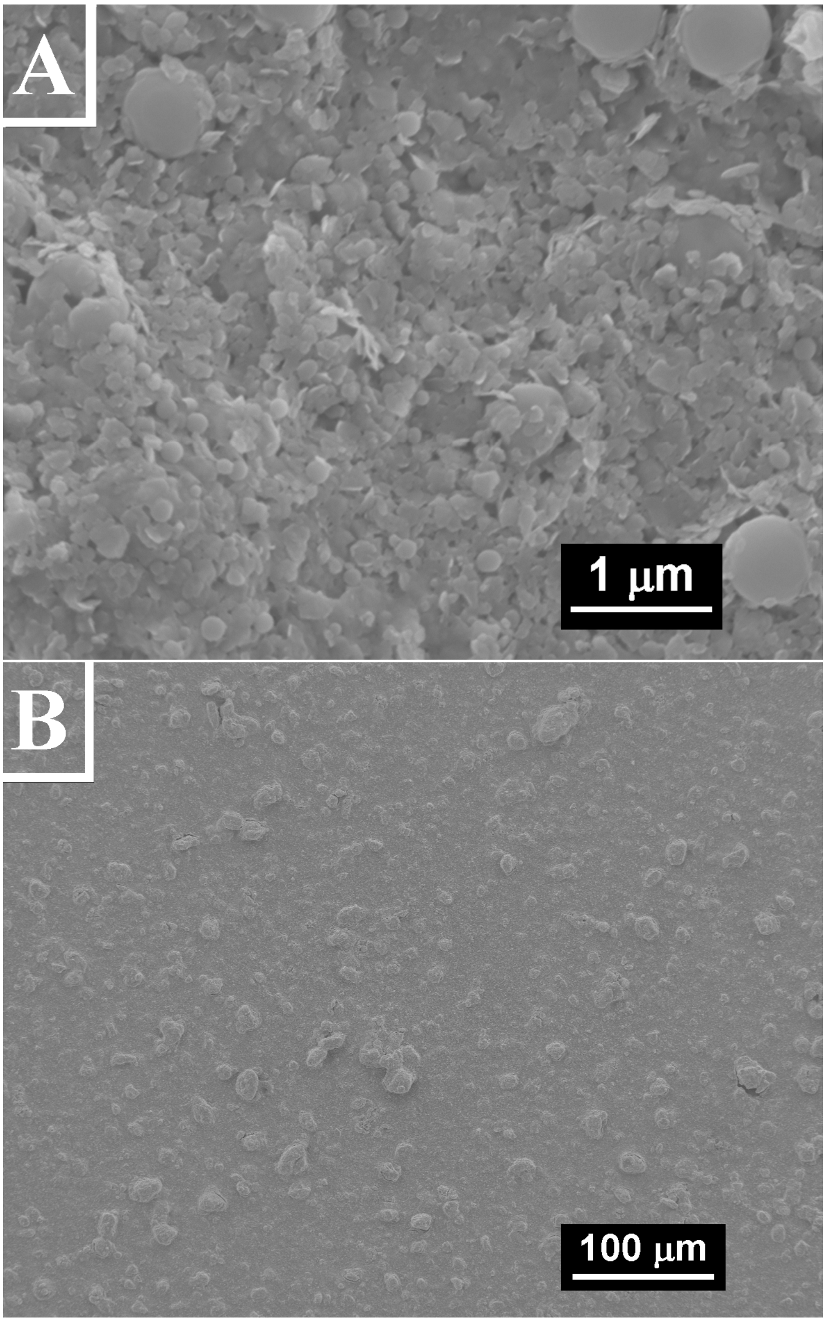

Fig. 5-33 SEM images of the surface of film prepared by EPD from 10 gL^{-1} clay suspension containing 1 gL^{-1} PVPBM and 0.5 gL^{-1} crystal violet in the solvent composed of 80% ethanol and 20% water (A)Higher magnification; (B)Lower magnification

5.2.3.4 Thermal analysis

The composite film was investigated by TGA and DTA methods. Fig.5-34 compares

TGA and DTA data for deposits prepared from 1 gL^{-1} and 10 gL^{-1} clay suspension, containing 1 gL^{-1} PVPBM and 0.5 gL^{-1} crystal violet. The TGA data in Fig5-34 showed reduction in sample mass mainly in the range of 50-500 ºC, which can be separated to two steps. The first step can be attributed to dehydration, while the second reduction is related to the burning process of PVPBM. The mass loss at 800 ºC was 64.4 and 48.1 % for deposits prepared from suspensions, containing 1 gL^{-1} and 10 gL^{-1} clay, respectively. The results indicated that deposit composition can be varied by the variation of clay concentration in the suspension.

DTA data in Fig.5-34 correlated well with the TGA data. The exothermic peaks in the corresponding DTA data in Fig.5-34(a,b) in the range of 180-550 ºC were attributed to the burning out of the polymer. The temperatures for main exothermic peaks coincided with the temperatures where the mass reduction was observed.

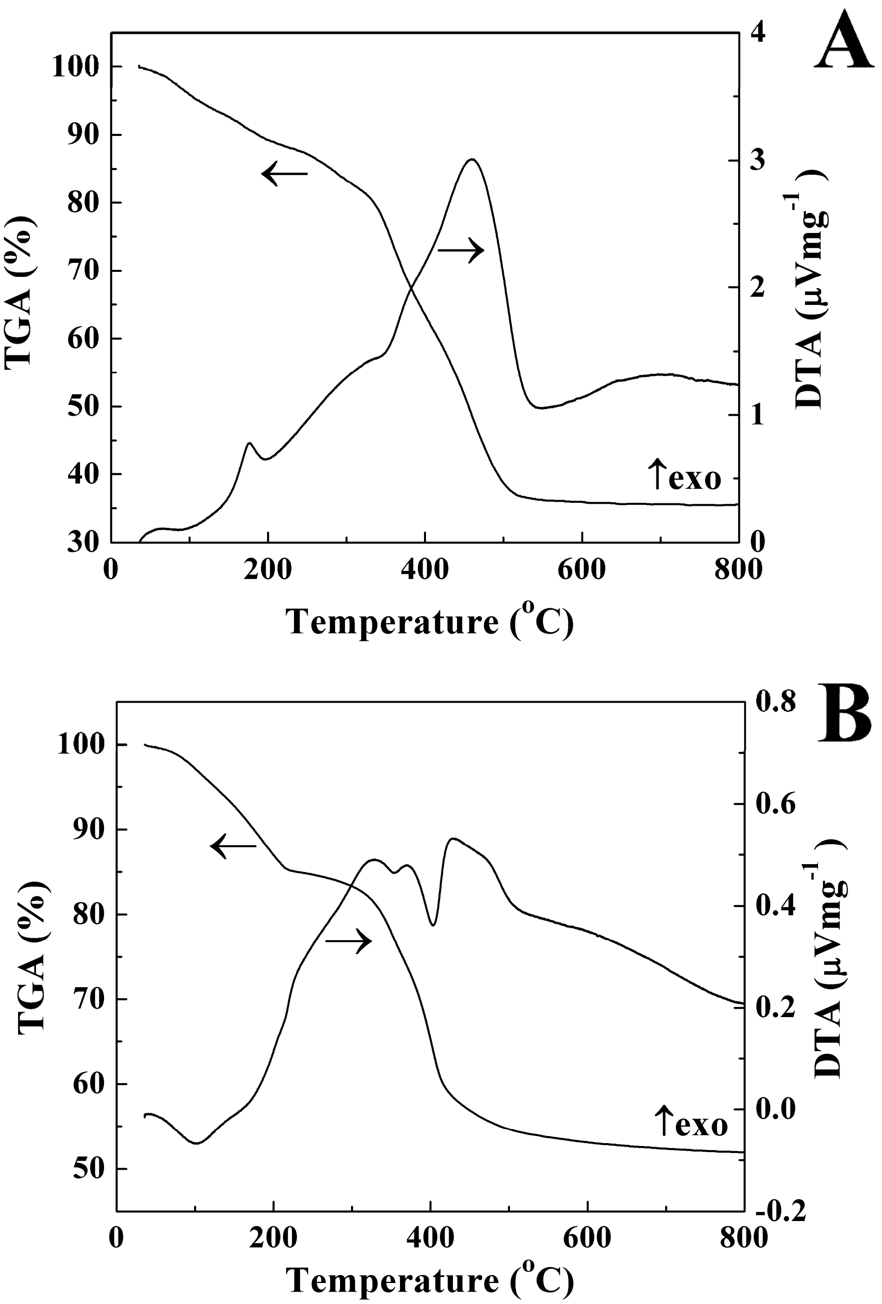

Fig. 5-34 TGA/DTA data for deposit prepared by EPD from (A) 1 gL^{-1} and (B) 10 gL^{-1} clay suspension, containing 1 gL^{-1} PVPBM and 0.5 gL^{-1} crystal violet in the solvent composed of 80% ethanol and 20% water

5.3 Electrochemical testing of coatings prepared by PVD and electroplating

5.3.1 Alloy substrates and coatings deposited by PVD and electroplating

AMPCO (copper alloy) and TZM (Mo-Ti-Zr-C alloy) are two important commercial alloys, widely used in industry. CrN, CrN-D, and TiC coatings were deposited by PVD. Ni coatings were deposited by electroplating. The samples were supplied by Mold Master company. The coatings were deposited using PVD and electroplating technologies developed at Mold Master Company.

5.3.2 Electrochemical tests

5.3.2.1 Impedance data

The coatings deposited on AMPCO940 and TZM alloys were studied by electrochemical impedance spectroscopy method. Fig.5-35 compared the impedance spectroscopy data for uncoated and Ni coated AMPCO940. The impedance data didn't show significant changes in the real part (Z') of the complex impedance $Z^*=Z'-iZ''$, presented in the Nyquist plot. The increased Z" values can be attributed to reduced surface area (roughness) and lower double layer capacitance of the coated sample. Similar results were obtained for CrN coated AMPCO940 (Fig.5-36). However, significant increase in Z' was observed for CrND coated AMPCO940, compared to uncoated alloy (Fig.5-37). This can be attributed to lower conductivity of the CrND film, which provided a barrier to electrolyte diffusion to the alloy surface. Such barrier can be beneficial for the corrosion protection of AMPCO940 alloy.

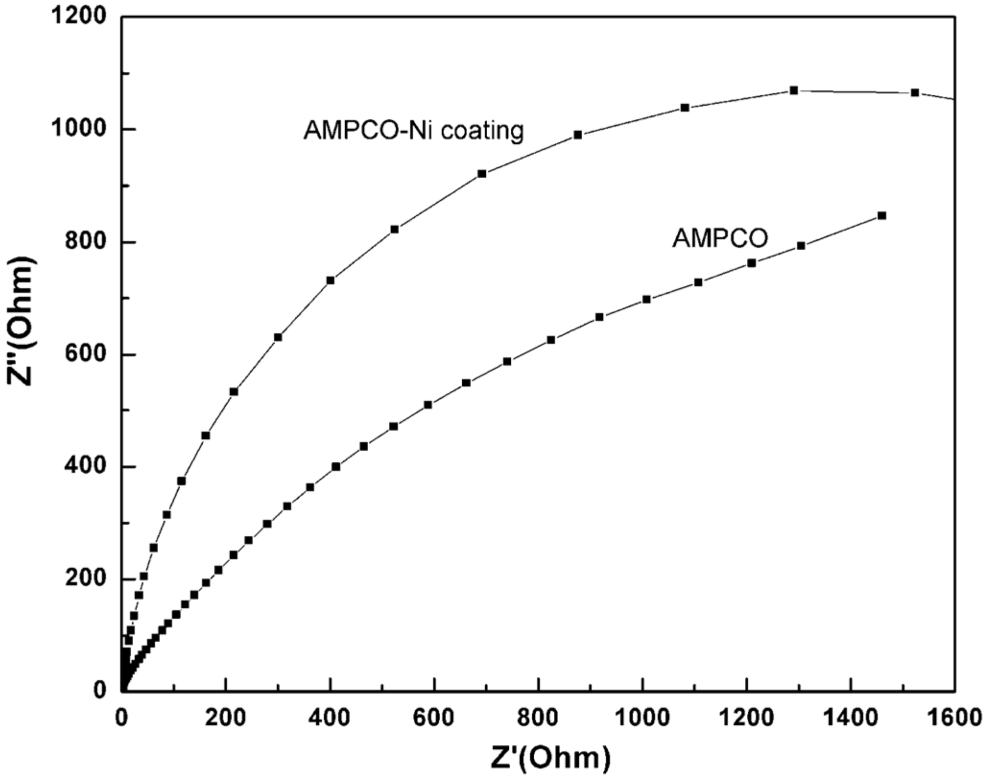

Fig. 5-35 Impedance plots for uncoated AMPCO alloy and Ni coated AMPCO

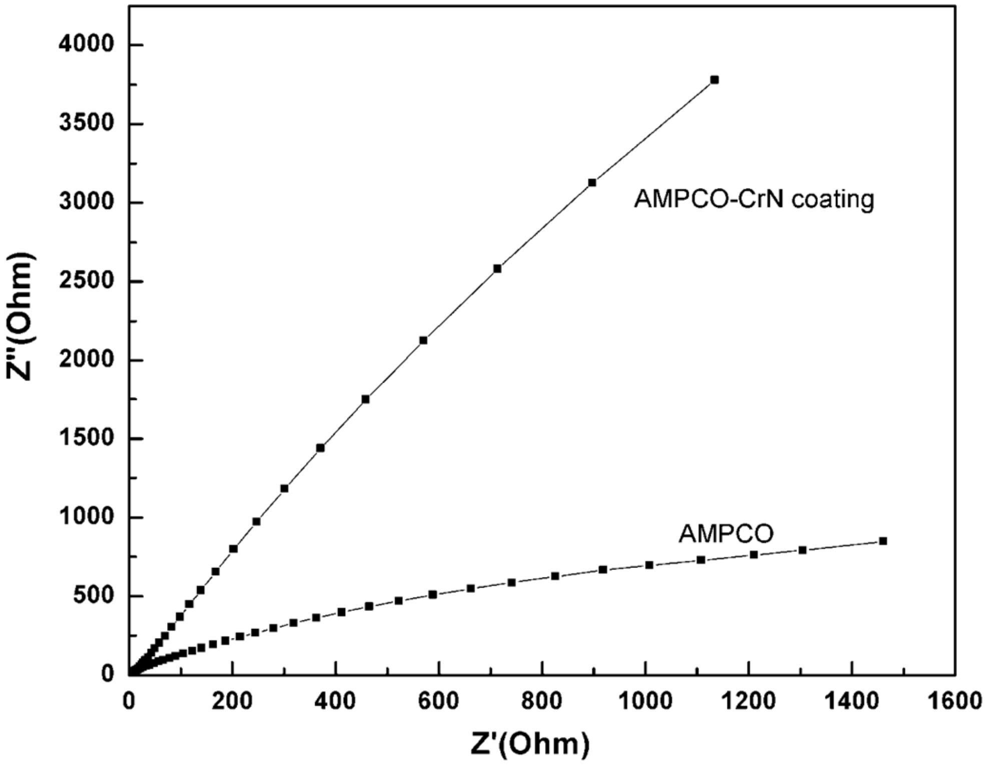

Fig. 5-36 Impedance plots for uncoated AMPCO alloy and CrN coated AMPCO

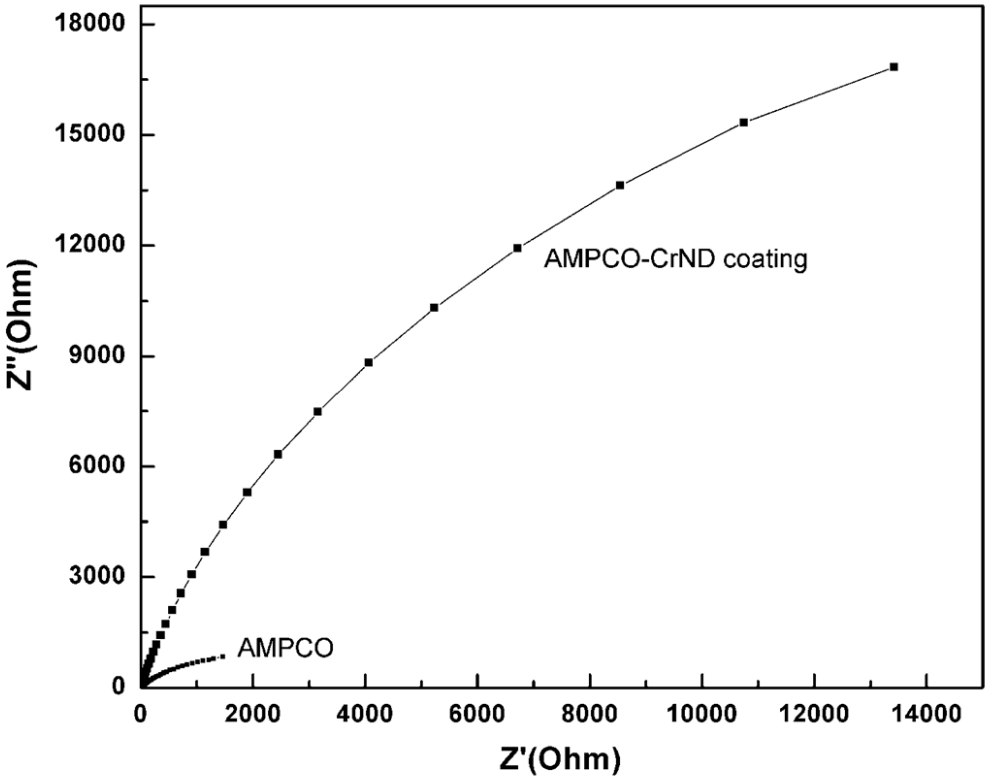

Fig. 5-37 Impedance plots for AMPCO alloy and CrN (D) coated AMPCO

Titanium-Zirconium-Molybdenum (TZM) is another type of alloy widely used in industry. Impedance spectroscopy studies showed that this alloy exhibits relatively high electrical resistivity, compared to AMPCO alloy. As a result, impedance spectroscopy data didn't show increase in Z' for the coated, compared to uncoated samples (Fig.5-38-5-40). TiC coated samples showed much lower Z' compared to uncoated TZM. It is suggested that the deposition of TiC resulted in reduction of metal ions in the thin surface oxide layer. This can result in lower chemical stability of coated alloy.

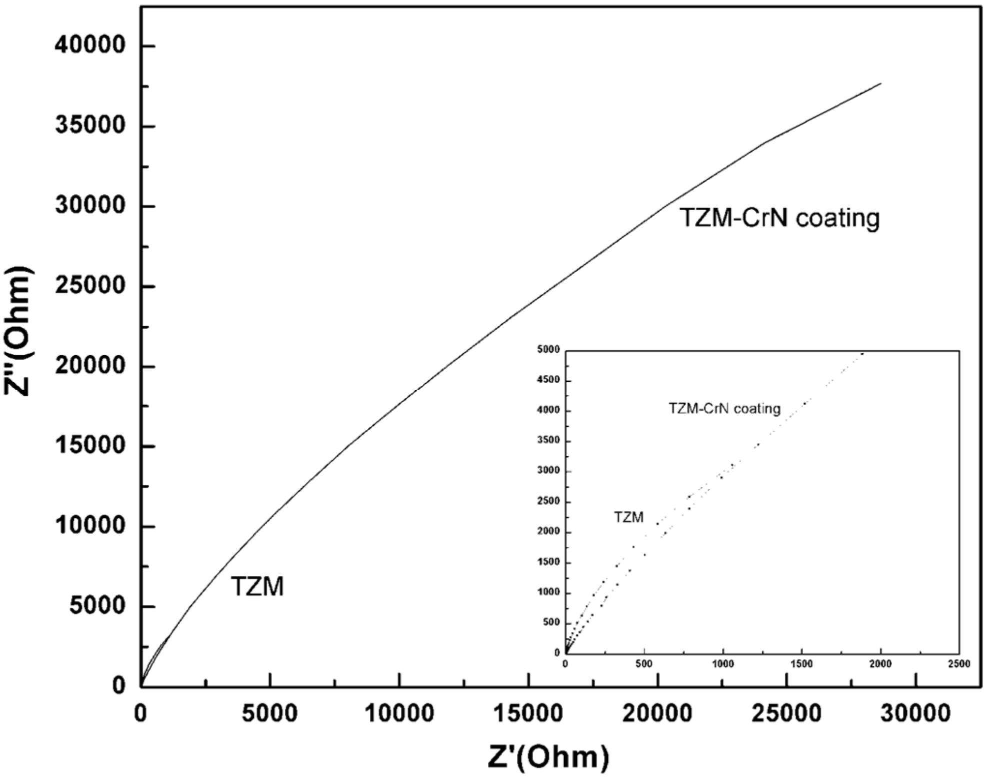

Fig. 5-38 Impedance plots for TZM alloy and CrN coated TZM

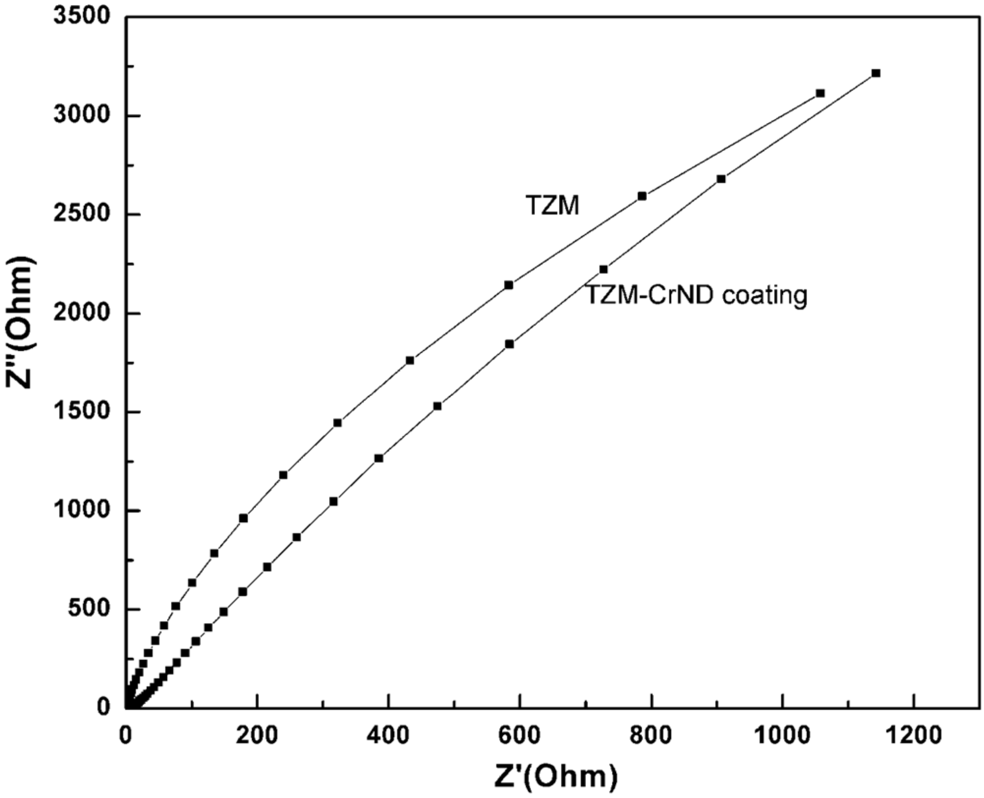

Fig. 5-39 Impedance plots for TZM alloy and CrN (D) coated TZM

.

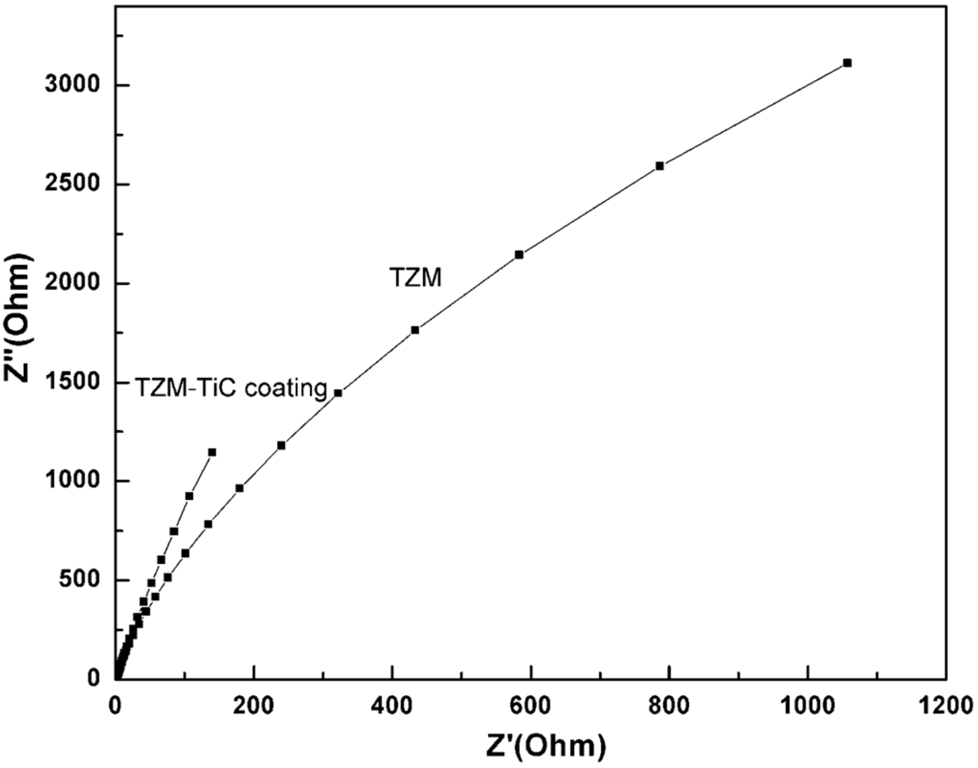

Fig. 5-40 Impedance plots for TZM alloy and TiC coated TZM

5.3.2.2 Tafel data

Fig.5-41 compares Tafel plots for Ni coated and uncoated AMPCO alloy. It is seen that the corrosion potential of the coated sample is more negative than the uncoated sample. However, at higher potentials the coated sample showed lower anodic current. The results indicate that electroplated Ni is not a very efficient coating to prevent corrosion.

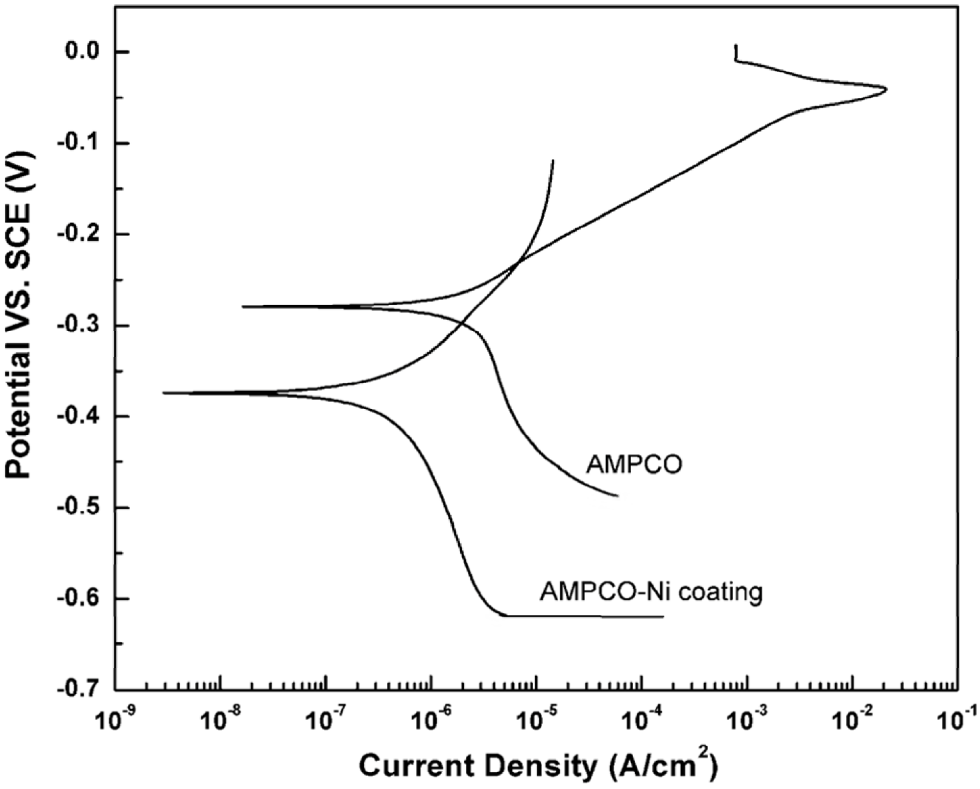

Fig. 5-41 Tafel plots for AMPCO alloy and Ni coated AMPCO

According to Fig.5-42, CrN performed much better than Ni coating. CrN coating clearly increased the corrosion potential and decreased the corrosion rate at the same time.

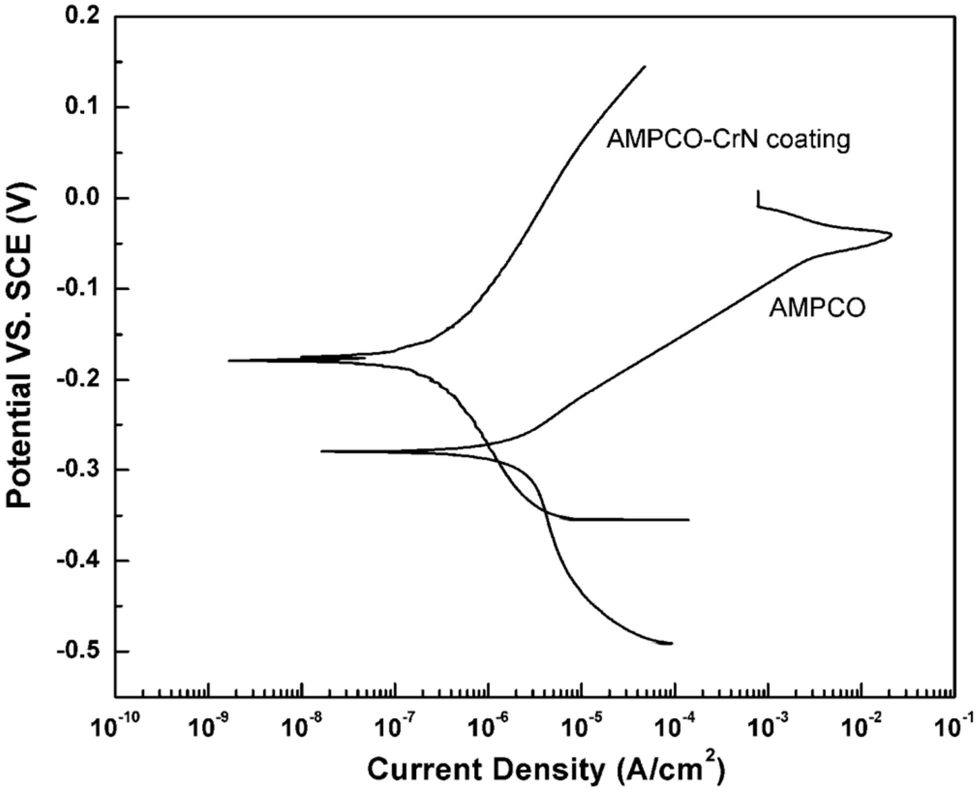

Fig. 5-42 Tafel plots for AMPCO alloy and CrN coated AMPCO

Fig.5-43 compares Tafel plots for CrN (D) coated and uncoated AMPCO. The increase of corrosion potential and reduction of anodic current was observed. However, CrN coatings showed better protection, compared to CrND, as indicated by higher corrosion potential and lower anodic current.

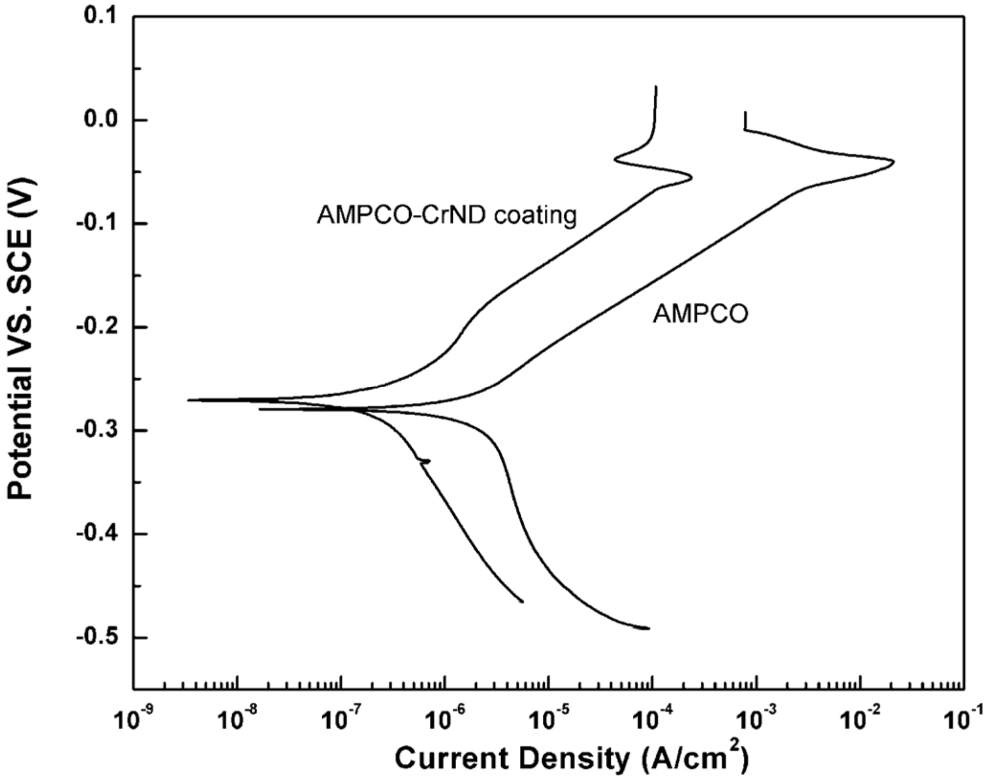

Fig. 5-43 Tafel plots for AMPCO alloy and CrN (D) coated AMPCO

Fig.4-44 compares the Tafel plots of CrN coated and uncoated TZM. With corrosion potential increased and rate decreased, CrN clearly improved electrochemical properties of TZM, though it did not have affected much on impedance much.

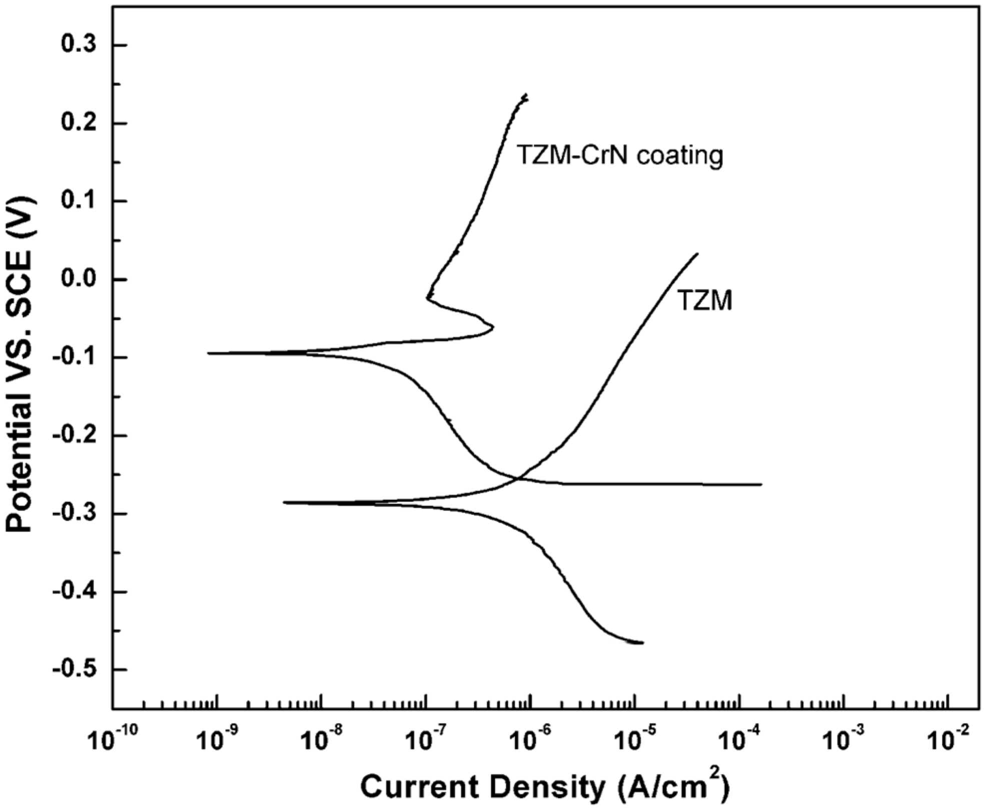

Fig. 5-44 Tafel plots for TZM alloy and CrN coated TZM

Fig.5-45 shows Tafel plot of CrN (D) coated and uncoated TZM. Corrosion potential of coated sample was higher than that of TZM, though they have close corrosion rates.

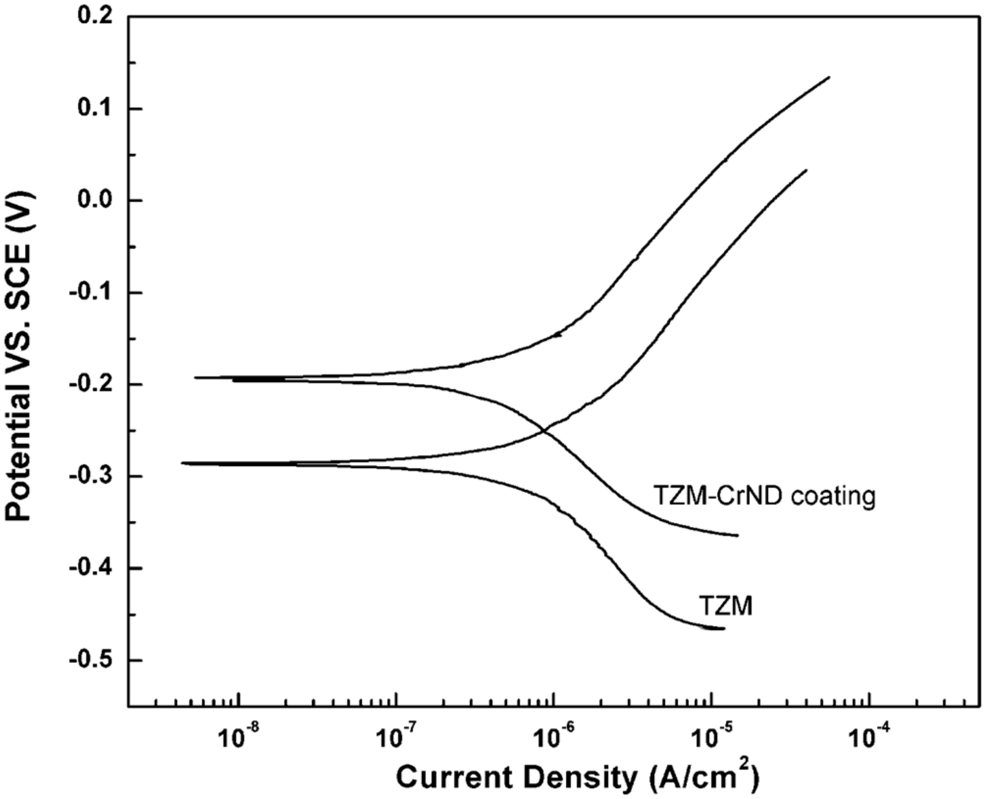

Fig. 5-45 Tafel plots for TZM alloy and CrN (D) coated TZM

TiC coated TZM showed significant reduction of the corrosion potential and indicated enhanced corrosion of the coated TZM, compared to uncoated TZM (Fig.5-46) in agreement with the impedance spectroscopy data.

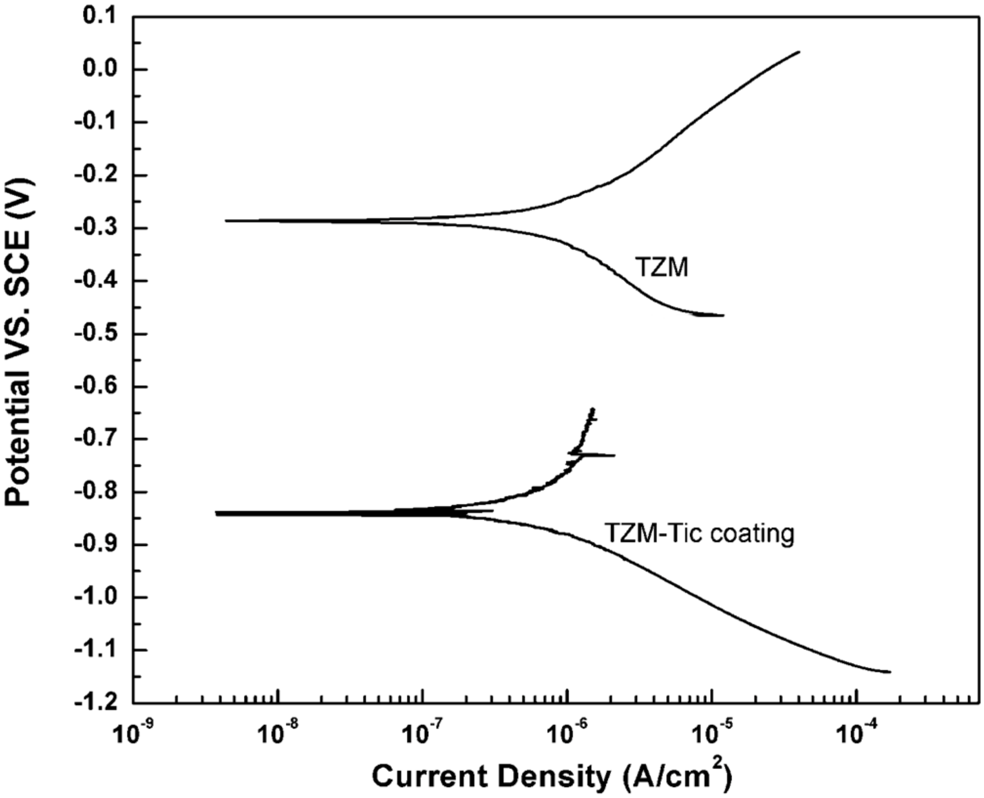

Fig. 5-46 Tafel plots for TZM alloy and TiC coated TZM

Fig.5-47 is a photo of samples following the Tafel test. Clearly the TiC coating on the surface had been corroded severely.

Fig. 5-47 Severe corrosion of TiC coated TZM after the corrosion test

6 Conclusions

I.

Nanostructured CeO_2 films were prepared by ELD and EPD methods. Benzoic acid provided efficient dispersion and charging of CeO_2 nanoparticles for EPD. The deposition yield can be controlled by the variation of deposition voltage, current density, deposition time and benzoic acid concentration. ELD and EPD resulted in the formation of porous CeO_2 films, which exhibited cracking. An electro-deposition method has been developed for the fabrication of PVP films. The deposition mechanism was based on the pH increase in the cathodic reactions, electrophoresis of the protonated PVP macromolecules and their charge neutralization and film formation at the cathode surface. The thickness of the PVP films was varied in the range of 0.1–3 μm by variation of the deposition time at constant current density or voltage.

II.

Two electrochemical strategies were developed for the co-deposition of CeO_2 and PVP, based on the electrodeposition of PVP and ELD or EPD of CeO_2. TGA, DTA, XRD and SEM studies showed the formation of composite films. The composition of the films can be adjusted by the variation of bath composition. The use of PVP allowed the formation of crack-free PVP-CeO_2 composite films. PVP films provided corrosion protection of stainless steel in aqueous NaCl solutions. Composite PVP-CeO_2 films prepared using ELD or EPD showed improved corrosion protection of stainless steel compared to pure PVP films.

III.

The EPD method has been deployed for the fabrication of PVPBM films. The method involved the protonation of PVPBM, electrophoresis of the charged polymer macromolecules, charge neutralization in the high pH region at the electrode surface and formation of water insoluble films. QCM and SEM data showed that the deposition yield can be controlled by the variation of polymer concentration, deposition voltage and deposition time. The EPD method allowed the formation of uniform and dense films. The thickness of the polymer films was varied in the range of 0.5-10 μm. The dispersion and deposition of CeO_2 was achieved using trans-cinnamic acid as a dispersant. The comparison of the deposition yield data for CeO_2 suspensions in ethanol and the mixed ethanol-water solvent showed that the pH increase at the electrode surface is an important factor controlling the particle discharge and film formation. Composite films were obtained as PVPBM-CeO_2 monolayers or PVPBM/PVPBM-CeO_2 laminates. The film thickness was varied in the range of 0.5-15 μm. The use of PVPBM with good film forming and binding properties allowed the room temperature deposition of composite materials. In this approach the problems related to the drying and sintering of pure CeO_2 films can be avoided. The films provided corrosion protection of stainless steel substrates in NaCl aqueous solutions. The method can be used for the fabrication of other organic-inorganic composites, containing PVPBM and inorganic nanoparticles of various functional materials.

IV.

Crystal violet has proved to be a promising additive which can be used to charge and disperse suspension particles in EPD processes. Clay is another commonly used particle in industry. Crystal violet works very efficiently with clay, in the presence of polymer PVPBM for the fabrication of composite films.

V.

Corrosion protection of CrN, CrND and TiC coatings prepared by PVD and Ni coating prepared by electroplating on AMPCO and TZM substrates has been investigated. CrN and CrN (D) provided corrosion protection of the substrates. CrN provided better corrosion protection than CrND. The Ni electroplated coating provided poor corrosion protection of AMPCO substrates. TiC coatings enhanced corrosion of TZM.

7 References

[1] Milton Ohring, Materials Science of Thin Films Deposition and Structure, second edition

[2] O.Knotek, F. Liiffler and G. Kriimer, Surface and Coatings Technology, 59 (1993) 14

[3] W. D. Miinz, F. J. M. Hauzer, D. Schulze and B. Buil, Surf. Coat. Technol. 49 (1991) 161.

[4] R. Buhl, H. K. Pulker and E. Mall, Thin Solid Films, 80 (1981) 114.

[5] E.Bergmann and E.Moll, in E.Broszeit, W. D. Miinz, H. Oechsner, K. T. Rie and G.-K.Wolf, Plasma Surface Engineering, Vol. 1, DGM, Oberursel, 1989, p. 547.

[6] H. Ehrich, B. Hasse, M. Mausbach and K.G.Miiller, J. Vat. Sci. Technol. A, 8 (3) (1990) 2160-64.

[7] J. Finken, E.W. Krentz, M. Krijsche, H. Sung, A. Voss, G. Erkens, O. Lemmer and T.Leyendecker, paper presented at the Int. Conf. on Metallurgical Coatings and Thin Films 91, San Diego, CA, April 1991.

[8] H.Schulz, Doctoral thesis, University of Karlsruhe, 1987.

[9] H. G. Prengel, Progress Report VDO, Ser. 5, No. 205, VDI, Diisseldorf, 1990.

[10] O. Knotek, F. Liiffler and H.G. Prengel, Proc. IPAT89, Geneva, CEP Consultants, Edinburgh, pp. 220-25.

[11] M. Stueber*, H. Holleck, H. Leiste, K. Seemann, S. Ulrich, C. Ziebert, Journal of Alloys and Compounds 483 (2009) 321–333

[12] M. Van Stappen, L.M. Stals, M. Kerkhofs, C. Quaeyhaegens, Surface and Coatings TechnoIogy 74-75 (i995) 629-633

[13] Ph. Steyer, A. Mege, D. Pech, C. Mendibidea, J. Fontaine, J.-F. Pierson. C.Esnouf, P. Goudeau, Surface & Coatings Technology 202 (2008) 2268–2277

[14]N. Selvakumar, Harish C. Barshilia, Solar Energy Materials & Solar Cells 98 (2012) 1–23

[15] I. Zhitomirsky, Advances in Colloid and Interface Science 97 (2002) 279

[16] I. Zhitomirsky, JOM-e Miner. Met. Mater. Soc. J. 52 2000

[17] I. Zhitomirsky, J. Eur. Ceram. Soc. 18 1998 849.

[18] P. Sarkar, P.S. Nicholson, J. Am. Ceram. Soc. 79 1996 1987.

[19] I. Zhitomirsky, Bull. Am. Ceram. Soc. 79 2000 57

[20] B.V. Derjaguin, L. Landau, Acta Physicochim. USSR 14 1941 633

[21] E.J.W. Verwey, J.T.G. Overbeek, Theory of the Stability of Lyophobic Colloids, Elsevier, Amsterdam, New York, 1948.

[22] N.G. Hoogeveen, M.A. Cohen Stuart, G.J. Fleer, J. Colloid Interface Sci. 182 1996 133.

[23] L. Sjostrom, T. Akesson, J. Colloid Interface Sci. 181 1996 645.

[24] T. Okubo, M. Suda, J.Colloid Interface Sci. 213 1999 565.

[25] I. Zhitomirsky, R. Chaim, L. Gal-Or, H. Bestgen, J. Mater. Sci. 32 1997 5205.

[26] S. Hayashi, Z. Nakagawa, A. Yasumori, K. Okada, J. Eur. Ceram. Soc. 19 1999 75.

[27] J. VanTassel, C.A. Randall, J. Eur. Ceram. Soc. 19 1999 955.

[28] T. Ishihara, K. Sato, Y. Takita, J. Am. Ceram. Soc. 79 1996 913.

[29] A.A. Foissy, G. Robert, Bull. Am. Ceram. Soc. 61 1982 251.

[30] P.S. Nicholson, P. Sarkar, X. Haung, J. Mater. Sci. 28 1993 6274.

[31] P. Ducheyne, S. Radin, M. Heughebaert, J.C. Heughebaert, Biomaterials 11 1990 244.

[32] Y. Matsuda, K. Imahashi, N. Yoshimoto, M. Morita, M. Haga, J. Alloys Compd. 193 1993 277

[33] S. Peulon, D. Lincot, Adv. Mater. 8 1996 166

[34] S.L. Jones, C.J. Norman, J. Am. Ceram. Soc. 71 1988 C190

[35] I. Zhitomirsky, Nanostruct. Mater. 8 1997 521

[36] M. Kosmulski, S. Durand-Vidal, J. Gustafsson, J.B. Rosenholm, Colloids Surf. A: Physicochem. Eng. Aspects 157 1999 245.

[37] P.M. Biesheuvel, H. Verweij, J. Am. Ceram. Soc. 82 1999 1451.

[38] J.J. Hermans, J. Polym. Sci. 18 1955 527

[39] H. Ohshima, J. Colloid Interface Sci. 228 2000 190

[40] H. Ohshima, Colloids Surf. A: Physicochem. Eng. Aspects 103 1995 249

[41] H. Ohshima, J. Colloid Interface Sci. 163 1994 474

[42] S. Levine, G.H. Neale, J. Colloid Interface Sci. 47 1974 520.

[43] H. Ohshima, J. Colloid Interface Sci. 188 1997 481.

[44] H. Ohshima, J. Colloid Interface Sci. 225 2000 233

[45] L. Gal-Or, I. Silberman, R. Chaim, J. Electrochem. Soc. 138 1991 1939

[46] J.A. Switzer, Bull. Am. Ceram. Soc. 66 1987 1521

[47] Y. Matsumoto, H. Adachi, J. Hombo, J. Am. Ceram. Soc. 76 1993 769

[48] Y. Matsumoto, T. Morikawa, H. Adachi, J. Hombo, Mater. Res. Bull. 27 1992 1319

[49] G.H.A. Therese, P.V. Kamath, Chem. Mater. 12 2000 1195

[50] L. Indira, P.V. Kamath, J. Mater. Chem. 4 1994 1487

[51] G.R. Lee, J.A. Crayston, J. Mater. Chem. 6 1996 187

[52] H. Koelmans, Philips Res. Rep. 10 1955 161

[53] A.E. Hughes, R.J. Taylor, B.R.W. Hinton, L. Wilson, Surf. Interface Anal. 23 1995 540

[54] A.T. Kuhn, C.Y. Chan, J. Appl. Electrochem. 13 1983 189.

[55] P.M.S. Monk, R. Janes, R.D. Partridge, J. Chem. Soc. Faraday Trans. 93 1997 3991.

[56] G.H.A. Therese, P.V. Kamath, Chem. Mater. 12 2000 1195.

[57] R. Chaim, I. Zhitomirsky, L. Gal-Or, H. Bestgen, J. Mater. Sci. 32 1997 389.

[58] M. Shirkhanzadeh, J. Mater. Sci. Lett. 10 1991 1415

[59] R.S. Jayashree, P.V. Kamath, J. Appl. Electrochem. 29 1999 449.

[60] G.H.A. Therese, P.V. Kamath, J. Appl. Electrochem. 28 1998 539.

[61] I. Zhitomirsky, A. Petric, Mater. Lett., in press.

[62] M. Izaki, J. Electrochem. Soc. 146 1999 4517.

[63] I. Zhitomirsky, L. Gal-Or, A. Kohn, H.W. Hennicke, J. Mater. Sci. Lett. 14 1995 807.

[64] I. Zhitomirsky, J. Eur. Ceram. Soc. 19 1999 2581.

[65] E.A. Meulenkamp, J. Electrochem. Soc. 144 1997 1664.

[66] I. Zhitomirsky, L. Gal-Or, S. Klein, J. Mater. Sci. Lett. 14 1995 60.

[67] I. Zhitomirsky, A. Kohn, L. Gal-Or, Mater. Lett. 25 1995 223.

[68] I. Zhitomirsky, L. Gal-Or, A. Kohn, M.D. Spang, J. Mater. Sci. 32 1997 803.

[69] I. Zhitomirsky, J. Mater. Sci. 34 1999 2441.

[70] R. Shacham, D. Avnir, D. Mandler, Adv. Mater. 11 1999 384.

[71] J.M. Zhang, C.J. Lin, Z.D. Feng, Z.W. Tian, J. Electroanal. Chem. 452 1998 235.

[72] S. Ban, S. Maruno, Jpn. J. Appl. Phys. 32 1993 L1577.

[73] Y. Matsumoto, H. Ohmura, T. Goto, J. Electroanal. Chem. 399 1995 91.

[74] F.-B. Li, R.C. Newman, G.E. Thompson, Electrochim. Acta 42 1997 2455.

[75] D.R. Brown, F.W. Salt, J. Appl. Chem. 15 1965 40.

[76] H.C. Hamaker, E.J.W. Verwey, Trans. Faraday Soc. 36 1940 180.

[77] H. Koelmans, J.T.G. Overbeek, Discuss. Faraday Soc. 18 1954 52.

[78] B. Ferrari, R. Moreno, P. Sarkar, P.S. Nicholson, J. Eur. Ceram. Soc. 20 2000 99.

[79] D. De, P.S. Nicholson, J. Am. Ceram. Soc. 82 1999 3031

[80] A.J. Aldykiewicz Jr., A.J. Davenport, H.S. Isaacs, J. Electrochem. Soc. 143 (1996)

147.

[81] K. Sambasivudu, Y.B. Reddy, J.S. Yadav, G. Sabitha, D. Shailaja, Int. J. Polym. Mater. 57 (2008) 891.

[82] K. Samba Sivudu, D. Shailaja, Mater. Lett. 61 (2007) 2167.

[83] Y. Li, K. Wu, I. Zhitomirsky, Colloids Surf. A 356 (2010) 63.

[84] K. Samba Sivudu, D. Shailaja, J. Appl. Polym. Sci. 100 (2006) 3439.

[85] P.A. Revell, M. Braden, M.A.R. Freeman, Biomaterials 19 (1998) 1579.

[86] A. Sari, C. Alkan, Polymer Composites 33 (2012) 92.

[87] H. Shafiee, A. Tagaya, Y. Koike, Journal of Polymer Science, Part B: Polymer Physics 48 (2010) 2029.

[88] T. Del Castillo-Castro, M.M. Castillo-Ortega, P.J. Herrera-Franco, Composites A 40 (2009) 1573.

[89] V.I. Zavrazhina, Y.P. Gladkikh, Protection of Metals 43 (2007) 100.

[90] P. Borah, A. Dutta, Ionics 14 (2008) 313.

[91] S.P. Armes, M. Aldissi, Polymer 31 (1990) 569.

[92] S.P. Armes, M. Aldissi, S.F. Agnew, Synthetic Metals 28 (1989) 837.

[93] R. Bouyahia, S. Djadoun, Journal of Thermal Analysis and Calorimetry 106 (2011) 927.

[94] R. Bouyahia, F. Metref, S. Djadoun, Macromolecular Symposia 263 (2008) 86.

[95] I. Zhitomirsky, Journal of the European Ceramic Society 18 (1998) 849.

[96] E. Pal, T. Seemann, V. Zollmer, M. Busse, I. Dekany, Colloid and Polymer

Science 287 (2009) 481.

[97] J. Vartiainen, M. Tuominen, K. Nättinen, Journal of Applied Polymer Science 116 (2010) 3638.

[98] K. Grandfield, I. Zhitomirsky, Materials Characterization 59 (2008) 61.

[99] I. Zhitomirsky, L. Gal-Or, Materials Letters 38 (1999) 10.

[100] X. Pang, T. Casagrande, I. Zhitomirsky, Journal of Colloid and Interface Science 330 (2009) 323.